FAULT CLASSIFICATION OF POLYMER SPUR GEAR USING ADVANCED SIGNAL PROCESSING AND MACHINE LEARNING TECHNIQUES

Ph.D. Thesis

By

ANUPAM KUMAR

1801103007

DEPARTMENT OF MECHANICAL ENGINEERING

INDIAN INSTITUTE OF TECHNOLOGY INDORE

July 2023

FAULT CLASSIFICATION OF POLYMER SPUR GEAR USING ADVANCED SIGNAL PROCESSING AND MACHINE LEARNING TECHNIQUES

A THESIS

Submitted in partial fulfillment of the

requirements for the award of the degree

of

DOCTOR OF PHILOSOPHY

by

ANUPAM KUMAR

1801103007

DEPARTMENT OF MECHANICAL ENGINEERING

INDIAN INSTITUTE OF TECHNOLOGY INDORE

July 2023

INDIAN INSTITUTE OF TECHNOLOGY INDORE

I hereby certify that the work which is being presented in the thesis entitled **FAULT CLASSIFICATION OF POLYMER SPUR GEAR USING ADVANCED SIGNAL PROCESSING AND MACHINE LEARNING TECHNIQUES** in the partial fulfillment of the requirements for the award of the degree of **DOCTOR OF PHILOSOPHY** and submitted in the **DEPARTMENT OF MECHANICAL ENGINEERING, INDIAN INSTITUTE OF TECHNOLOGY INDORE** is an authentic record of my own work carried out during the time period from July 2018 to July 2023 under the supervision of **Prof. ANAND PAREY,** Professor and the co-supervision of **Prof. PAVAN KUMAR KANKAR**, Professor, Department of Mechanical Engineering, IIT Indore.

The matter presented in this thesis has not been submitted by me for the award of any other degree of this or any other institute.

ANUPAM KUMAR

This is to certify that the above statement made by the candidate is correct to the best of my/our knowledge.

03/07/2023

Prof. ANAND PAREY

03/07/2023

Prof. PAVAN KUMAR KANKAR

ANUPAM KUMAR has successfully given his/her Ph.D. Oral Examination held on **November 20, 2023**.

20/11/2023

Prof. ANAND PAREY

20/11/2023

Prof. PAVAN KUMAR KANKAR

ACKNOWLEDGEMENT

I would like to extend thanks to my enthusiastic supervisor, **Prof. Anand Parey**, who has constantly supported me throughout my research journey. My Ph.D. has been an amazing experience, and I thank Prof. Parey wholeheartedly, not only for his tremendous academic support but also for believing in me and providing me with many other opportunities which helped me gloss for overall development. I am thankful to my co-supervisor, **Prof. Pavan Kumar Kankar**, for his immense guidance and support during my Ph.D. journey. Only his inspiring thoughts make me more enthusiastic with every passing day.

I would like to thank my Ph.D. progress committee members, **Dr. Eswara Prasad Korimilli** and **Dr. Girish Chandra Verma**, for their valuable suggestions right from the beginning of my research work. I express my sincere thanks to **Prof. Shanmugam Dhinakaran,** Head of the Department of Mechanical Engineering, for providing me with the opportunity and necessary infrastructure to carry out my research work.

I would like to thank the technical staff of the Central Workshop of IIT Indore for their valuable work supporting my experimental set-up. I would like to give a special thanks to Mr. Sandeep Patil, Deputy Manager of vibration and noise control Lab, for every stage of my experiments.

I acknowledge with a deep sense of thankfulness to my current and previous laboratory colleagues Mr. Dada Saheb Ramteke, Dr. Palash Dewangan, Dr. Pavan Gupta, Dr. Jatin Prakash, Dr. Vinod Singh Thakur, Mr. Nagendra Singh Ranawat, Mr. Yogesh Andhale, Mr. Santosh Yadav, Mrs. Pallavi Gautam, Ms. Akanksha Chaudhari, Dr. Vikas Sharma, Dr. Naresh Kumar Raghuwanshi, Dr. Ankur Saxena, Dr. Yogesh Pandya**,** and all my Vibration and Noise Control Lab and System Dynamics Lab members for always standing there through my trough and crest during my Ph.D.

journey. They all have been accommodating and constantly encouraged me throughout the time we spent together.

I would like to thank all colleague researchers' friends who have been highly supportive, especially Dr. Anuj Kumar, Mr. Rajnish Modanwal, Mr. Devashish Chorey, Mr. Vivek Rana, Mr. Pankaj Gupta, Mr. Vishal Jagdale, Mr. Ram Mohril, Mr. Bhavesh Chaudhary for their endless support and encouragement during the course of my research.

I will be failing in my duties if I do not extend my thanks to my grandparents, Late Gayrti Devi and Late Yamuna Singh Azad, my mother **Mrs. Pramila Devi**, and my father, **Mr. Satyendra Narayan Singh**, for their enormous support, sincere advice, and guidance. They sacrificed many things and always stood by to support me at every moment of my life. I could not imagine the success of my Ph.D. journey without them. I would like to thank them for their constant support and love. I would also like to thank my father-in-law, **Mr. Vinay Kumar Singh** for his faith and love.

A very special thanks and love to my beloved wife, **Dr. Vaishali Raj** for her unconditional love and care. I extend my love and gratitude to my lovely sisters **Mrs. Alka Rani, Mrs. Sonam Singh**, **Pushpanjali Singh,** and other family members for their love and moral support, which made this journey successful. I am also grateful to my brothers-in-law, **Dr. Vijay Kumar Singh**, **Mr. Vikram Chauhan, Mr. Vaibhav Kumar Singh, and Mr. Vivek Kumar Singh** for their endless support, love, and blessings. I would also like to thank my niece and nephews, **Harsh Singh, Devesh Singh, Vinayak Chauhan, Vaibhavi Chauhan, Wamika Singh & Vihana Singh** for being my stress buster. I am also thankful to all those who helped and supported me directly or indirectly during this journey.

Above all, I would like to thank the Almighty for everything he has done for me.

Anupam Kumar

DEDICATION

To my grandparents'

Late Gayatri Devi and

Late Yamuna Singh Azad

for their blessings, immeasurable love, care, and unwavering support

ABSTRACT

Polymer gears possess numerous advantages over metal gears, including their low weight, low vibration and noise, affordability high corrosion resistance, and ease of manufacturing. These characteristics make polymer gears highly suitable for power transmission applications in various domains such as aviation, electric vehicles, textile machines, windshield wipers, printers, packaging machines, and mixers. Over the past few decades, extensive research has been conducted on polymer gear materials, loading conditions, the influence of gear pairs, and tooth modifications. Among these studies, researchers have identified that polymer gears often fail due to wear, pitting, and thermal damage. Researchers have employed a variety of techniques to modify the teeth of polymer gears, such as inserting steel pins into the internal holes of the gear teeth. This modification aims to enhance gear durability by mitigating thermal effects on the teeth. However, surprisingly, there is a significant gap in research exploring how these tooth modifications affect gear noise and vibration levels. Apart from that, only a few research studies have been conducted on detecting faults in polymer gears. Therefore, the objective of this thesis is to investigate the influence of tooth modification on the noise and vibration characteristics of polymer gears. Furthermore, the study aims to develop approaches for detecting and classifying faults in polymer gears.

To achieve this, first a test rig was designed and constructed specifically for conducting polymer gear tests under various load and speed conditions. To explore tooth modifications in polymer gears, Two tooth modifications and one without tooth modification gear were explored in terms of their vibration and noise levels. The results obtained from these modified gears were compared with those of unmodified gears, both in polymer-polymer gear pairs and polymer-metal gear pairs.

Furthermore, the early detection of faults in polymer gears using vibration analysis is crucial to avoid catastrophic failures. However, the

vibration signals of polymer gears are typically weak and susceptible to ambient noise, especially at the early stages of fault development. This poses challenges in extracting signal features using traditional signal analysis methods. Therefore, in this study, the following methods have been developed for polymer gear fault classification: One of the approaches to early polymer gear pitting fault detection is by kurtosis based variational mode decomposition (VMD). Firstly, acquired polymer gear vibration signals are decomposed by VMD. After that select the informative decomposed signals using kurtosis and obtained a more sensitive signal. Subsequently, condition indicators, namely kurtosis and crest factor, are extracted from the more sensitive signal. The analysis reveals that both indicators exhibit an increase in values corresponding to the severity of faults. The first step involves decomposing the acquired signal using empirical wavelet transform (EWT) and selecting a sensitive signal. Various features are then extracted from the selected signal. These features are divided into three feature sets. The first set includes root mean square (RMS), crest factor, shape factor, and kurtosis. The second set consists of Hjorth parameters (HP)-based features, while the third feature set combines the features from the first and second sets. Subsequently, different machine learning models, namely K-nearest neighbors (KNN), linear discriminant analysis (LDA), and support vector machine (SVM), are trained using the three distinct feature sets to classify the polymer gear faults. The results demonstrate that when the EWT decomposition method is combined with KNN, there is a significant improvement in classification accuracy. Specifically, the third feature set achieves a superior accuracy rate of 99.3%. Furthermore, a comparison is made between the classification accuracy of empirical mode decomposition (EMD) and the raw signal-based method. Next, to develop a classification model for classifying the one healthy and five different levels of simulated pitting faults of polymer gear with maximum accuracy. In the case of the healthy gear, there were no pits present on the tooth surface. However, in the case of Fault 1 through Fault 5, the number of pits on the tooth surface ranged from one

to five. A double decomposition technique with an ensemble learning model has been proposed. To achieve this, a double decomposition technique has been employed, combining EMD and Discrete Wavelet Transform (DWT). This process enables the extraction of a set of entropy features (EF) and HP are extracted following the decomposition. After that, different machine learning classifiers namely SVM, ensemble learning, and decision tree were trained with three different feature sets (EF, HP, and a combination of EF and HP) to classify the early pitting faults of polymer gears. The performance of the double decomposition technique is evaluated and compared with EMD and DWT-based decompositions separately. The result reveals that the best classification accuracy is achieved by double decomposition with ensemble learning classifiers and trained with a combination of EF and HP feature sets. Furthermore, six different deep learning models have been developed, tested, and compared for the classification of polymer gear multiclass faults with minimum computational time. For this, the first complete ensemble empirical mode decomposition with the adaptive noise (CEEMDAN) is used for signal decomposition and getting an enhanced signal. The results show that the hybrid design deep learning model, combining long short-term memory (LSTM) and gated recurrent unit (GRU), gives impressive accuracy. The hybrid model achieved a maximum accuracy of 99.6% while significantly minimizing computational time compared to the other designed models. Furthermore, the proposed model was also compared to traditional machine learning models. The findings support the superiority of the deep learning model in terms of both accuracy and computational efficiency. In this manner, the thesis provides experimental and data-driven approaches for the fault classification of polymer gears.

Keywords: Polymer gear; teeth modification; noise; vibration; fault classification; VMD; EWT; double decomposition; Hjorth parameters; LSTM; GRU.

TABLE OF CONTENTS

LIST OF FIGURES

LIST OF TABLES

NOMENCLATURE

N	Sample number
y_i	i^{th} vibration signal
C_i	i^{th} intrinsic mode functions
r_n	n^{th} residual component
ω_k	Center frequencies
λ	Lagrangian multipliers
τ	Noise tolerance
f_{gm}	Gear mesh frequency
$2f_{gm}$	Harmonic of gear mesh frequency
$u_e(t)$	Upper envelope
$l_e(t)$	Lower envelope
$r_1(t)$	Residue function
$\varphi_n(\omega)$	Scaling function
$\psi_n(\omega)$	Wavelet function
φ_0	Standard deviation of white noise
μ_{th}	Threshold
E_{Le}	Log energy entropy
E_{th}	Threshold entropy
E_{sure}	Sure entropy
E_{sha}	Shannon entropy
E_{ne}	Norm entropy

ACRONYMS

PP	Polymer Pinion
PG	Polymer Gear
PPSP	Polymer Pinion with Steel Pin
PPH	Polymer Pinion with Hole
SG	Steel Gear
VFD	Variable Frequency Drive
DAQ	Data Acquisition System
RMS	Root Mean Square
CF	Crest Factor
SPL	Sound Pressure Level
VMD	Variational Mode Decomposition
EMD	Empirical Mode Decomposition
CIs	Condition Indicators
IMF	Intrinsic Mode Functions
VMF	Variational Mode Functions
EWT	Empirical Wavelet Transform
ML	Machine Learning
KNN	K-Nearest Neighbors
LDA	Linear Discriminant Analysis
SVM	Support Vector Machine

HP	Hjorth parameters
SF	Statistical Features
DWT	Discrete Wavelet Transform
TP	True Positives
TN	True Negative
FP	False Positives
FN	False Negative
CEEMDAN	Complete Ensemble Empirical Mode Decomposition with Adaptive Noise
CNN	Convolution Neural Network
DNN	Deep Neural Network
RNN	Recurrent Neural Network
LSTM	Long Short-Term Memory
BiLSTM	Bidirectional LSTM
GRU	Gated Recurrent Unit
ABC	Artificial Bee Colony
CC	Correlation Coefficient
RCMDE	Refined composite multiscale dispersion entropy
RCMFE	Refined composite multiscale fuzzy entropy
MDF	Median frequency

Chapter 1

Introduction and literature review

1.1 Introduction

Gears are mechanical components designed to transmit motion and power between shafts through the gradual engagement of teeth [1]. While early gear designs prioritized reliability, the performance requirements for gears have evolved over time. Modern transmission systems now demand gears with increased load-carrying capacity, higher operational speeds, minimized noise and vibration, lighter weight, and cost-effectiveness in production and operation.

In response to these demands, engineers have developed innovative methods to enhance the power density of vehicle powertrains while reducing the mass of components. One such approach involves leveraging plastic materials in gear manufacturing, enabling the creation of lightweight designs that are both cost-effective and efficient.

1.2 Polymer gears and their usages

Polymers have always attracted a lot of interest from gear designers because of their low material density and lower material costs. Polymer gears (PGs) were first introduced in the 1950s and have since undergone rapid development, with advantages such as the ability to operate with minimal or no lubrication, high resilience, and internal damping capacity [2–4]. Despite these benefits, certain inherent limitations, such as inadequate flexural strength and surface durability, have limited the load-carrying capacity of PGs, resulting in their early use being restricted to lightly loaded motion transmission applications.

However, recent advancements in polymer materials, lubrication conditions, and manufacturing processes have led to the development of polymer resins with superior and consistent material properties, significantly improving the load-carrying capacity of PGs [5]. As a result, PGs have become viable alternatives to metal gears in power transmission applications, such as textile industries, vehicle engines, and motorbikes [6–8]. For instance, the use of polymer gears in automobile engineering has led to a reduction of 70% in mass, 80% in inertia, and 9% in fuel consumption [9]. The combination of high load-carrying ability and low weight is opening new avenues for polymer gears in industries, including e-bikes, aviation, and new energy vehicles.

In addition to that, the choice of material for the mating gear has a significant impact on various parameters of polymer gear (PG) performance, including fatigue life, operating temperature, and failure mode [10]. PGs can be used in two types of material engagements: metal-polymer and polymer-polymer pairings, each offering specific advantages in terms of operational performance and cost. Depending on the specific application, a polymer-polymer gear pair can offer greater benefits compared to a metal-polymer gear pair, such as reduced weight, cost savings, and overall cost-effectiveness. Furthermore, utilizing materials with similar stiffness for both the driver and driven gears helps to prevent the stiffness mismatch commonly observed in metal-polymer gear pairs.

1.3 Failure modes of PGs

Under harsh working conditions, such as heavy loads, high running speeds, and elevated temperatures, PGs may experience catastrophic failure due to various reasons, including cracking at the root, wear, pitting, and cracking at the pitch circle, as depicted in Figure 1.1 [11]. During operation, the pitch point of the gear experiences elevated temperatures, which can weaken the material strength and lead to cracking at the pitch circle. Singh et al. [11] have shown that unlubricated gears fail due to surface wear, local melting,

and pitting, whereas lubricated conditions lead to failures primarily at the root. Lu et al. [12] conducted experiments and observed slight pitting around the pitch line in polymer gears. As the loading cycle increases, more pits appear near the pitch line, with a depth ranging from 1 to 2 mm. Another study by Illenberger et al. [13] focused on analyzing the development of pitting in high-performance plastic gears. They found that pitting damages mainly occur in the dedendum flank region of the gear in single tooth contact. Furthermore, the extent of the flank area affected by pitting increases with the number of load cycles. It is crucial to detect these defects at an early stage to prevent catastrophic failures.

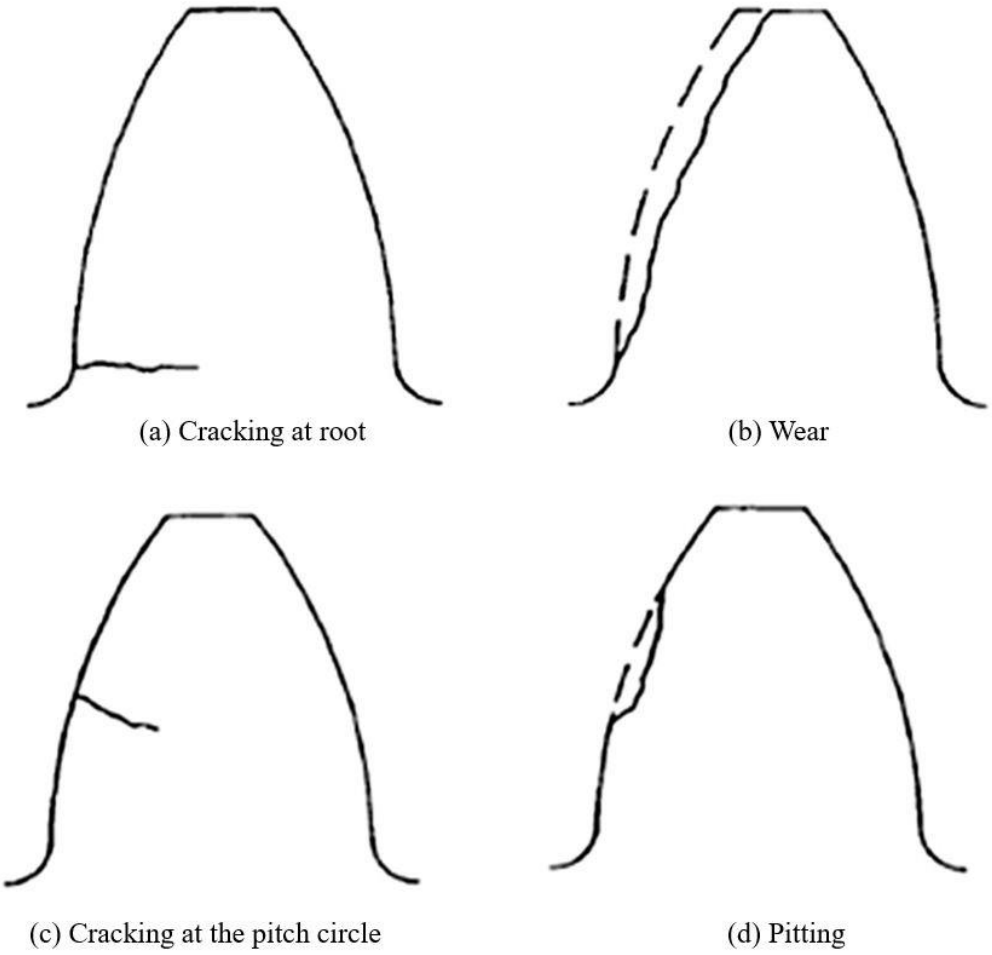

Figure 1.1 Different types of polymer gear failures [11].

One major drawback of PGs is their low thermal conductivity, which can lead to thermal failure. To overcome this limitation, researchers have employed various techniques to enhance the performance of PGs by modifying their tooth design. Kim [14] studied durability improvement methods for plastic spur gears. The approach involved inserting a steel pin into the internal hole of the gear tooth. The findings demonstrated a decrease in tooth surface temperature, resulting in a reduced wear rate and an increased service life for the gear. Another investigation conducted by Senthilvelan and Gnanamoorthy [15] focused on examining the impact of gear tooth fillet radius on gear performance. The results revealed that gears with higher tooth fillet radius exhibited superior service life under all loading conditions. These research efforts highlight the importance of implementing tooth modifications in PGs to mitigate thermal issues and enhance their overall performance.

1.4 Machine condition monitoring

Machine condition monitoring (CM) plays a crucial role in ensuring the reliable and cost-effective operation of industrial facilities. CM involves continuously monitoring the machine to detect faults at an early stage, allowing timely action to be taken before a breakdown or catastrophic failure occurs. By implementing continuous CM, planned maintenance and repairs can be scheduled, leading to more efficient and environmentally friendly operations. Various technologies have been employed to enhance the applicability, accuracy, and reliability of CM systems [16]. Real-time machine data acquisition and processing have gained wide acceptance in CM due to their ability to detect faults early. Selecting the most suitable CM system is critical for increasing machine availability, performance, and lifespan, reducing spare parts inventories, and preventing breakdown repairs.

In the industry, maintenance accounts for 15-40% of the costs of manufacturing [17]. Therefore, it is crucial to implement an effective maintenance strategy to minimize these additional expenses. One approach to

achieving this goal is through the implementation of condition based maintenance (CBM) or maintenance based on structural health monitoring. CBM has gained popularity among companies due to its ability to prevent unnecessary breakdowns and recommend maintenance actions only when necessary. By adopting CBM, plants can save significant amounts of time and money.

Various techniques are utilized in the industry for machine monitoring. These include visual and aural inspections, temperature monitoring, wear debris analysis, vibration analysis, acoustic emission analysis, noise analysis, and more. Visual and aural inspections rely on skilled personnel who assess the machine's condition using their visual senses, but these methods have limitations in effectively detecting early-stage faults [18].

Temperature monitoring involves the use of sensors like thermocouples, thermal cameras, and thermometers to track and measure machine temperatures [19]. This monitoring process is essential for identifying excessive heat generation, which can serve as a significant indicator of faults.

Wear debris analysis is another important traditional method used in industrial CM. It aims to determine the level of contamination and the size of wear particles present in the lubricant [20,21].

Acoustic emission (AE) [22,23] monitoring involves the detection of stress waves generated in materials due to deformation, such as crack initiation or dislocation movement. These waves typically fall within the ultrasonic frequency range of 20 KHz to 1 MHz.

Vibration monitoring is a robust approach that can be applied to CM for all types of industrial machines. Vibration-based monitoring techniques are effective in detecting various types of faults, including issues with gears and bearings, misaligned parts, eccentric shafts, and improper clearances. Vibration analysis has been widely utilized in approximately 82% of fault diagnosis approaches [24,25].

1.5 Vibration analysis for gearbox fault analysis

Gearbox failures can occur in various ways during operation, often accompanied by increased noise and vibration as warning signs before complete failure. The gearbox vibration signal is a complex non-stationary signal that includes multiple components under real-time operating conditions, such as shaft frequency, tooth meshing frequency, harmonics, fault transients, and noise [26,27]. The behavior of the gearbox vibration signal is influenced by physical characteristics such as operating speed, load, gear tooth meshing, tooth surface condition, and friction [28–33]. Additionally, the presence of other components within the gearbox, like bearings, impacts the gearbox vibration signal. Thus, the acquisition of vibration signals and subsequent signal processing play crucial roles in detecting gear faults.

Shipley [34] studied one of the primary causes of gearbox breakdowns is localized or widespread faults in the gear teeth. Vibration analysis utilizing signal processing methods has demonstrated effectiveness in identifying gearbox defects under constant speed conditions [35–39]. Vibration signals are captured by accelerometers mounted on the gearbox bearing casing. Operating variables, including speed variations and gear teeth meshing, contribute to the modulation of gearbox vibration signals [28]. These modulations can mask existing fault-related modulations [40–42]. Therefore, signal processing techniques are employed to analyze gearbox vibration signals for the detection of faults.

1.6 Overview of signal processing techniques to detect gear faults

Signal processing techniques are widely used for gear fault analysis to extract valuable information from vibration signals and identify potential faults in gear systems. These techniques help to analyze the characteristics of vibration signals and detect specific patterns or anomalies associated with gear faults. The vibration signal from the gearbox demonstrates a mixture

of deterministic and random elements [43]. Random signals can be classified as stationary or non-stationary, while deterministic signals can be further categorized as periodic or non-periodic. Signal processing techniques are adept at extracting important information from these signals. Several methods have been developed for the early detection of gearbox faults [21,36,44]. However, each method has its limitations. Some commonly employed signal processing techniques for gear fault analysis include:

1.6.1 Time domain analysis

Time domain analysis is a commonly used signal processing technique for detecting gear faults in machinery. It involves examining the vibration signals obtained from gear systems in the time domain to identify any abnormalities or patterns that indicate the presence of faults. Time domain analysis involves examining the amplitude changes of a signal over time to detect transient impulses caused by fault phenomena in the time domain vibration signal [45]. This approach is commonly utilized to identify the presence of gear faults.

Another important aspect of time domain analysis is the calculation of statistical parameters. These parameters include root mean square (RMS) values, peak values, kurtosis, skewness, and crest factor. By comparing the statistical parameters of vibration signals from healthy gears with those from faulty gears, significant deviations can be detected, indicating the presence of gear faults. The most commonly used statistical parameters in gear fault analysis include peak value, RMS, crest factor, and kurtosis [46]. Time synchronous averaging (TSA) is a traditional time domain analysis technique used to extract periodic waveforms from noisy signals. TSA involves dividing the vibration signal into contiguous segments of equal length, which is usually the shaft rotation period. These segments are then averaged to enhance the synchro-nous vibration signal with periodic shaft movement, while random non-synchronous components are attenuated or canceled [47].

1.6.2 Frequency domain analysis

Frequency domain analysis is another signal processing technique for gear fault detection, which involves examining the frequency content of vibration signals to identify specific fault-related frequencies and their associated characteristics [48]. One of the most used techniques in frequency domain analysis is the Fast Fourier Transform (FFT). The FFT converts the time domain vibration signal into the frequency domain. In a frequency domain graph, the y-axis (ordinate) represents the amplitude of the displacement, velocity, or acceleration, while the x-axis (abscissa) represents the frequency. This graph provides a visual representation of how the amplitude of the signal varies at different frequencies.

In gear fault detection, the FFT can be used to identify the presence of specific frequencies associated with gear faults, such as the gear meshing frequency and its harmonics. The FFT can also be used to analyze the sidebands around the gear meshing frequency, which can indicate the presence of defects such as pitting, wear, or cracks in the gear teeth [49].

1.6.3 Time-frequency domain analysis

Time-frequency domain analysis is a technique used to analyze signals that exhibit time-varying frequency content. It combines the advantages of both time domain and frequency domain analyses by providing information about how the frequency content of a signal changes over time. A time-frequency plot provides a comprehensive representation of a signal by depicting all components within a specific frequency range. It displays these components sequences, causality, and frequency variations over time in a single plot [38].

Time-frequency domain analysis is a powerful tool for analyzing non-stationary signals, such as those generated by gear faults. However, it can be challenging to extract meaningful information from these complex signals using traditional signal processing techniques. Therefore, advanced

signal processing methods have been developed to overcome these challenges and improve the accuracy of gear fault detection.

One such method is wavelet transform, which is widely used for the time-frequency analysis of non-stationary signals. It decomposes the signal into different frequency bands and provides information about the amplitude and phase of each component. Wavelet-based techniques have been successfully applied to detect gear faults [50,51]. Other advanced signal processing techniques include empirical mode decomposition (EMD) [52], ensemble empirical mode decomposition (EEMD) [53], Hilbert-Huang transforms (HHT) [54], and adaptive filtering algorithms, among others. They aim to improve the signal quality, denoise the data, and enhance the detection of fault-related features in the time-frequency domain. However, these methods require expert judgments to determine the health of the gearbox. As a result, modern industrial applications choose fault detection methods that can determine machine health statuses automatically. Therefore, the gear fault diagnosis in vibration signals has been enhanced by the integration of advanced signal processing techniques with machine learning algorithms. Machine learning (ML) algorithms, including artificial neural networks (ANN), support vector machines (SVM), decision trees (DT), and deep learning models, have demonstrated significant potential in automatically analyzing and classifying gear faults with promising outcomes [55–57].

1.7 Overview of machine learning techniques

ML and data-driven techniques have proven to be effective in defect detection by utilizing existing sensor data. These methods enable timely and reliable fault detection with minimal human intervention, leading to cost savings and improved system performance.

For ML algorithms to work effectively, access to data is crucial. ML algorithms require a set of features to represent the data, which can have continuous, discrete, or binary values. If the instances are labeled with

known accurate outputs, it is considered supervised learning [58], while unsupervised learning [59] does not involve labeling the samples.

The selection of appropriate features plays a vital role in recognizing fault characteristics and enhancing the performance of ML algorithms. These features can be extracted from the acquired signals in the time domain [50,60–62], frequency domain [63,64], and time-frequency[65–68].

To improve efficiency, feature subset selection techniques can be applied to remove unnecessary and redundant data, reducing dimensionality. This process ensures that only relevant features are utilized in the ML algorithms [69]. A generalized fault detection procedure for rotating machines using ML is depicted in Figure 1.2.

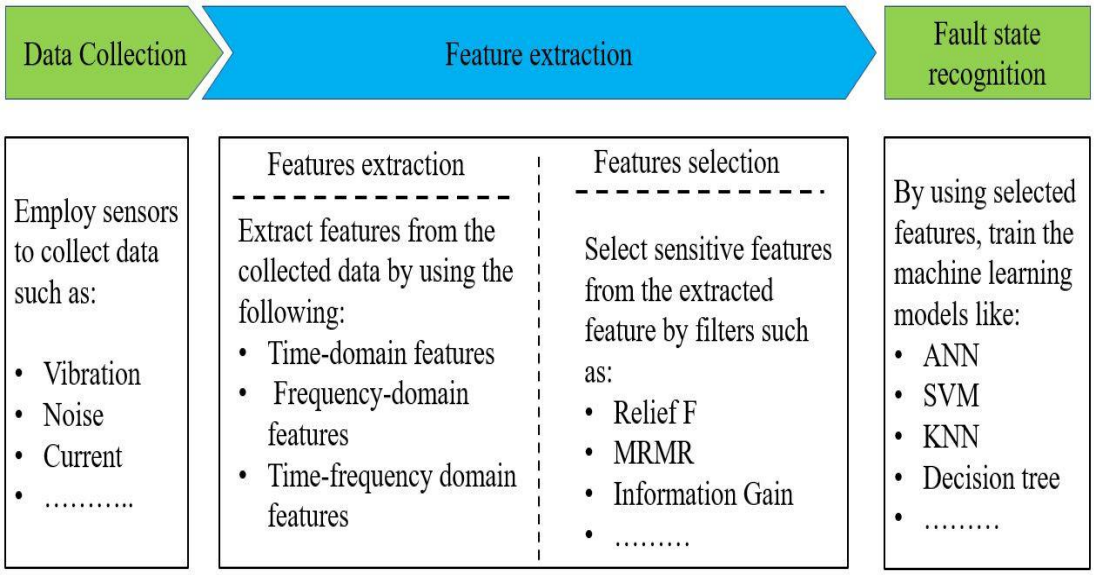

Figure 1.2 Fault detection procedure of rotating machine using traditional machine learning methods.

Vernekar [70] conducted a study on automated fault detection of gears using vibration signals. Features were extracted from the signals, and the J48 algorithm was employed for sensitive feature selection. Fault classification was performed using the ANN algorithm. In another study, Samanta [62] compared ANN and SVM for gear fault detection. Genetic algorithms (GA)

were utilized for feature extraction, and SVM exhibited higher classification accuracy compared to ANN. Saravanan et al. [67] investigated the effectiveness of wavelet-based features for fault detection using ANN and proximal SVM. Feature vectors were extracted from Morlet wavelet coefficients, and sensitive features were selected using the J48 algorithm.

1.8 Overview of deep learning techniques

Deep learning models can extract high-level features from raw input data by leveraging multiple layers within the network. This approach has found success in various domains, including image processing, speech recognition, and natural language processing [71,72].

There are two common techniques for applying deep learning algorithms. The first approach involves transforming the one-dimensional (1D) signal into a two-dimensional (2D) representation, such as a time-frequency representation. This transformed representation is then used to train a convolutional neural network (CNN) to capture underlying patterns. The second strategy involves directly feeding the signals into deep networks, such as 1D CNNs or recurrent neural networks (RNNs), to extract hidden patterns. CNN [73,74] is a type of feed-forward neural network that incorporates convolution operations and deep structures. Researchers [74–78] have utilized 1D CNNs with raw vibration signals as input and successfully developed end-to-end diagnosis models for gear fault classification. Furthermore, Li et al. [79] investigated gear fault detection using Bi-directional long short-term memory (BiLSTM) and compared it with long short-term memory (LSTM). Other alternative deep learning techniques, such as the combination of CNN and Gated Recurrent Unit (GRU) for gear fault detection [80] and the utilization of autoencoders for detecting gear pitting [81], have also been explored in gear failure diagnosis. The fault classification procedure for rotating machines using deep learning is illustrated in Figure 1.3.

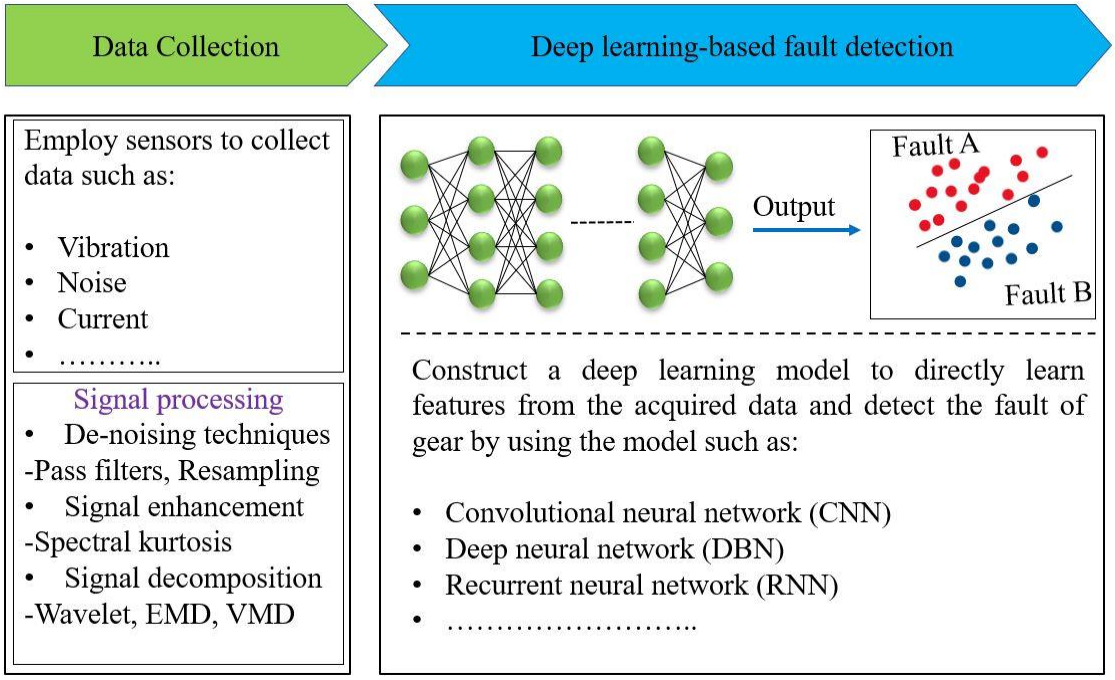

Figure 1.3 Fault detection of rotating machine using deep learning techniques.

1.9 Conclusions

It is found from the above literature survey; PGs have emerged as viable replacements for metal gears in power transmission applications. This is due to advancements in polymer materials, lubrication conditions, and manufacturing techniques. However, it is important to note that PGs can experience catastrophic failure under harsh working conditions during long-term operations. The main types of failure observed in PGs are cracking at the root, wear, cracking at the pitch circle, and pitting.

In the field of gear fault diagnosis, vibration signal analysis has proven to be a valuable tool for early and reliable defect identification. Three different approaches have been employed for gear fault detection: the signal processing method-based approach, the machine learning-based approach, and the deep learning-based approach. Within the signal processing approach, three different analysis methods have been utilized: time-domain analysis, frequency-domain analysis, and time-frequency domain analysis.

ML approaches have demonstrated the ability to accurately identify gear defects with minimal human intervention. Various ML algorithms have been explored, and the selection of the most suitable algorithm depends on factors such as data availability, desired learning rate, desired accuracy level, types of defects being addressed, and the engineer's comfort with the techniques. The ML process typically involves data collection, feature extraction, and fault classification.

Deep learning techniques have been applied to construct end-to-end diagnosis models that can automatically learn features from collected data and recognize the health status of machines.

1.10 Outcomes of the literature review

The existing literature on PGs, including their applications and failure modes, has been thoroughly examined. Additionally, a comprehensive review of various condition monitoring methods, with a specific focus on vibration-based monitoring techniques, has been conducted. The significance of vibration-based techniques in detecting various faults in gears is presented in detail. Here are the key findings derived from the literature review.

- Temperature is a critical factor influencing the failure of PGs. To enhance the lifespan of PGs and reduce tooth surface temperature, several tooth modification methods have been developed.
- However, there is a lack of research on how tooth modification in PGs affects other properties such as vibration and noise. Therefore, it is crucial to investigate the impact of tooth modification on the vibration and noise generated by gears under different operating conditions.
- PGs have established themselves as an attractive alternative to traditional metal gears in a plethora of applications. During operation, PGs mainly fail due to pitting, wear, cracking at the root, and cracking at the pitch circle. But, there is a lack of research on PGs fault detection.

- Commonly acquired signals for gear fault analysis include vibration, noise, motor current signature, and acoustic emission. Vibration signals carry detailed fault information and are widely used in the condition monitoring of metal gears. However, it is important to focus on analyzing vibration signals specifically for polymer gear fault detection.
- Identifying the severity of faults is crucial for initiating appropriate corrective actions. However, the literature lacks sufficient information on severity identification for PG faults.
- In the literature, fault detection techniques for metal gears are typically categorized into signal processing-based, machine learning-based, and deep learning-based methods. Therefore, there is much scope in these techniques for PGs fault detection.
- ML techniques typically involve three main steps: (i) acquiring the signal, (ii) pre-processing the acquired signal and extracting relevant features, and (iii) utilizing these feature data to train the ML algorithm. The success of the ML algorithm in classifying different gear faults depends on factors such as the signal types, the sensitivity of the selected features, and the domain from which the features are extracted. The domains commonly used for feature extraction are time, frequency, and time-frequency. However, it is important to note that not all ML models perform equally well in all cases. Therefore, there is a need to develop a reliable learning algorithm that gives a higher accuracy with fewer features and which is robust to gear operating conditions and surrounding noise.
- From the literature review in the case of DNN, features are extracted from CNN there is no need for manual feature extraction. However, it is beneficial to reduce the dimensionality and variability of the data to facilitate faster and more efficient training of RNNs. This can be achieved through dimensionality reduction techniques or manual feature extraction from the signals. However, there is

limited investigation into manual feature extraction approaches specifically within the context of DNN techniques. Developing a DNN model that achieves high classification accuracy while minimizing computational time is therefore crucial.

Based on the literature outcomes, the aims and objectives of the thesis work can be derived and presented in the subsequent section.

1.11 Objectives

The current research aims to improve fault detection in polymer gears through the development and application of advanced signal processing and machine learning techniques. Based on the literature review and the outcomes discussed, the following objectives have been derived:

i. Investigate the impact of teeth modifications on the vibration and noise characteristics of polymer gears, aiming to understand how these modifications affect the level of vibration and noise under different operating conditions.
ii. Develop a robust fault detection method for polymer gears using advanced signal processing techniques, focusing on extracting relevant features from the vibration signals to accurately identify faults.
iii. Compare the performance of different ML classifiers using various feature sets extracted from decomposed signals, aiming to identify the most effective combination of features and classifier for polymer gear fault classification.
iv. Develop a novel approach that combines double decomposition with supervised machine learning techniques, to achieve early fault classification in polymer gears and improve the overall accuracy of the fault detection process.
v. Design and develop a deep learning model specifically tailored for polymer gear fault detection, with a focus on achieving high classification accuracy while minimizing computational time.

1.12 Organization of thesis

The thesis is organized into the following chapters:

Chapter 1: Introduction and literature review

This chapter provides an introduction to the research topic and reviews previous works related to polymer gears. It discusses different methods of gear fault detection, including signal processing methods, machine learning methods, and deep learning methods. The chapter concludes with the research motivation and objectives of the thesis.

Chapter 2: Effect of teeth modifications on vibration and acoustic characteristics

In this chapter, the impact of teeth modifications on the vibration and acoustic characteristics of polymer gears is investigated. The design and development of an experimental setup for evaluating noise and vibration characteristics are described in detail. A comparison is made between different types of engagements, such as metal-polymer and polymer-polymer material pairs, with modified and unmodified gears. The chapter concludes with a summary of the findings.

Chapter 3: Early pitting fault detection using kurtosis based VMD

This chapter presents the methodology for detecting early pitting faults in polymer gears using kurtosis based VMD. A comparison is made between the proposed method, empirical mode decomposition (EMD), and raw signal for polymer gear fault detection. The chapter concludes with a summary of the findings.

Chapter 4: Supervised machine learning model for early fault detection

In this chapter, a supervised ML model for early fault detection in polymer gears using vibration signals is presented. Different classifiers and combinations of feature sets are analyzed, and the effect of different

decomposition methods on classifier accuracy is studied. The chapter concludes with a summary of the findings.

Chapter 5: Classification of polymer gear pitting faults using double decomposition and Hjorth parameters

This chapter demonstrates the use of the double decomposition method combined with Hjorth parameters and entropy features for polymer gear fault classification. The chapter concludes with a summary of the findings.

Chapter 6: Hybrid deep learning model for polymer gear multiclass fault classification

In this chapter, a hybrid deep-learning model is developed for multiclass fault detection in polymer gears with high accuracy and low computational time. A comparison is made between the deep learning model and the hybrid deep learning model in terms of accuracy and computational time. Various ML classifiers are also compared with the proposed model. The chapter concludes with a summary of the findings.

Chapter 7: Conclusion and Future Scope

This chapter provides an overall conclusion of the thesis and discusses the future scope of the study.

Chapter 2

Effect of teeth modifications on vibration and acoustic characteristics of polymer gears

2.1 Introduction

Several studies have been conducted to explore different aspects of PGs, including materials [82], teeth modification [14,15,83–85], and performance parameters such as the effect of gear-pair [86–89], rotational speed, loading condition [90–93], and reinforcement [94–98]. Recent research by Hriberšek and Kulovec [99] has investigated the impact of voids on the durability of PGs.

In recent decades, researchers have placed great emphasis on investigating wear and thermal damage in polymer gears [3,100]. Many researchers have reported plastic gear failures caused by high temperatures resulting from the low thermal conductivity of polymer materials, which shortens their lifespan [101]. Therefore, some investigations have focused on developing novel design methods to reduce excessive heat accumulation and increase the service life of PGs. For instance, Kim [14] proposed a durability improvement method by drilling an internal hole or inserting a steel pin into the teeth surface. This study indicates that reducing teeth surface temperature and modification enhances the service life. Koffi et al. [102] investigated the influence of five different teeth configurations on temperature and mechanical behaviors, including teeth with no hole, axial cooling hole, tapped axial hole, radial and axial cooling hole, and tapped radial and tapped axial cooling hole. Furthermore, Mertens and Senthilvelan [103] experimentally studied the impact of air cooling on the performance of polymer gears, while Düzcükoğlu [104] modified polyamide gears by drilling cooling holes across the face width of the pitch circle and below the root circle.

The results indicated that the modified gear exhibited 5-20°C lower surface temperature and improved wear resistance compared to the unmodified gear.

In addition to wear and tooth modification analysis, noise generation is a significant concern for machines using PGs. Researchers have investigated the effects of different materials and gear pairs on noise generation in polymer gears. For example, Dearn [105] compared the sound pressure levels (SPL) of polyoxymethylene (POM) against POM, POM against dissimilar material, and POM against steel gear pairs, and found that the SPL for POM against POM was higher. Nozawa et al. [106] investigated the effect of a polymer sheet-adhered gear paired with a steel gear operating under constant rotational speed with varying torque and observed a significant reduction in noise during operation. Hoskins et al. [107] studied the dynamic behavior of polymer gears in terms of noise and found that SPL increases with increased load and speed at all operating conditions. Singh and Siddhartha [108] investigated the noise emissions of functionally graded materials during operation and observed that the noise is directly proportional to speed and not influenced by torque.

After reviewing the existing literature, it can be observed that various studies have focused on improving the performance of PGs by modifying gear teeth, using different gear materials, and pairing gears with dissimilar materials. However, there is a lack of research on the vibration and noise emissions from PGs. Excessive gear vibration and noise can significantly impact machine performance. Thus, it is crucial to study the vibration and noise levels produced by polymer gears. To the best of the author's knowledge, no prior study has investigated the effect of teeth modification on the acoustic noise and vibration characteristics of polymer gears. The present study aims to fill this research gap by examining the impact of two types of tooth modifications, namely, hole-type pinion and insert steel pin-type pinion, on the vibration and noise levels of various gear pairs. The

study will experimentally measure the vibration and noise levels of polymer gear pairs under different operating conditions, such as speed and torque.

2.2 Details of the test gears

2.2.1 Gear material

This study examines two different gear-pairing materials: polymer and steel gear (SG) material. The material used for polymer gear (PG) in this research is MC901 (Nylatron), a modified nylon 6 grade known for its stable properties, mechanical strength, flexibility, and damping characteristics. MC901 is commonly used in bearings, gears, wheels, and custom parts and is identified by its blue color. The material used for SG in this study is S45C, a carbon steel that contains 0.45% carbon. Table 2.1 provides the material properties of MC901 and S45C gears, and Table 2.2 outlines the specifications of the pinion and gear utilized in this study.

Table 2.1 Material properties of the MC901 and S45C.

Material properties	MC901 (Nylatron)	S45C (Carbon steel)
Hardness	120 (R scale)	220 (Brinell)
Poisson's ratio	0.40	0.30
Thermal conductivity (W/mK)	0.23	49.8
Tensile strength (MPa)	96	690

2.2.2 Specimen preparation

This study investigates the effect of tooth modifications on vibration and noise levels of PG by employing two types of modifications: polymer pinion with a hole (PPH) and polymer pinion (PP) with a steel pin inserted in a hole (PPSP). Figure 2.1 shows the location and size of the holes in the pinion teeth, which have a radius of 0.5 mm and are drilled at the junction

of the base circle and the centerline of the pinion teeth. Figure 2.2 presents the PP gear in its unmodified form and with the two modifications, PPH and PPSP, shown in Figure 2.2 (b) and Figure 2.2 (c), respectively. Table 2.3 provides an overview of the various gear pairs tested in this study.

Table 2.2 Specification of pinion and gear.

Gear parameters	Pinion	Gear
Face width (mm)	20	20
Pitch circle diameter (mm)	40	60
Bore diameter (mm)	14	14
Number of teeth	20	30
Pressure angle	20°	20°
Module (mm)	2	2

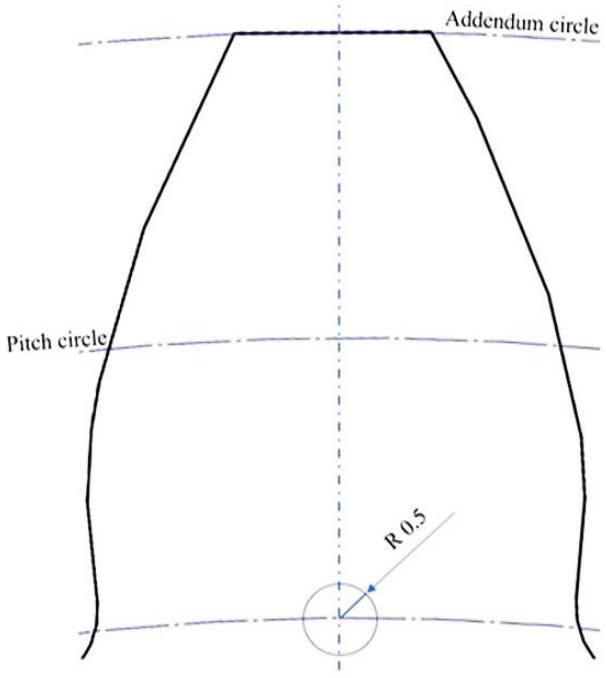

Figure 2.1 Schematic illustration of location and dimension of drilled holes in the pinion.

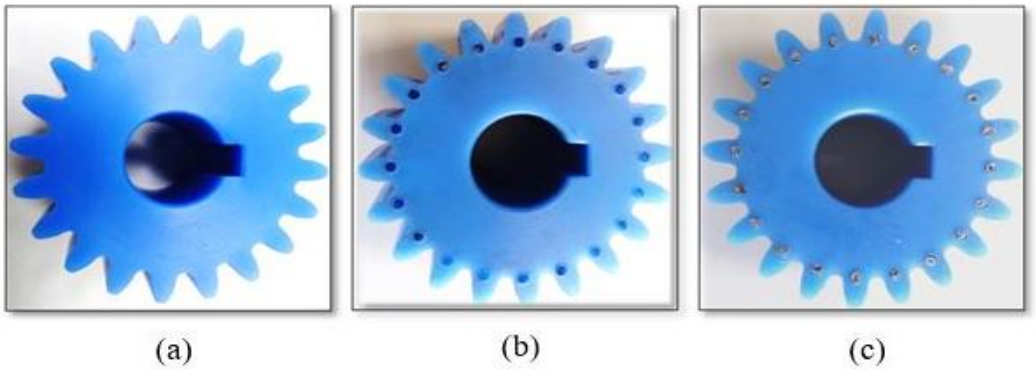

Figure 2.2 (a) Polymer pinion without modification (PP), (b) Polymer pinion with hole (PPH), (c) Polymer pinion with steel pin inserted in the hole (PPSP).

Table 2. 3 Overview of the various test gear pairs.

Gear pair	Description
A	Polymer pinion paired with polymer gear (PP/PG).
B	Polymer pinion with a hole paired with polymer gear (PPH/PG).
C	polymer pinion with a steel pin inserted in the hole paired with polymer gear (PPSP/PG).
D	Polymer pinion paired with steel gear (PP/SG).
E	Polymer pinion with a hole paired with steel gear (PPH/SG).
F	Polymer pinion with steel pin inserted in the hole paired with steel gear (PPSP/SG).

2.3 Gear test rig and testing procedure

2.3.1 Gear test rig

To conduct the experiments, a gear test rig has been developed in the Gear Fault Diagnosis Laboratory at IIT Indore, as shown in Figure 2.3. The test

rig is composed of an AC motor, a variable frequency drive (VFD), a bearing housing plate, a fixed plate, a gearbox, and a magnetic brake. The CAD design of the fixed plate, split bearing housing plate, bearing housing plate, and gearbox is presented in Figure 2.4. The split-bearing housing plate consists of two components: a top plate and a bottom plate. The housing plate is designed in a way that allows for easy removal of the shaft, making it convenient to change gears for testing purposes frequently. The AC motor is capable of running at speeds up to 2900 rpm and is connected to the input shaft of the gear through a coupling. The output shaft is linked to a manually adjustable magnetic brake, which applies the required test torque. A VFD is utilized to regulate the motor speed. The technical information of the various components of the experiment is specified in Table 2.4.

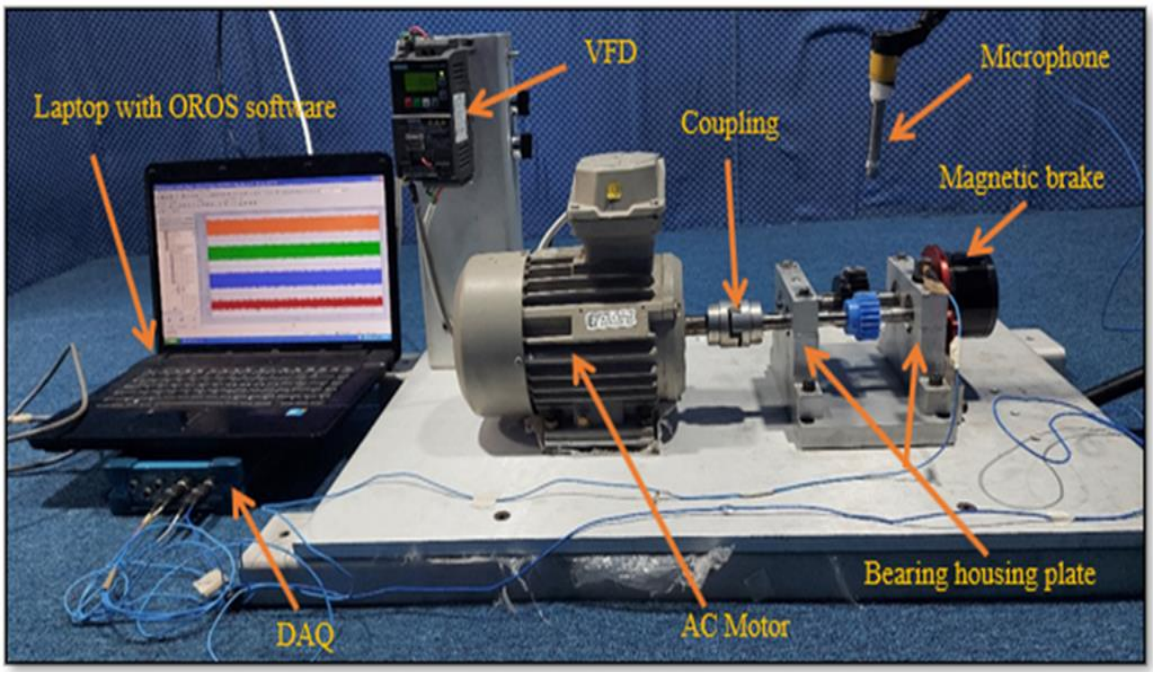

Figure 2.3 Experimental setup with DAQ.

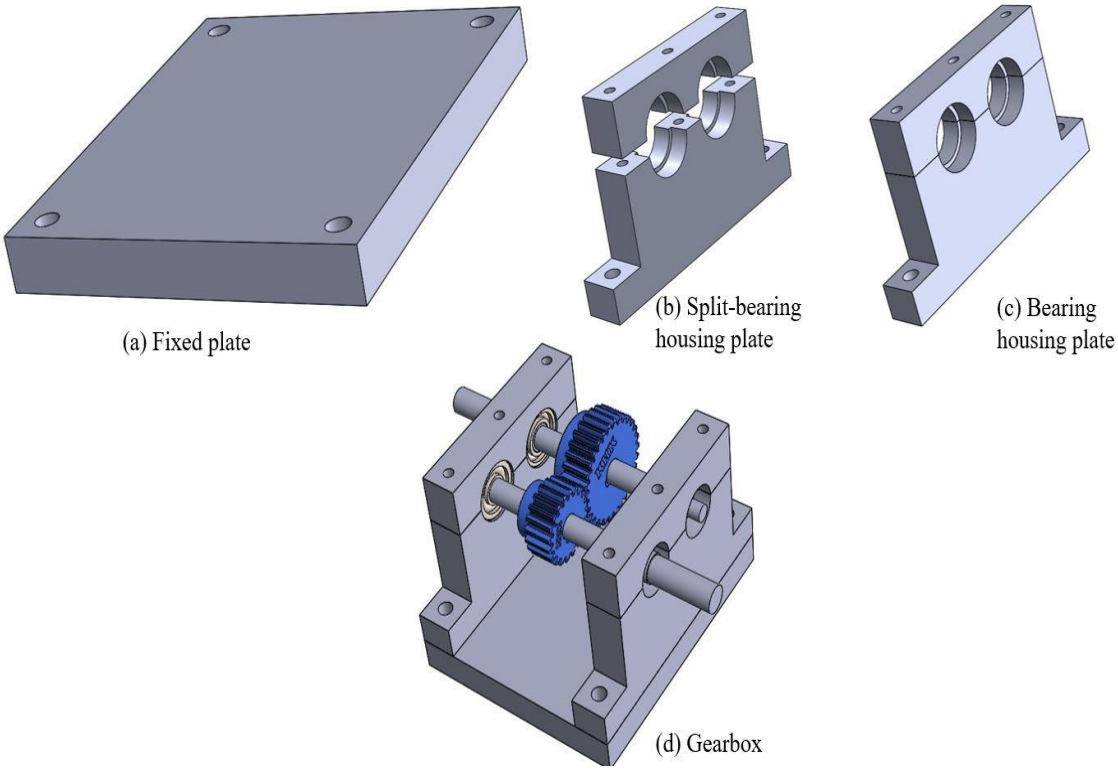

Figure 2.4 CAD designs (a) fixed plate (b) split-bearing housing plate(c) bearing housing plate and (d) gearbox.

2.3.2 Surface roughness measurement

All the tested gears are directly purchased from KHK, which is manufactured by hobbing process. To minimize gear noise, surface roughness should be kept to a minimum. Therefore, the maximum surface roughness (R_{max}) and average surface roughness (R_a) of the test gears are measured. The values of R_{max} and the R_a of the test gears are measured by using Marsurf LD-130 (from Mahr Metrology, Germany). The value of R_{max} and R_a of a polymer spur gear before and after tip relieving is measured by tracing a 2 μm diameter probe for a section length of 2mm on the left and right flank surfaces of its randomly chosen two teeth. A total of four values of Rmax and four values of R_a are measured, and their arithmetic mean is used for further analysis. The R_{max} and R_a values for each gear are listed in Table 2.5.

Table 2.4 Technical specifications of various components of the experimental setup.

S. No	Component name	Technical specification
Electrical equipment		
1	Induction motor	Three phase, 0.75 HP, pre-wired, rpm range 0-2900 rpm
2	VFD	Variable frequency drive with multi-featured front panel programmable controller
3	Tachometer	
4	Data acquisition system	NVGate OR-34, 4 channels, 102.4 KS/s
Mechanical equipment (Bearing housing components)		
1	Shaft	Step shaft with different diameter, 14 mm diameter
2	Bearings	Four deep groove ball bearing (bearing number is 6003-2Z and 6300-2Z) mounted in an aluminum horizontal split housing
3	Fixed plate	210×152×20 mm is the dimension of a fixed plate
4	Split-bearing housing plate	Two parts- Top and bottom parts made with aluminum material
5	Bearing housing plate	Assembled the top and bottom parts of split bearing housing by the bolt. 180×20×100 mm is the dimension.

Table 2.5 The values of surface roughness.

Surface roughness parameters	Polymer Pinion (PP)	Polymer gear (PG)	Steel gear (SG)
R_{max} (µm)	2.615	2.847	2.998
R_a (µm)	0.383	0.473	0.493

2.3.3 Vibration measurement

Vibration measurements are performed to analyze the vibration of the test PGs. The tri-axial accelerometer (PCB-Piezotronics 356A26, S/N: 355339) is mounted on the top of the bearing housing, as shown in Figure 2.5 (a), to capture the vibration signals. The accelerometer is connected to an OROS-OR34 data acquisition system (DAQ) to acquire the vibration signature of the test polymer gears. The DAQ is further connected to a laptop with NV Gate software for analyzing the captured signals. The test gears are run at different rotating shaft speeds (500 rpm, 800 rpm, 1100 rpm, and 1400 rpm) with applied torque levels of 2 Nm, 3 Nm, and 4 Nm. The vibration signature of 10 seconds is captured from various gear pairs (A-F), with a sampling frequency of 12.8 kHz.

2.3.4 Acoustic measurements

For acoustic measurements, a microphone (PCB model number-378A21) is placed 5 cm away from the test gear, as illustrated in Figure 2.5 (b).

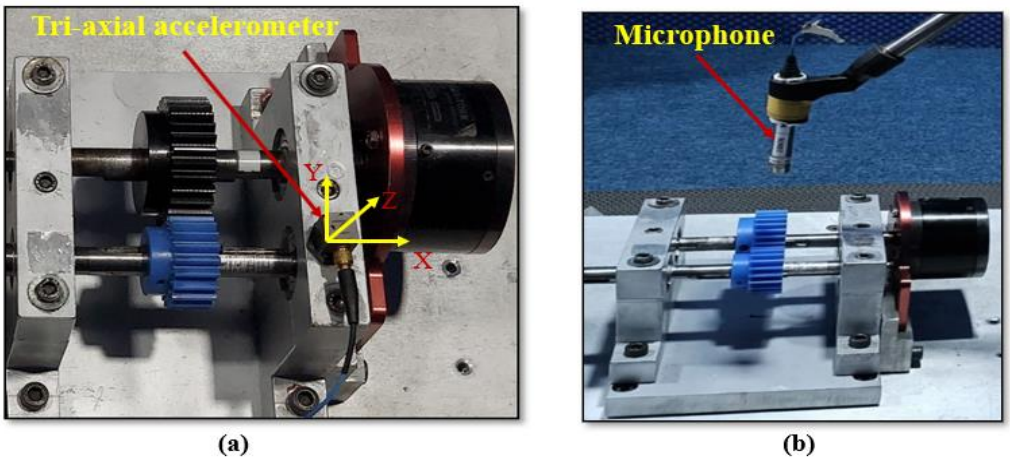

Figure 2.5 (a) Vibration measurement using a tri-axial accelerometer and (b) Acoustic measurement using a microphone.

The microphone is connected to an OROS-OR34 data acquisition system (DAQ) to record the noise signature of the test polymer gears. The DAQ is further connected to a laptop with NV Gate software for analyzing the

captured signals. Acoustic signals are recorded for all six gear pairs at various speeds and torques mentioned in section 2.2.3.

2.4 Results and discussion

This section presents the analysis of experimentally recorded vibration and acoustic data from various gear pairs under different operating conditions.

2.4.1 Vibration signal analysis

In this experimental study, vibration signals were acquired in three different directions: the x-axis, y-axis, and z-axis. The signals along the z-axis were used in the analysis as they contained the highest amplitude vibration signals. Figure 2.6 shows the time-domain vibration signals for A and D type gear pairs at various speeds and a constant 4 Nm torque. It can be observed that the amplitude of time-domain signals of A and D type gear pairs increases with an increase in speed.

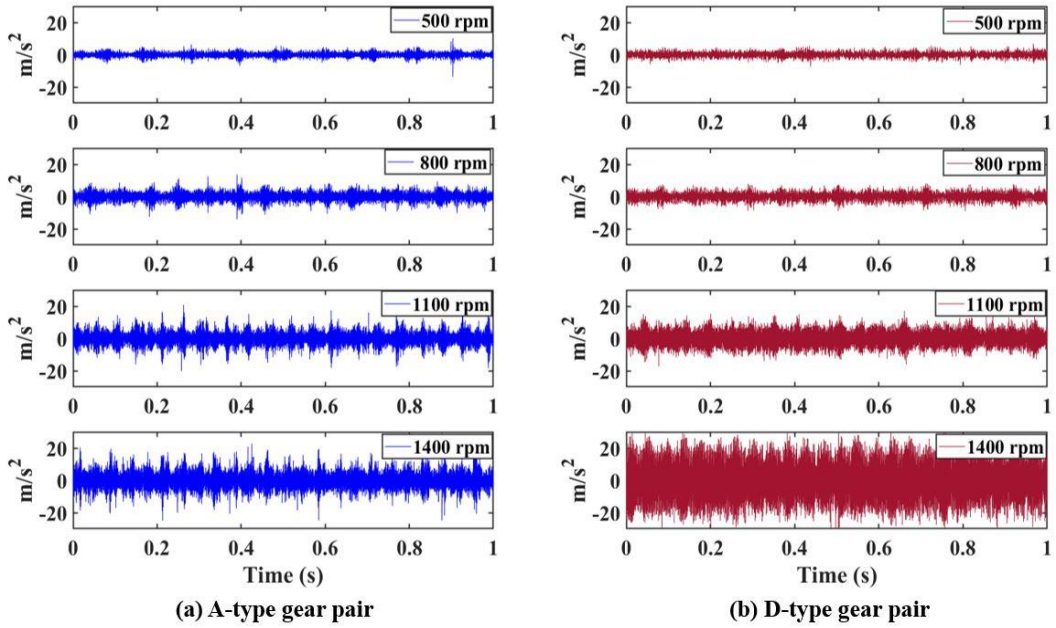

Figure 2.6 Time-domain vibration signal for A and D type gear pairs with various speeds at 4 Nm.

Figure 2.7 shows the time-domain vibration signals of A and D type gear pairs at different applied torque and a constant 1400 rpm speed. Figure 2.7 (a) indicates that the amplitude slightly increases with load. Figure 2.7 (b) reveals that the amplitude is nearly constant for 2 Nm and 3 Nm, but it increases at 4 Nm. This suggests that the loading conditions do not significantly affect the time-domain signal of A type and D type gear pairs.

Figure 2.8 illustrates the time-domain waveform of different gear pairs (A to F) at 1400 rpm speed and at 4 Nm torque. The A gear pair has the lowest amplitude (-20 m/s^2 to 20 m/s^2), while the E gear pair has the highest amplitude (-50 m/s^2 to 50 m/s^2) compared to the other gear pairs. The B-type gear pair has the highest amplitude among the A, B, and C type gear pairs, whereas the A type has the lowest amplitude. Similarly, when comparing the D, E, and F type gear pairs, the E type gear pair has the highest amplitude, while the D type gear pair has the lowest. Relying only on vibration amplitude to study the impact of teeth modification may mislead the analysis because the amplitude is also affected by the speed.

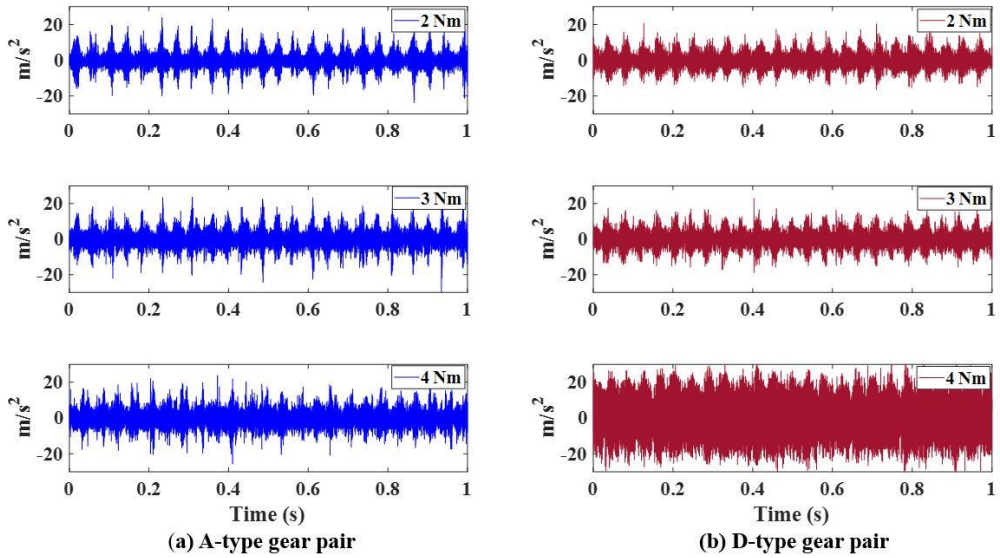

Figure 2.7 Time-domain vibration signal for A and D gear pairs under various torques at 1400 rpm.

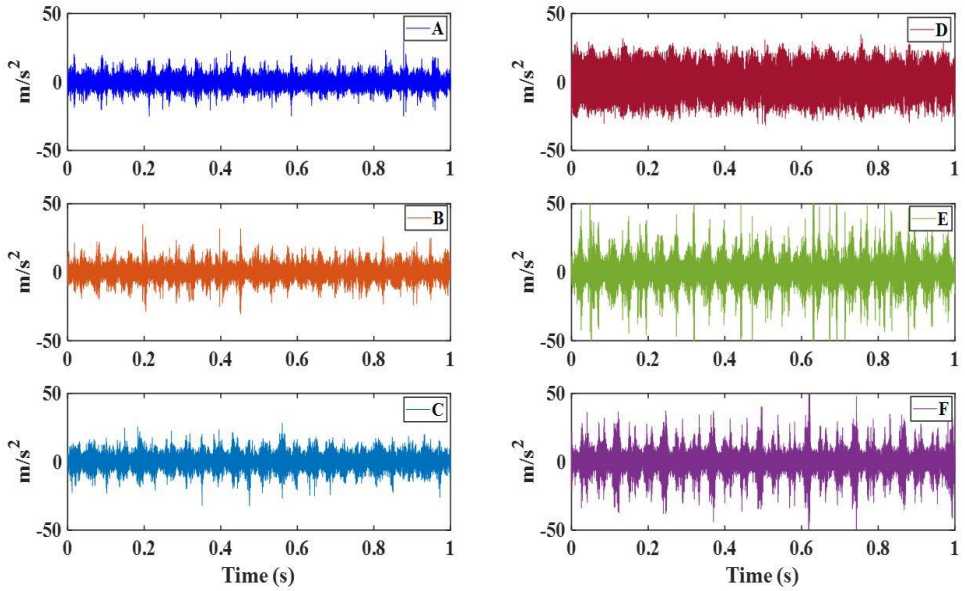

Figure 2.8 Comparison of different types of gear pairs (A to F) at 1400 rpm under 4 Nm.

Typically, the root mean square (RMS) [109] values of vibration signals are utilized to assess the overall vibration level of gearboxes. Therefore, in this study, the RMS value is calculated from the vibration signals obtained at various operating conditions. The RMS value is considered to be the most informative because it is directly related to the energy content of the vibration signal.

$$RMS=\sqrt{\frac{1}{N}\left[\sum_{i=1}^{N}(y_i)^2\right]} \qquad 2.1$$

Where N is the sample number, and y is the vibration signal.

To compare the impact of teeth modification on vibration, the RMS has been computed for all experimental conditions. Table 2.6 presents the RMS values obtained from vibration signals for A, B, and C type gear pairs under different conditions. Across all experimental conditions, the percentage increase in RMS for the B type gear pair relative to A is greater than that of the C type gear pair relative to A. The results in Table 2.6 reveal that the % increase in RMS for the B-type gear pair relative to A ranges between

5.3 to 20, while for the C type gear pair, it ranges between 0.22 to 17.2. The analysis of RMS performance for A, B, and C type gear pairs at different speeds and torques is shown in Figure 2.9. From Figure 2.9 (a–c), it can be observed that for all applied torques, the values of RMS increase as the rotational speed increases. The A-type gear pair has the minimum RMS value at every speed, while the B-type gear pair has the maximum RMS value. The RMS values of A, B, and C type gear pairs exhibit only minor changes at all input speeds under all loading conditions. When comparing the RMS values of A, B, and C type gear pairs, the values are as follows: A < C < B.

Table 2.6 RMS values of A, B, and C-type gear pairs.

Experimental conditions		Gear pair conditions			% Increase with respect to A	
Torque	Speed (rpm)	A	B	C	B	C
2 Nm	500	1.026	1.232	1.097	20.044	6.92
	800	2.094	2.205	2.168	5.299	3.53
	1100	3.229	3.750	3.72	16.159	15.233
	1400	4.233	4.894	4.747	15.61	12.14
3 Nm	500	1.228	1.398	1.28	13.8	4.225
	800	2.382	2.539	2.523	6.618	5.928
	1100	3.654	4.147	3.687	13.494	0.91
	1400	4.664	5.49	5.466	17.727	17.196
4 Nm	500	1.424	1.59	1.43	11.175	0.438
	800	2.484	2.884	2.616	16.094	5.334
	1100	3.754	4.212	3.762	12.218	0.22
	1400	4.934	5.792	5.681	17.388	15.122

Table 2.7 presents the RMS values and their percentage increase for D, E, and F type gear pairs under various experimental conditions. The table reveals that the E type gear pair shows a higher percentage increase in RMS values with respect to the A type gear pair compared to the F type gear pair under all experimental conditions. Specifically, the % increase in RMS values for the E type gear pair with respect to the D type gear pair ranges from 7.63 to 101.6, while for the F type gear pair, it ranges from 0.04 to 47.22. At 500 rpm under all applied torque conditions, the % increase in RMS values for both E and F-type gear pairs is minimal.

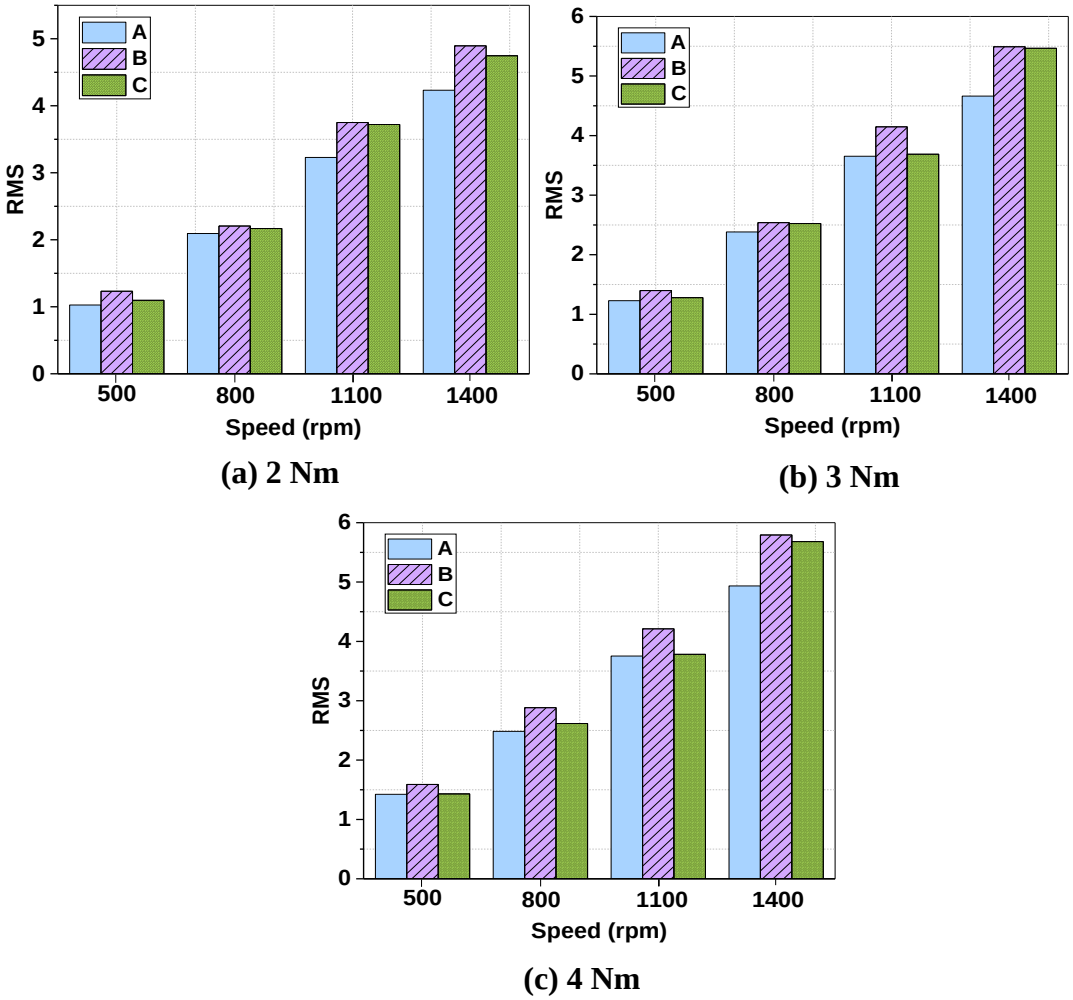

Figure 2.9 Performance of A, B, and C type gear pairs at different speeds and different torques (a) 2 Nm, (b) 3 Nm, and (c) 4 Nm.

Table 2.7 RMS values of D, E, and F type gear pairs.

Experimental conditions		Gear pair conditions			% Increase with respect to A	
Torque	Speed (rpm)	D	E	F	E	F
2 Nm	500	1.1	1.24	1.213	12.915	10.69
	800	1.86	3.75	2.479	101.6	33.17
	1100	3.37	5.54	3.633	64.243	7.73
	1400	4.239	7.66	6.24	80.7	47.2
3 Nm	500	1.18	1.36	1.35	15.316	14.4
	800	1.993	2.91	2.935	46.05	47.225
	1100	3.827	6.57	4.451	71.61	16.322
	1400	4.85	8.49	7.266	75.13	49.8
4 Nm	500	1.484	1.6	1.485	7.63	0.043
	800	2.235	3.474	3.112	55.48	39.27
	1100	4.54	7.41	5.365	63.13	18.18
	1400	8.871	11.94	10.31	34.59	16.157

The performance comparison of D, E, and F type gear pairs at various speeds and torques is shown in Figure 2.10. It can be observed that the RMS values for the E and F type gear pairs are higher than that of the D type gear pair for a given speed and torque condition. The E type gear pair has the highest RMS value at all speeds and torques. There is minimal variation in the RMS value for D, E, and F type gear pairs at 500 rpm for all applied torques. The RMS values increase with increasing speed and torque.

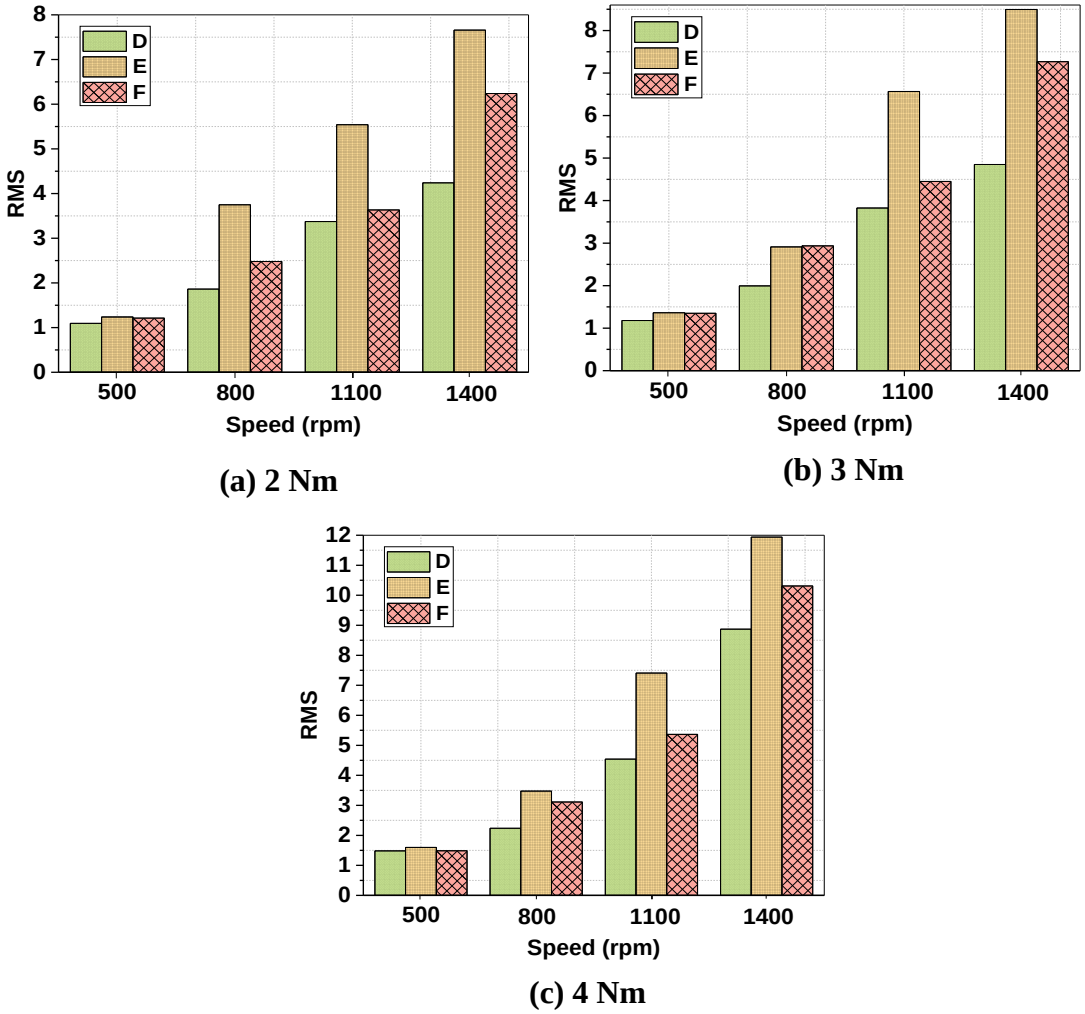

Figure 2.10 Performance of D, E, and F type gear pairs at different speeds and different torques (a) 2 Nm, (b) 3 Nm, and (c) 4 Nm.

2.4.2 Acoustic signal analysis

To investigate the impact of teeth modifications on noise generation, acoustic signals were captured under various speed and torque conditions. Figure 2.11 shows the time-domain acoustic signals for A and D type gear pairs at 4 Nm and different speeds. The X-axis indicates the time in seconds (s), while the Y-axis represents the acoustic pressure in Pascals (Pa). As speed increases, the amplitude of the acoustic pressure also increases. The D type gear pair exhibits slightly higher acoustic signal amplitude compared to the A type gear pair. At 1400 rpm, the maximum amplitude of the A-type gear

pair ranges from -1.37 Pa to 1.37 Pa, while the D type gear pair ranges from -2 Pa to 2 Pa.

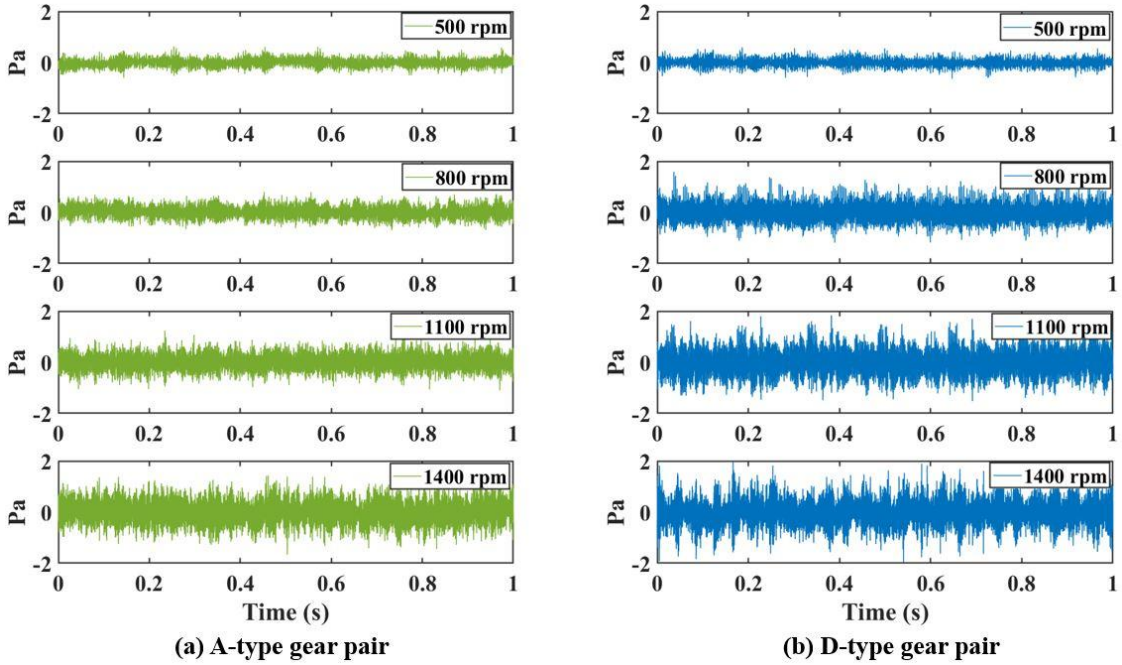

Figure 2.11 Time-domain acoustic signal for A and D type gear pairs at various speeds at 4 Nm.

Figure 2.12 shows the time-domain acoustic signal for gear pairs A to F operating at 1400 rpm and a torque of 4 Nm. At 1400 rpm and 3 Nm, gear pairs of both A, B, and C types and D, E, and F types have little impact on the magnitude of the acoustic signal. However, the D, E, and F-type gear pairs exhibit slightly higher amplitude than the A, B, and C type gear pairs. The sound pressure level (SPL) in dBA was then calculated from the captured acoustic signals for all experimental conditions.

Table 2.8 presents the SPL (dBA) values of A, B, and C type gear pairs, as well as their percentage increase for different speed and torque conditions. The results show that the percentage increase in SPL for the B-type gear pair with respect to A is higher than the C type gear pair with respect to the A type gear pair under all experimental conditions. The

percentage increase in SPL with respect to the A-type gear pair for the B type gear pair ranges from 0.56 dBA to 5.17 dBA, while for the C type gear pair, it ranges from 0.36 dBA to 2.30 dBA.

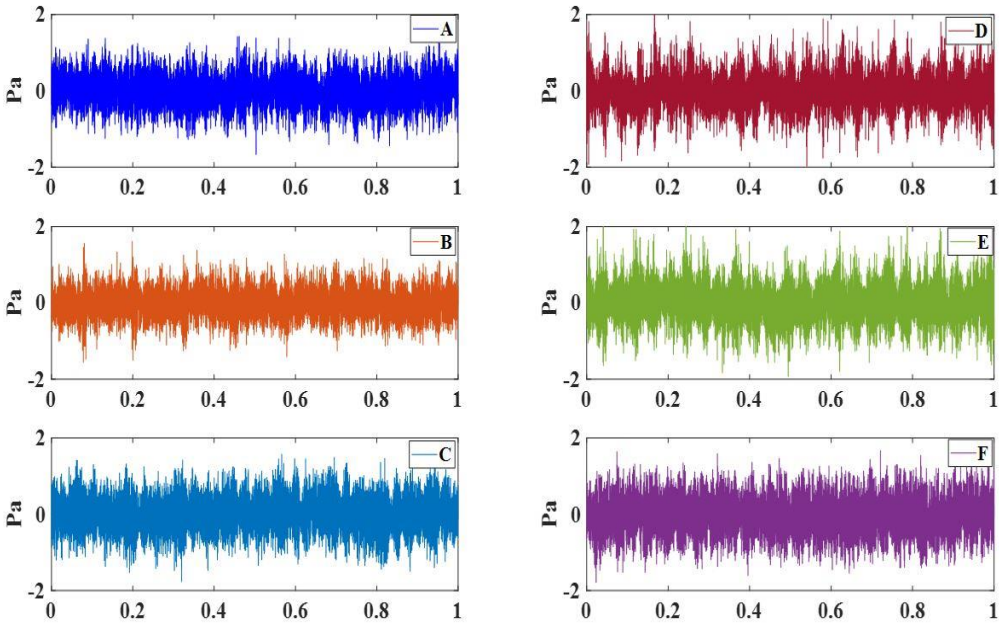

Figure 2.12 Time-domain acoustic signal of various gear pairs (A to F) at 1400 rpm under 3 Nm.

Figure 2.13 depicts the impact of rotational speed and applied load on the sound pressure level (SPL) for the A, B, and C type gear pairs. As the rotational speed and applied torque increased, the SPL of all gear pairs also increased. The result indicates that the A-type gear has lower SPL as compared to B and C type gear paired under all experimental conditions. Moreover, the B-type gear pair generated the highest noise levels among all gear pairs for all rotational speeds and applied torques.

Table 2.9 presents the SPL (dBA) values for D, E, and F type gear pairs and the percentage increase in SPL for E and F type gear pairs with respect to the D type gear pair under various speed and torque conditions. The percentage increase in SPL for the E type gear pair is higher than that of the F type gear pair under all experimental conditions. From Table 2.9, it can be observed that the E type gear pair and the F type gear pair exhibit a

percentage increase in SPL ranging from 0.92 dBA to 4.69 dBA and 0.47 dBA to 3.61 dBA, respectively, with respect to the D type gear pair.

Table 2.8 SPL (dBA) values of A, B, and C type gear pairs.

Experimental conditions		Gear pair conditions			% Increase with respect to A	
Torque	Speed (rpm)	A	B	C	B	C
2 Nm	500	73.2	74.4	74.2	1.6	1.4
	800	79.1	80.1	79.8	1.3	0.9
	1100	80.1	81.1	80.8	1.3	0.94
	1400	82.5	85.9	84.4	4.1	2.3
3 Nm	500	74.3	76.1	75.5	2.4	1.6
	800	80.5	84.6	81.7	5.5	1.5
	1100	81.1	82.6	81.8	1.9	0.9
	1400	84	87.2	85	3.81	1.2
4 Nm	500	75.9	77.6	77.1	2.1	1.5
	800	80.5	82.2	81.5	2.1	1
	1100	83.2	83.7	83.5	0.6	0.4
	1400	86	87.7	86.5	1.9	0.6

In Figure 2.14, the impact of D, E, and F type gear pairs on sound pressure level (SPL) is depicted under various speeds and torques. The graph shows how changes in rotational speed affect the noise emissions of these gear pairs. As the rotational speed increases, the SPL (dBA) of all three gear pairs (D, E, and F) also increases. This correlation suggests that the noise emissions are influenced by the speed at which the gears rotate. The D type gear pair generally exhibits lower noise emissions across various experimental conditions, while the E type gear pair produces higher noise emissions. This study provides insights into the noise characteristics of different gear and can be valuable for designing quieter gear systems or selecting appropriate gear pairs for specific applications.

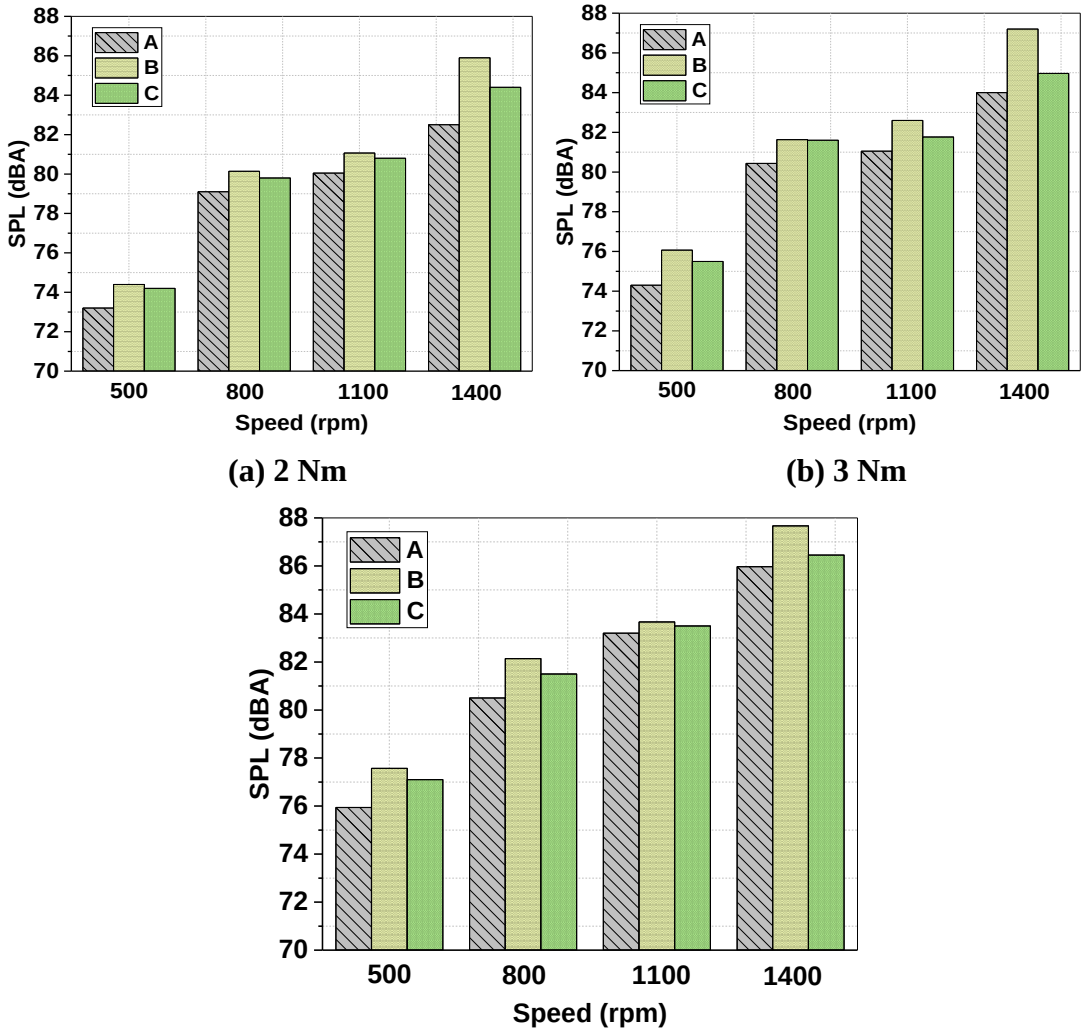

(a) 2 Nm **(b) 3 Nm**

(c) 4 Nm

Figure 2.13 Effect of applied load and rotational speed on SPL for A, B, and C-type gear pairs at (a) 2 Nm, (b) 3 Nm, and (c) 4 Nm.

Table 2.9 SPL (dBA) values of D, E, and F type gear.

Experimental conditions		Gear pair conditions			% Increase with respect to D	
Torque	Speed (rpm)	D	E	F	E	F
2 Nm	500	75.3	76.6	75.65	1.73	0.47
	800	78.95	82.55	81.8	4.56	3.61
	1100	82.05	85.9	84.1	4.69	2.5
	1400	84.85	87.8	87.3	3.48	2.89
3 Nm	500	76.6	77.4	77	1.05	0.52
	800	81.3	83.9	83.55	3.2	2.77
	1100	83.25	86.9	85.35	4.38	2.52
	1400	85	88.4	87.95	4	3.47
4 Nm	500	76.65	78.5	77.3	2.41	0.85
	800	82.8	84.6	84.25	2.17	1.75
	1100	86.25	87.7	87	1.68	0.87
	1400	87.4	88.2	88.05	0.92	0.74

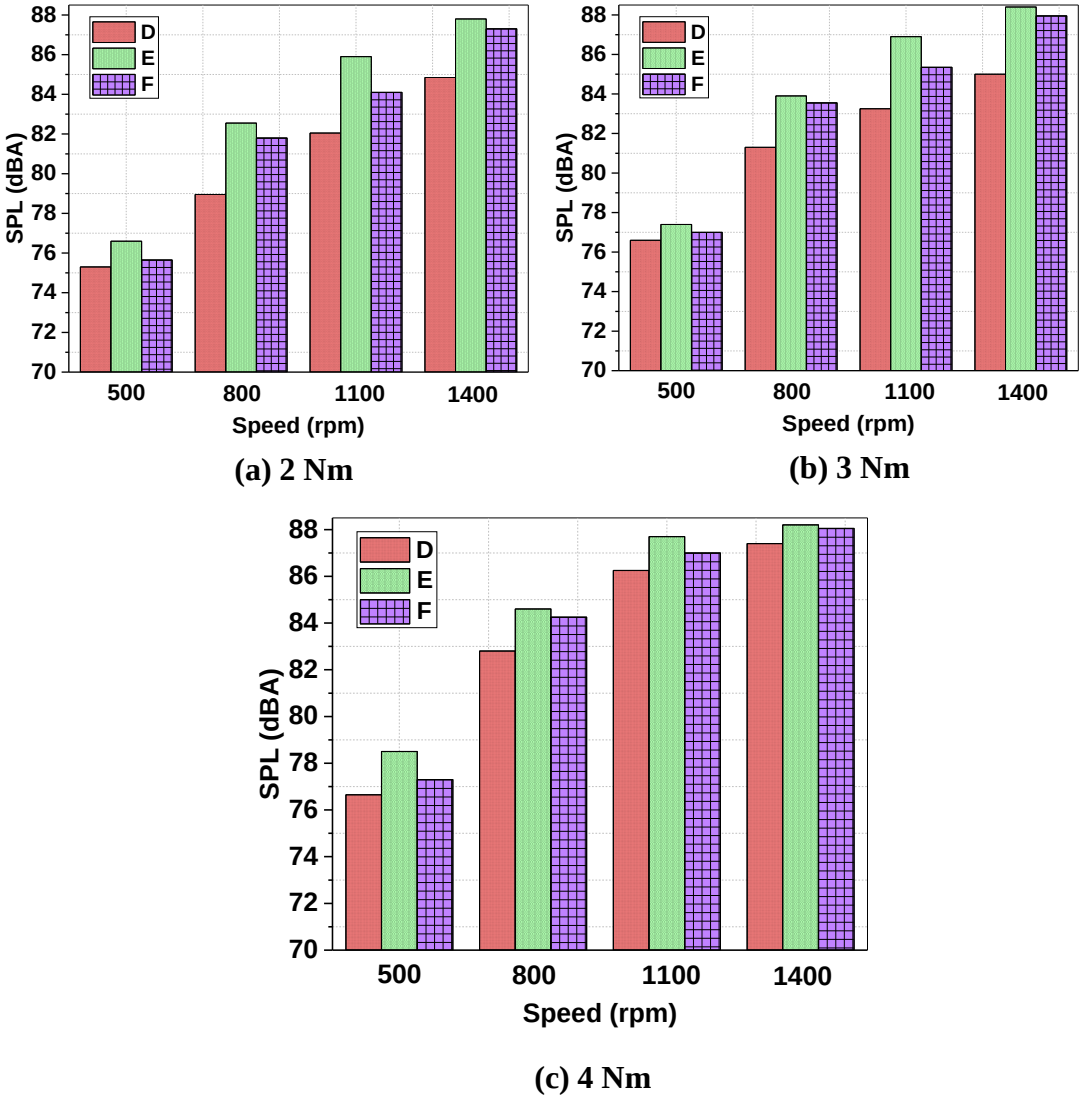

Figure 2.14 Effect of applied load and rotational speed on sound pressure level (SPL) for D, E, and F-type gear pairs (a) 2Nm, (b) 3 Nm, and (c) 4Nm.

2.5 Conclusions

This chapter presents the findings of an experimental study conducted to evaluate the impact of teeth modifications on noise and vibration levels of PGs. The study involved testing various gear combinations (A, B, C, D, E, and F) under different speeds and load conditions. The following conclusions were drawn from the study:

- Firstly, it was found that the vibration and noise levels of all gear pairs (A, B, C, D, E, and F) increased with an increase in rotational speed and torque. This suggests that higher speeds and loads result in greater vibration and noise levels. This phenomenon can be explained by the fact that as speed escalates, the gear teeth engage and disengage more frequently. This rapid interaction occurs because the teeth rotate at a faster pace, increasing the frequency of contact between them. Simultaneously, higher torque exerts a stronger force on the gear teeth. When these factors combine increased speed and torque the frequency of impacts or contacts among the gear teeth rises significantly. These repeated impacts generate vibrations within the system.
- Secondly, when comparing the vibration and noise levels of gear pairs A, B, and C, the results indicated that the B-type gear pair exhibited the maximum noise and vibration level under all operating conditions, while the A-type gear pair had the minimum noise and vibration level. The increased noise and vibration in the B-type gear pair can be attributed to enhanced tooth deflection, a result of the presence of holes in the gear teeth. These holes lead to amplified gear vibration and noise, underlining their significant impact on the overall performance of the gear system.
- Thirdly, when comparing the vibration and noise levels of gear pairs D, E, and F, the E-type gear pair demonstrated the maximum noise and vibration level under all operating conditions, while the D-type gear pair exhibited the minimum noise and vibration level. In the case of E-type gear paired the tooth deflection is increased caused by the presence of the hole, thus amplifying the overall gear vibration and noise.

Chapter 3

Polymer gear early pitting fault detection using kurtosis based VMD

3.1 Introduction

PGs may experience catastrophic failure under harsh working conditions, such as heavy loads, high running speeds, and high temperatures. In various studies, pitting is a common failure in PGs [12,13]. Therefore, detecting these defects at an early stage is important to prevent catastrophic failure.

Detecting faults in PGs using vibration signals is challenging due to the generation of weak signals as compared to metallic gear. Furthermore, local defects can cause non-stationary signals that are difficult to distinguish from heavy noise generated by machine components and the operating environment. Therefore, a suitable signal denoising technique is necessary to cancel out the noise and highlight the fault features present in the signal.

Empirical Mode Decomposition (EMD) is a robust time-frequency analysis technique that enables the decomposition of a non-stationary and non-linear signal into a number of intrinsic mode functions (IMFs) and residuals [110]. IMFs usually gain a better signal-to-noise compared with that raw vibration signals, making the fault frequencies easy to obtain. Parey et al. [111] have conducted experimentation and simulation to authenticate the effectiveness of the EMD process, to detect the gear fault severity. Statistical parameters such as kurtosis and crest factor values of signals were taken for fault diagnosis. Singampalli et al. [112] studied the application of EMD based condition indicators (CIs) for the prediction of fault severity in a spur gear through vibration signals. However, EMD has a disadvantage called the mode mixing phenomenon, thereby leading to a misinterpretation of the signal's physical characteristics. Variational mode decomposition (VMD)

is an improved IMF extraction technique that overcomes the mode mixing and reconstruction errors of EMD. The major characteristics of VMD are ensuring maximum bandwidth for the computed IMF and excellent performance in the presence of nonstationary signals [113]. However, selecting a proper IMF is a challenging task, and the fault signature is weak in sensor-acquired signals. The extraction of CIs plays a crucial role in identifying faults in polymer gears. Previous research [110,114] has shown that kurtosis and crest factor are highly sensitive CIs for fault detection, and thus are used in this study.

The above work encouraged us to apply the VMD technique to analyze a polymer gear fault. The present work focuses on the in-depth investigation, of the fault detection of a polymer spur gear through vibration signals. Once acquiring the vibration signals, employ the VMD algorithm to decompose the signal into a number of variational mode functions (VMFs). Thereafter, VMFs have been selected using the kurtosis method. After that CIs are extracted from the sensitive VMF and analyzed for fault detection. Furthermore, compared the CIs extracted from raw signal and kurtosis based EMD with those obtained from the kurtosis based VMD technique.

3.2 The background of EMD, and VMD

3.2.1 Empirical mode decomposition

EMD is a signal processing method used to analyze nonlinear and non-stationary signals by decomposing them into smaller forms known as intrinsic mode functions (IMFs). It was proposed by Huang et al. [115]. The method involves decomposing the vibration signals into several IMFs through a shifting process. The IMFs have two defining characteristics: (a) the difference between the extreme values at zero crossings must be equal to or less than one, and (b) their mean value, which is obtained by averaging the upper and lower envelopes, is zero. The sifting process for the EMD method is described in the following step-by-step process:

1. Identify all the local maxima and local minima of a signal y(t).

2. Upper envelope $u_e(t)$ is generated by connecting all local maxima, while a lower envelope $l_e(t)$ is generated by connecting all local minima via cubic spline interpolation.

3. The mean envelope m_1 determine by equation 3.1.

$$m_1(t) = \frac{u_{e(t)+l_e(t)}}{2} \quad 3.1$$

4. The first component $h_1(t)$ is determined by equation 3.2.

$$h_1(t) = y(t) - m_1(t) \quad 3.2$$

5. Check to see if $h_1(t)$ satisfies the criteria of an IMF.

6. If $h_1(t)$ is an IMF, it is designated as the first IMF.

$$c_1(t) = h_1(t) \quad 3.3$$

If $h_1(t)$ is not an IMF, take it as the original signal $y(t)$ and repeat the procedures (1)-(4) up to the k times to components $h_k(t)$ until the first IMF $c_1(t)$ that meets the IMF criteria is found.

7. The residue function $r_1(t)$ is determined by equation 3.4.

$$r_1(t) = y(t) - c_1(t) \quad 3.4$$

Consider $r_1(t)$ to be a new signal $y(t)$ and repeat the procedures (1)-(6) to find the other IMFs likes $c_2(t)$, $c_3(t)$, $c_4(t)$, …….$c_j(t)$. As a result,

$$r_2(t) = r_1(t) - c_2(t) \quad 3.5$$

$$r_3(t) = r_2(t) - c_3(t)$$

…….

…….

$$r_j(t) = r_{j-1}(t) - c_j(t)$$

When the monotonic function is achieved for the residue $r_j(t)$, the shifting process will come to an end.

8. The last step, by adding all the IMFs and residue, gets the EMD of the original signal.

$$y(t) = \sum_{i=1}^{j} c_i(t) + r_j(t) \qquad 3.6$$

where $x(t)$ is a signal, which is the sum of IMFs, $c_i(t)$ symbolizes the IMF and $r_j(t)$ represents the residual component. The last IMF (c_n) has the lowest frequency components, whereas the first IMF (c_1) has the highest frequency components.

3.2.2 Variational mode decomposition

The VMD decomposes a real value input signal y(t) into several discrete modes y_k (t) or variational intrinsic mode functions (VMFs) that hold specific sparsity features. Each VMF is compact around the center frequencies ω_k. The process of decomposition steps are as follows [113],

$$\min_{\{y_k\}\{\omega_k\}} \left\{ \sum_k \left\| \partial_t \left[\left(\partial(t) + \frac{j}{\pi t} \right) * y_k(t) \right] e^{-j\omega_k(t)} \right\|_2^2 \right\} \qquad 3.7$$

Where, $Y(t) = \sum_{k=1}^{k} y_k$, $\{y_k\} = \{y_1, \ldots . y_k\}$ is the set of all modes and $\{\omega_k\} = \{\omega_1, \ldots . \omega_k\}$ are center frequencies.

To solve the reconstructing constraint, Lagrangian multipliers (λ) are employed. The extended Lagrangian, on the other hand, is written as [113]:

$$L\left(\left\{y_k\right\},\ \left\{\omega_k\right\},\ \lambda\right)=\alpha\sum_k\left\|\partial t\left[\left(\partial(t)+\frac{j}{\pi t}\right)*y_k(t)\right]e^{-j\omega_k(t)}\right\|_2^2+\left\|y(t)-\sum_k y_k(t)\right\|_2^2$$
$$+\left\langle\lambda(t),\ y(t)-\sum_k y_k(t)\right\rangle$$

3.8

In equation 3.8 α denotes the penalty factor. During the n+1 iteration, the predicted component and associated center frequency may be calculated as follows:

$$\hat{y}_k^{n+1}(\omega)=\frac{\hat{x}(\omega)-\sum_{i\neq k}\hat{y}_i(\omega)+\frac{\lambda(\omega)}{2}}{1+2\alpha\left(\omega-\omega_k\right)^2} \tag{3.9}$$

$$\omega_k^{n+1}=\frac{\int_0^\infty\omega\left|\hat{y}_k(\omega)\right|^2\mathrm{d}\omega}{\int_0^\infty\left|\hat{y}_k(\omega)\right|^2\mathrm{d}\omega} \tag{3.10}$$

$\hat{x}(\omega),\hat{s}_k(\omega),\hat{s}_k(\omega)$ and $\hat{\lambda}(\omega)$ a representation of Fourier transform of $x(t),\ y_k(t),\ y_k^{n+1}(t)$ and $\lambda(t)$ respectively, in Equ. 3.9 and 3.10. The following expression can be used to represent the update λ :

$$\hat{\lambda}^{n+1}(\omega)=\hat{\lambda}^n(\omega)+\tau\left[x(\omega)-\sum_k\hat{y}_k^{n+1}(\omega)\right] \tag{3.11}$$

letter n denotes the number of iterations.

In this study, the parameters, namely, the mode number K are set to 4, noise tolerance τ is set to 0, and the moderate bandwidth restriction α is set to be default value 2000.

3.3 Condition indicators

3.3.1 Kurtosis

Kurtosis is a statistical tool used to analyze the signal, defined as the signal's fourth normalized moment. Its mathematical expression is shown in equation 3.12.

$$Kurtosis = \frac{N\sum_{i=1}^{N}\left(y_i - \overline{y}\right)^4}{\left(\sum_{i=1}^{N}\left(y_i - \overline{y}\right)^2\right)^2} \qquad 3.12$$

Where N is the number of points in the time vibration signal y,

y_i is the i_{th} point in the time domain-based signal y, and $\overline{y}$ is the mean of the signal.

3.3.2 Crest factor

The ratio of a signal's peak value to its RMS value is known as the crest factor (CF), which is mathematically expressed in equation 3.13.

$$CF = \frac{\max\left(y_i\right)}{\sqrt{\frac{\sum_{i=1}^{N}\left(y_i\right)^2}{N}}} \qquad 3.13$$

Where N is the number of points in the time vibration signal y

y_i is the i_{th} point in the time domain-based signal y.

3.4 Experimental study

3.4.1 Test setup

The experimental setup used in this study is depicted in Figure 3.1. To drive the experimental setup, an AC motor with a maximum rotational speed of 2850 rpm was used. The motor was connected to a 19-mm shaft with a

tolerance of 0.05 mm through a flexible coupling to minimize the effects of misalignment and vibration transmission from the motor. On the other end of the shaft, a pulley and belt arrangement were mounted, which was further coupled with a newly designed spur gear assembly. A magnetic brake was used on the output shaft of the gear assembly to apply the torque during testing.

3.4.2 Gear material and measurement conditions

In the previous chapter, section 2.2, the gear material, specification, and properties were discussed in detail. This chapter focuses on the examination of three types of gear faults, namely no fault, slight pitting, and severe pitting using vibration signals. The polymer gear signals are obtained for all three types of faults, at various operating conditions. To conduct the experiments, the gear assembly is driven by an AC motor at three different speeds, 25 Hz, 30 Hz, and 35 Hz, while three torque conditions, 1 Nm, 2 Nm, and 3 Nm, are used at each speed. The tachometer is used to monitor the speed of the gear input shaft. To measure the vibration signals, a tri-axial accelerometer (PCB-Piezotronics 355339) is fixed on the bearing housing using adhesive, as shown in Figure 3.1(b).

The sampling frequency of signal acquisition is 12.8 kHz. To simulate circular pits, a micro-milling machine is used to artificially form the pits on the pinion gear tooth surface while keeping the size within an acceptable range, as illustrated in Figure 3.2. A circular pit has a diameter and depth of approximately 2 mm and 0.2 mm, respectively. The gear in Figure 3.2 (a) represents the no-fault condition. For slight pitting, three pits are seeded on a single tooth surface, as shown in Figure 3.2 (b). To represent the progress of the fault, i.e., severe pitting fault, five pits are seeded on the same tooth surface, as seen in Figure 3.2 (c).

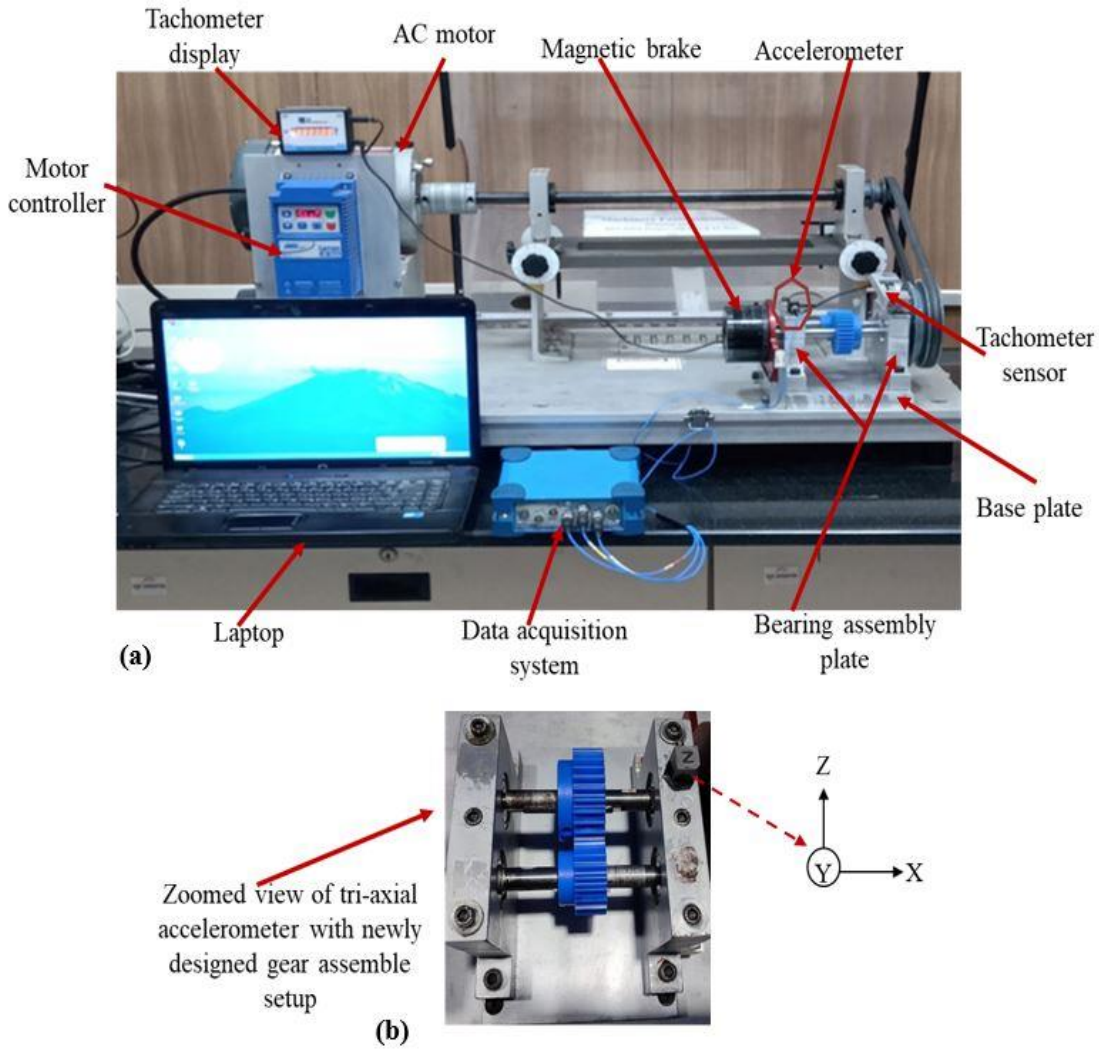

Figure 3.1 Experimental setup with designed gear assembly setup.

3.4.1 The proposed methodology

In this study, a method is proposed to address the challenge of selecting an appropriate VMF from a range of VMFs, which is a difficult task in traditional signal decomposition techniques. The objective is to achieve early fault detection in polymer gears using vibration signals. The method is based on the concept of kurtosis, which serves as an indicator of the non-Gaussian behavior of vibration signals.

Initially, the acquired signal is decomposed using VMD to obtain a set of VMFs. Among these VMFs, the two VMFs with the highest kurtosis

values are selected for further analysis. The VMF with the highest kurtosis is expected to contain the most fault-related information among all the decomposed VMFs. Additionally, considering the presence of noise interference during weak fault diagnosis, the VMF with the second-highest kurtosis value is also included. Therefore, two VMFs are chosen as the most informative for fault detection. By focusing on these selected VMFs, the method reduces the computational cost associated with analyzing all the VMFs. It enables a focused investigation of crucial frequency bands for extracting fault features. Furthermore, these selected VMFs are combined to obtain a more sensitive signal. Subsequently, CIs are computed from the sensitive signal. The analysis of these CIs is conducted to detect faults in polymer gears. The methodology employed in this study is depicted in Figure 3.3.

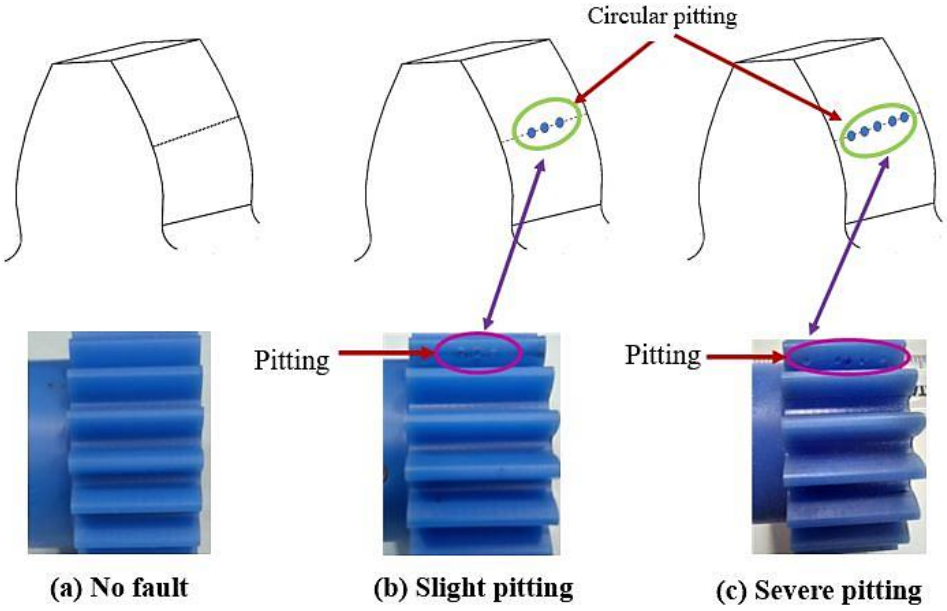

Figure 3.2 Schematic view corresponding to polymer gear with artificially fabricated pitting faults.

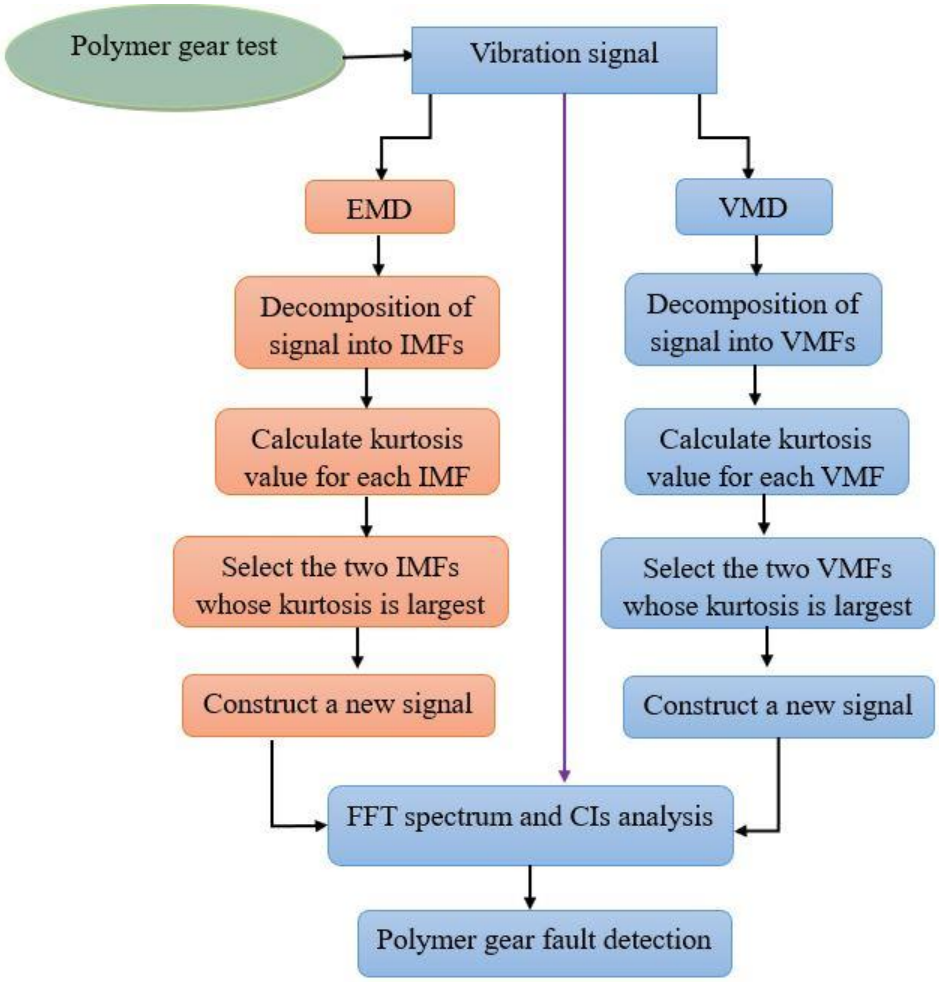

Figure 3.3 Methodology for the pitting fault detection of the polymer spur gear.

3.5 Results and discussion

To detect early pitting faults in polymer gear, vibration signals were acquired under different speed and torque combinations, using a tri-axial accelerometer. Although the amplitude of the captured vibration signals varied in three directions (x-axis, y-axis, and z-axis), the z-axis signal seemed most relevant, as the tangential force acts along this axis at the pinion and gear interface. Therefore, only the z-axis signals were examined and analyzed for further analysis of the polymer gear fault detection.

The vibration signals obtained at 3 Nm torque and 25 Hz speed for various levels of pitting faults in the polymer gear are illustrated in Figure

3.4. As shown, the signal amplitude increased with the severity of pitting. However, relying solely on the vibration amplitude may not be sufficient for accurate diagnosis due to its sensitivity to speed variations.

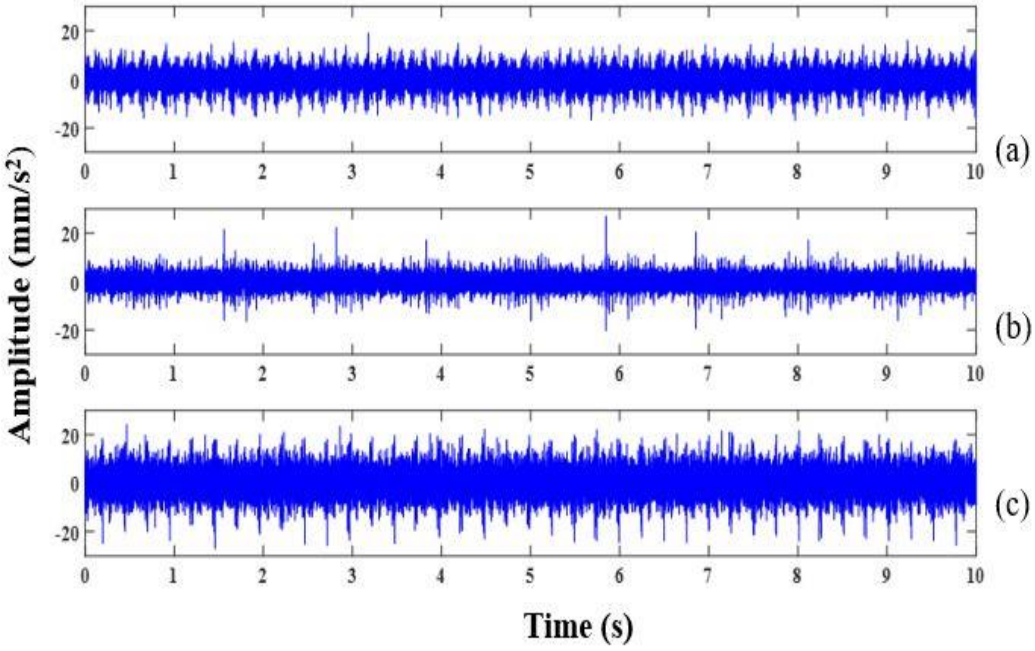

Figure 3.4 Raw time signal of polymer gear, (a) No fault, (b) slight pitting, (c) severe pitting.

Therefore, the use of appropriate CIs is crucial for detecting pitting in polymer gears. In this study, kurtosis and crest factor are two essential CIs that can be utilized to identify faults in polymer gears.

Table 3.1 displays the CIs obtained from a raw signal. However, the values of CIs do not exhibit a consistent trend with the advancement of pitting faults, which may be due to material properties, vibration, and noise from other components. To overcome this unreliable trend, this study proposes the kurtosis based VMD.

Table 3.1 CIs values of raw vibration signals at 30 Hz speed.

CIs		Torque (Nm)		
	Gear conditions	1 (Nm)	2 (Nm)	3 (Nm)
Kurtosis	No fault	7.40	6.10	7.33
	Slight pitting	7.20	6.65	6.05
	Severe pitting	6.86	6.15	9.95
Crest factor	No fault	6.01	6.97	7.61
	Slight pitting	6.16	6.81	7.12
	Severe pitting	9.29	8.49	15.05

3.5.1 IMF extraction

In this study, the acquired signals are decomposed into corresponding VMFs by using VMD to have a better understanding of the fault characteristics. Each acquired signal under different operating conditions and fault conditions is decomposed into 4 VMFs by using VMD, as shown in Figure 3.5. Figures 3.5 (a) and 3.5 (b) display the VMF components for no-fault and severe pitting faults at 3 Nm torque and 30 Hz speed, respectively. Each IMF carries different information about the original signal. In the literature, several methods, such as correlation coefficient, entropy, and standard deviation, are used to select an optimum IMF from the decomposed ones. Kurtosis is a robust index used to determine this impulsive behavior in vibration signals. Therefore, in this study focus on the two VMFs with maximum kurtosis value, is used to determine the maximum kurtosis in VMFs. The analysis was conducted using MATLAB R2020b software.

A list of kurtosis results is presented in Table 4. VMF 3 and VMF 4, hold the maximum kurtosis values, which are 3.5 and 4.9 for healthy and 9.6 and 8.7 for severe pitting, similarly, the kurtosis value is also extracted for slight pitting conditions. After that add these selected VMFs and obtained a sensitive signal for further fault detection because they indicate the

maximum deviation from the Gaussian behavior for a random signal and the presence of the highest impulsiveness. The sensitive signal is analyzed in the time and envelope spectrum as shown in Figure 3.6 at 3 Nm torque and 30Hz speed.

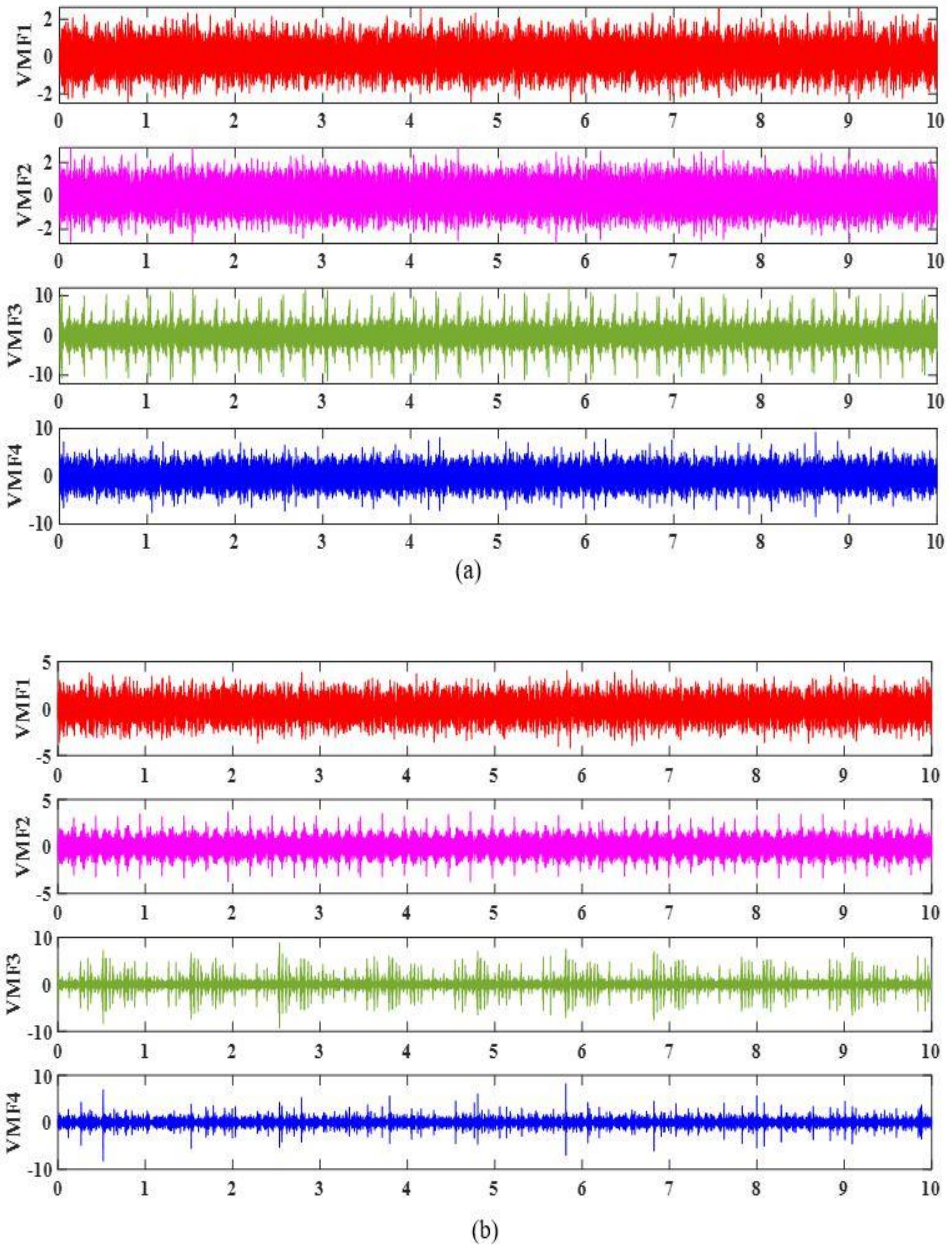

Figure 3.5 The VMD decomposition results in (a) no-fault and (b) severe pitting fault conditions.

Table 3.2 Kurtosis results for VMFs at 30 Hz speed and 3 Nm torque.

	VMF			
	VMF-1	VMF-2	VMF-3	VMF-4
No fault	2	2.4	3.5	4.9
Severe pitting	3.5	3.7	9.6	8.7

Specifically, Figure 3.6 (a-c) presents the time-domain waveform of the sensitive signal under 30 Hz speed and 3 Nm torque for no fault, slight fault, and severe fault conditions. The waveform reveals an increase in spikes with fault severity. Additionally, Figure 3.6 (d-f) demonstrates the envelope spectrum of the sensitive signals for different gear conditions at 3 Nm torque and 30 Hz speed. The envelope spectrum highlights the gear mesh frequency (f_{gm}) and its harmonics ($2f_{gm}$, $3f_{gm}$). The amplitude of f_{gm} is 0.157 m/s^2 for the no-fault gear. However, for polymer gears with slight and severe pitting faults, the amplitude of f_{gm} increases with an increase in fault severity. Specifically, for slight and severe pitting, the f_{gm} amplitude is 0.279 m/s^2 and 0.362 m/s^2, respectively. Apart from that, simultaneously extracting the CIs namely kurtosis and crest factor from the sensitive signals for identifying the polymer gear faults.

3.5.2 CIs extraction from sensitive signals and identification of polymer gear faults

The CIs extracted from the sensitive signals are presented in Table 3.3. The results indicate that the CI values are at a minimum when there are no faults present and increase as the severity of pitting faults increases. This trend holds true for all three torque and speed conditions evaluated. Based on these findings, it can be concluded that the CIs derived from the sensitive signals are effective in detecting early pitting faults in polymer gears.

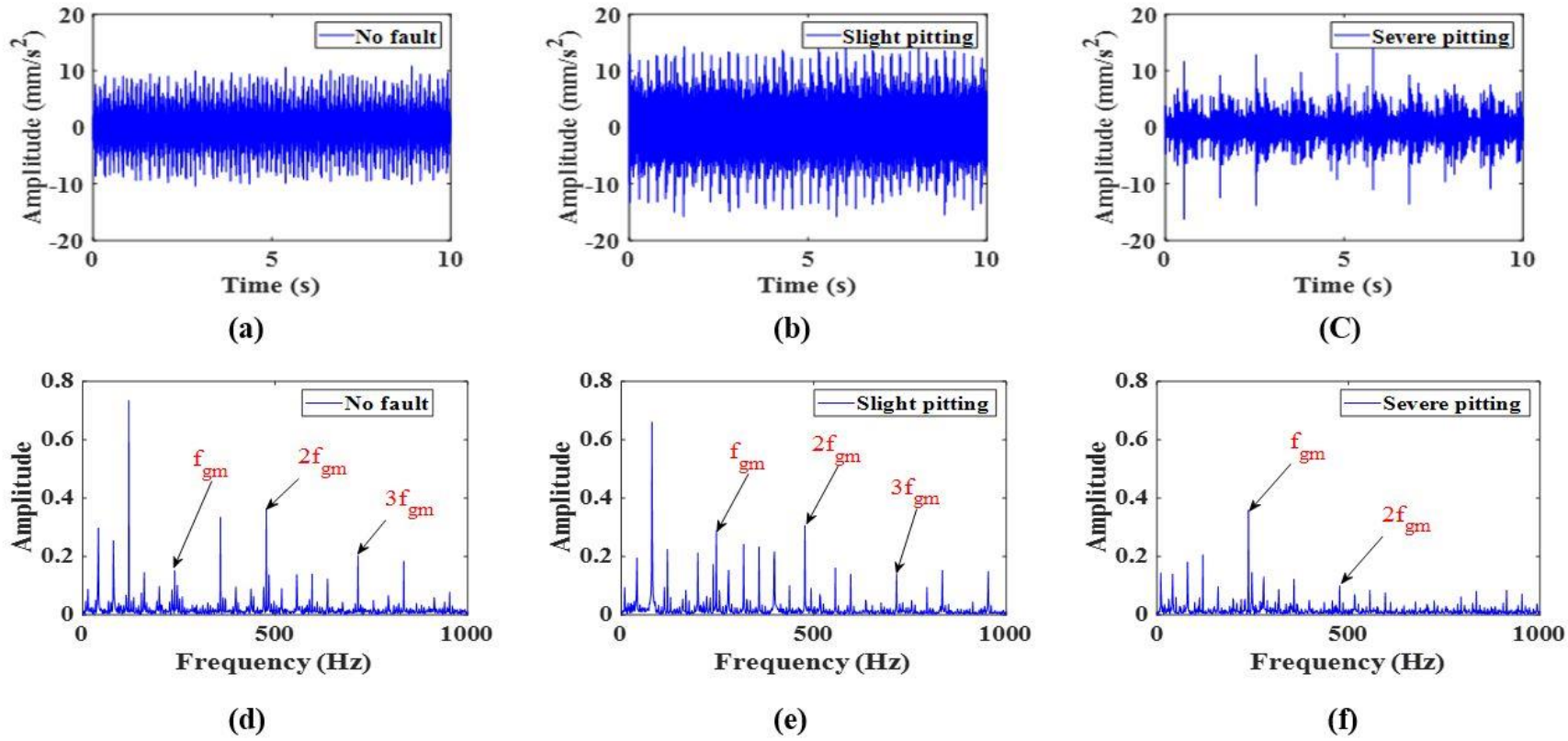

Figure 3.6 Time waveform and envelope spectrum of kurtosis-VMD-based reconstructed signals at 3 Nm speed and 30Hz torque.

Table 3.3 Performance of CIs for kurtosis-VMD-based reconstructed signals at 30 Hz speed.

CIs	Gear conditions	Loads (Nm)		
		1 (Nm)	2 (Nm)	3 (Nm)
Kurtosis	No fault	3.66	3.77	3.82
	Slight pitting	9.25	8.83	6.93
	Severe pitting	14.15	16.38	16.93
Crest factor	No fault	4.08	4.36	4.95
	Slight pitting	7.44	6.44	6.6
	Severe pitting	14.63	17.56	15.1

The study also compares the effectiveness of CIs obtained from the sensitive signal which is obtained from kurtosis based VMD method with those obtained from the raw signal and kurtosis based EMD method under different experimental scenarios.

The comparison of kurtosis and crest factor performance between the raw and decomposed signals which is based on kurtosis based VMD and EMD is shown in the Figures. 3.7 and 3.8, respectively. In these figures, the torque varies row-wise while the speed is constant, and the speed varies column-wise while the torque is constant.

As shown in Fig. 3.7 (a-i), the kurtosis extracted from the raw signals and the sensitive signal generated using kurtosis based EMD method exhibit an irregular trend with varying fault conditions. In contrast, the kurtosis indicator value obtained from the sensitive signal generated using kurtosis based VMD method increases with the severity level of pitting. Specifically, the kurtosis value is lowest for the no-fault condition and highest for the severe pitting condition, consistent with all three torque and speed combinations.

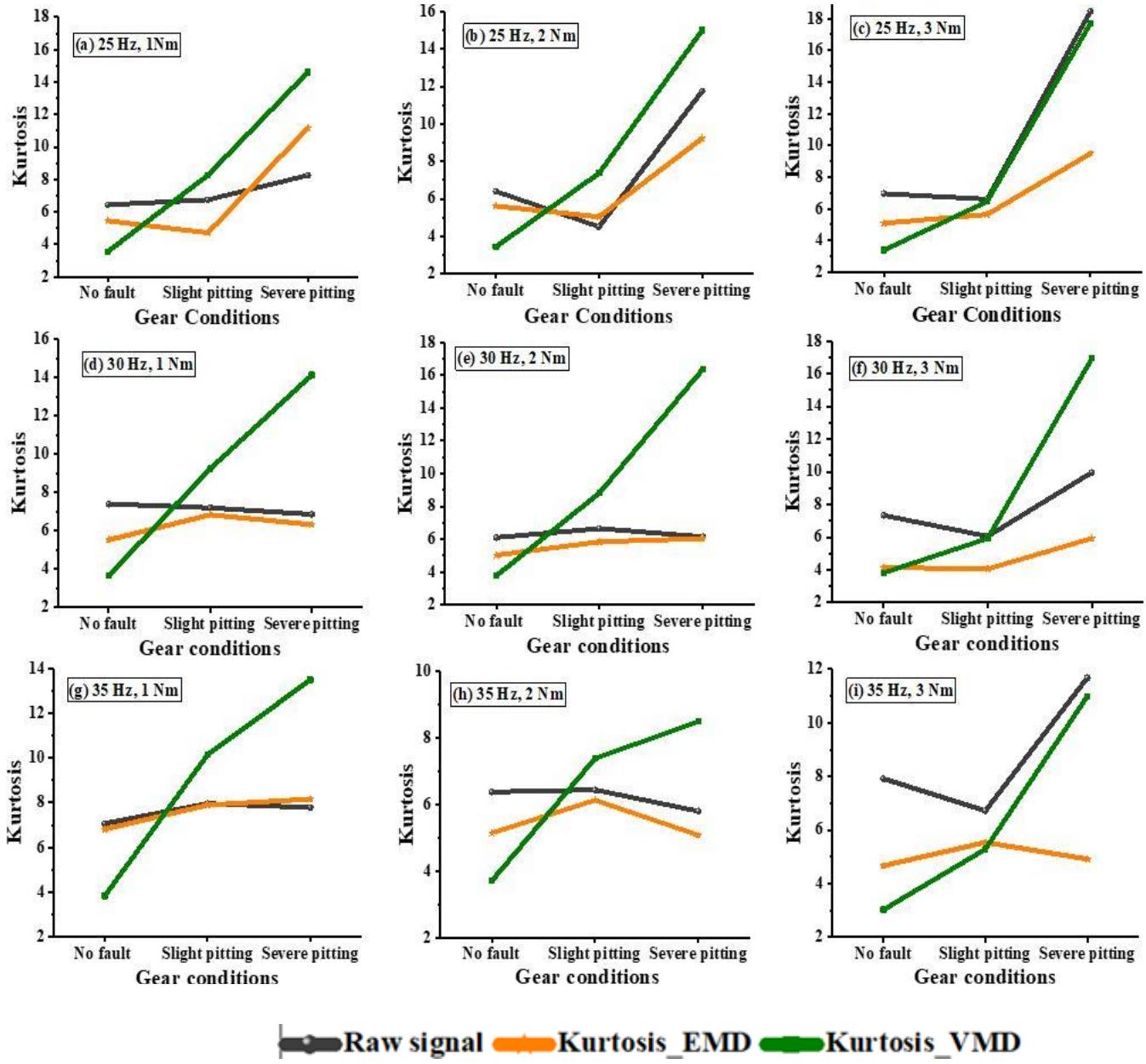

Figure 3.7 Comparison of kurtosis performance between raw and decomposed signals.

Based on Figure 3.8 (a-i), it is evident that the crest factor values obtained from raw signals and sensitive signal which is based on kurtosis based EMD show an irregular pattern with the severity of faults. In contrast, for a sensitive signal, which is obtained by kurtosis based VMD, the crest factor value

is the smallest for no-fault and increases with the severity of the fault. The comparison of CIs extracted from raw signal and kurtosis based EMD fails to detect early pitting faults in polymer gear. However, the CIs extracted from the kurtosis based VMD are effective in detecting early pitting faults at different speeds and loads.

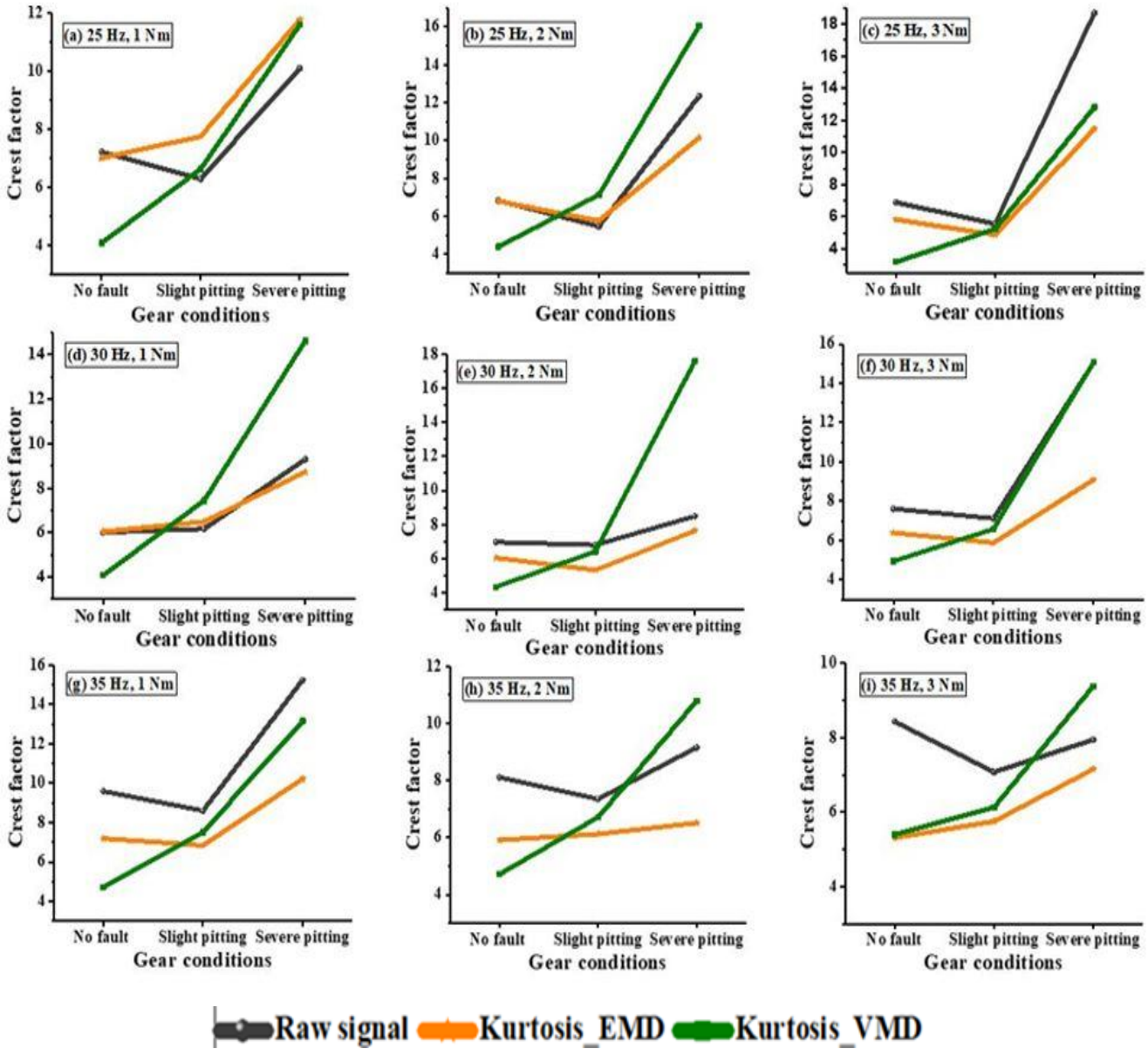

Figure 3.8 Comparison of the crest factor performance between raw and decomposed signals.

The proposed method-based result demonstrates the detection of gear defects under various experimental situations.

3.6 Conclusion

To meet the high-reliability criteria of the polymer gears, this study presents a novel method to detect early pitting faults in polymer gear using kurtosis based VMD. The proposed method consists of two primary steps. In the first step, the raw vibration signals are decomposed using VMD. The kurtosis of each decomposed signal, namely VMF, is retrieved, and the first two VMFs with higher kurtosis values are picked and added to obtain a more sensitive signal. In the second step, the CIs, namely kurtosis and crest factor, is extracted from the sensitive signal, and analysis is performed for early fault detection of polymer gear. In addition, upon a newly constructed signal, the envelope spectrum is investigated to detect the early fault based on the gear mesh frequency noticed. To verify the performance of the proposed method, the CIs are compared which are extracted from kurtosis based EMD, and raw signal. The raw signal-based CIs, such as kurtosis and crest factor, failed to detect the level of faults. Similar behavior is also observed when the CIs are extracted from kurtosis based EMD.

On the other hand, when CIs are computed from kurtosis based VMD, the CIs values increase with fault severity. The experimental results show that the proposed fault detection methods can detect polymer gear's fault more effectively, which will reduce any catastrophic failure. The proposed fault detection approach is further validated in the presence of additive noise at various levels.

Chapter 4

Supervised machine learning model for early fault detection

4.1 Introduction

Traditional fault detection methods rely on specialists to diagnose rotating machine faults correctly and take a long time. Additionally, traditional maintenance procedures are complicated, time-consuming, and expensive.

To address these challenges, In recent years, researchers have studied a large number of fault classification algorithms. Among them, the gear fault classification algorithms mainly include support vector machine (SVM) [116], artificial neural network (ANN) [67], and deep learning [117]. Chen et al. [68] proposed a gearbox fault diagnosis model based on a wavelet support vector machine. The results show that it has a stronger generalization ability and higher diagnostic accuracy than artificial neural networks and support vector machines with random extraction parameters. Lie and Zuo [118] studied the identification of gear crack level using K nearest neighbor classification algorithm.

In recent years, a variety of statistical features (SF) have been used to classify gear faults, including mean, variance, skewness, kurtosis, crest factor, shape factor, sample entropy, fuzzy entropy, Shannon entropy, and approximate entropy.

Hjorth parameters (HP) are a set of features based on statistical calculations that have been used in many studies to effectively describe the characteristics of the EEG signal [119]. In recent years, many studies have used HP to extract information from different bio-signals and have achieved

successful results, including the detection of the heart rate from the electrocardiogram (ECG) signal [120].

Finally, at the classification phase, an appropriate classification model is developed for each class by one of several classification methods. In previous studies, different classification methods have been used to classify the faults, including K-nearest neighbors (KNN), SVM, linear discriminant analysis (LDA), quadratic discriminant analysis (QDA), and decision tree.

Most of the studies are focused on the fault classification of metal gears using vibration signals. The main challenge in fault classification from the vibration signals is the detection of faults with high accuracy in the early stages.

This chapter proposes an innovative approach to detect early pitting faults by utilizing vibration signals from a polymer gear setup. The methodology adopted for fault detection and classification is shown in Figure 4.1. To accomplish this, two decomposition methods viz., EMD and empirical wavelet transform (EWT) are applied on the raw signals to obtain the mode functions (MFs). Based on the energy ratio most sensitive MF, is selected which will be referred to as representative MF in the rest of this study. The most sensitive MF is then used for extracting the common SF and HP. After extracting the features, classifiers like LDA, KNN, and SVM are used to classify the polymer gear faults i.e., healthy, slight pitting, moderate pitting, and severe pitting. Also, classification accuracy is compared with the raw signal (without decomposition) based method.

4.2 Experimental study

This study examines one healthy gear and three gears with simulated pitting faults, including slight, moderate, and severe pitting. The pitting faults are created on the pinion gear tooth surface using a micro-milling machine with a pit depth of 0.2 mm and a diameter of 2 mm. The healthy gear has no

faults, while the slight pitting gear has two pits, the moderate pitting gear has four pits, and the severe pitting gear has five pits on the tooth surface, as depicted in Figure 4.2.

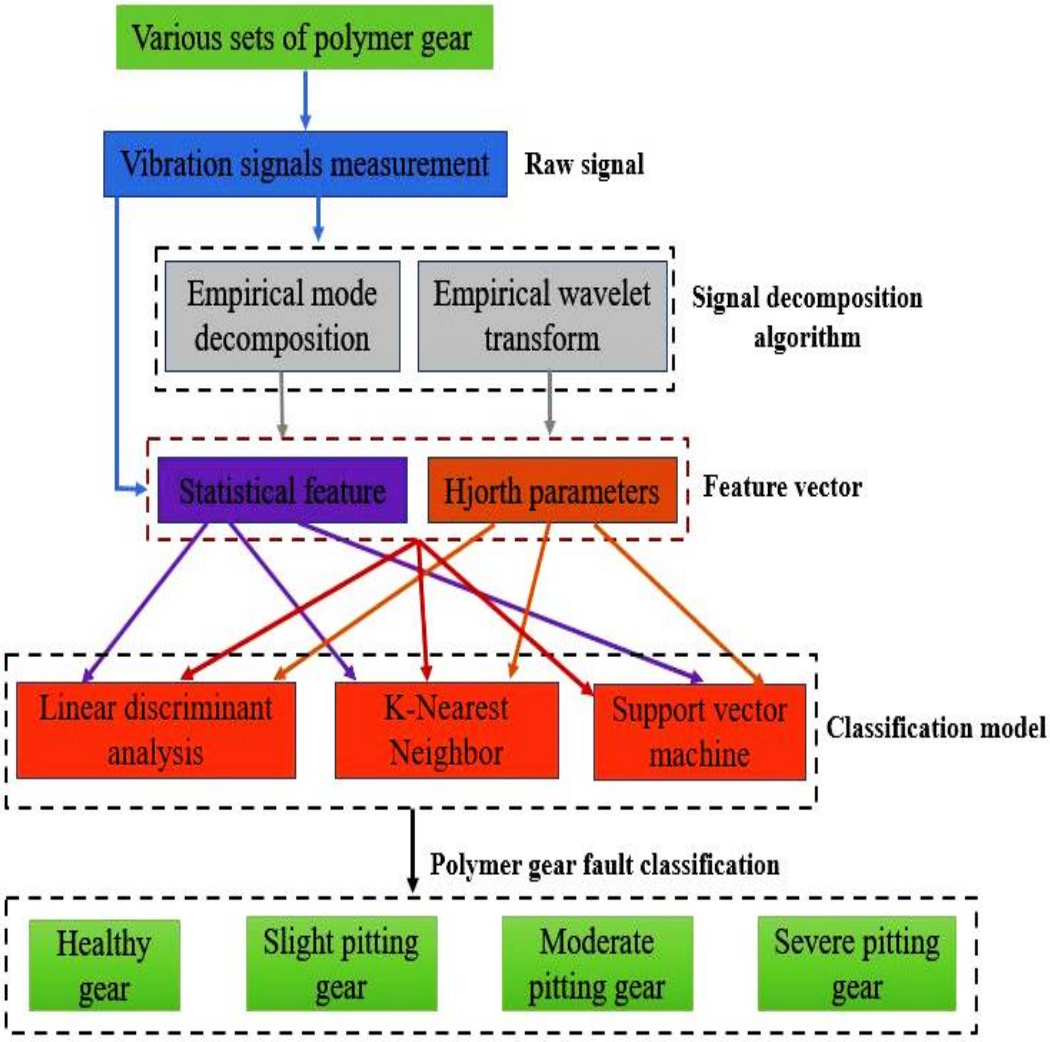

Figure 4.1 Methodology adapted for fault detection in polymer gears.

The vibration signals are captured using a tri-axial accelerometer (PCB-Piezotronics 355339) installed vertically on the top of the bearing housing through a direct adhesive mounting technique, as depicted in Figure 3.1. OROS-OR34 data acquisition system (DAQ) is used to record the vibration signature of the test gears, and the captured signals are visualized using NV Gate software on a laptop. The study captures raw vibration signals at three different speeds (10 Hz, 20 Hz, and 30 Hz) and a combination

of four applied torque (no load, 1 Nm, 2 Nm, and 3 Nm) from a healthy gear and three faulty gear conditions. Each vibration signal is captured for 10 seconds with a sampling frequency of 12.8 kHz. The detailed specification of the test gears is described in Table 2.2. To extract more suitable features, each acquired signal is decomposed into frequency sub bands using two methods: empirical wavelet transforms (EWT) and empirical mode decomposition (EMD).

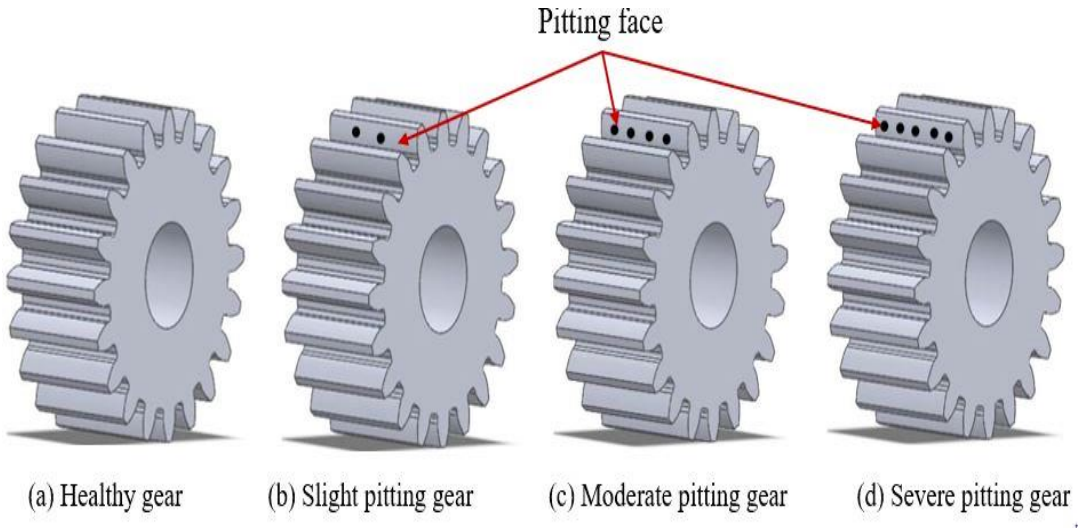

Figure 4.2 Simulated tooth pitting on polymer gears.

4.3 Signal decompositions

4.3.1 Empirical mode decomposition

A comprehensive explanation of EMD has been previously discussed in Section 3.2.1. In this study, the vibration signal was decomposed into 10 mode functions (MFs), and the first 6 MFs are displayed in Figure 4.3. The most sensitive MF was selected based on an energy ratio criterion to extract the optimal features of the signal.

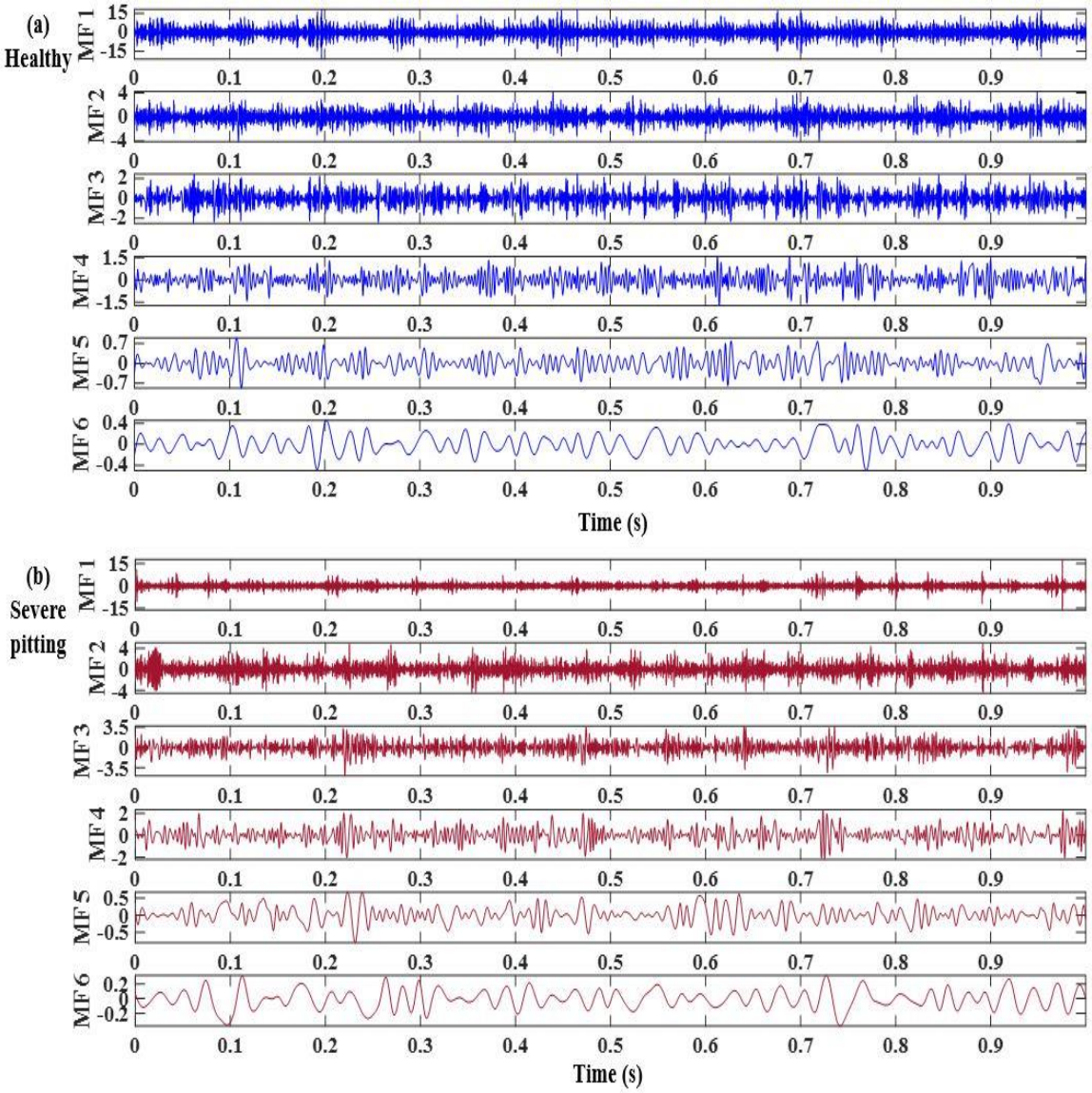

Figure 4.3 EMD-based MFs extracted from polymer gear vibration signal at 30 Hz speed and 3 Nm load condition.

4.3.2 Empirical wavelet transform

EWT is a signal decomposition technique that adapts to the signal being analyzed and it was developed by Gilles [121]. EWT uses segmentations of the Fourier spectrum of the original signal to create a wavelet filter bank that can divide the signal into sub-signals with a compact support Fourier spectrum. The primary steps involved in EWT are as follows:

Bandpass filters are built using empirical wavelets. In each segment, the empirical scaling function $\varphi_n(\omega)$ and wavelet function $\psi_n(\omega)$ are defined as follows:

$$\varphi_n(\omega)=\begin{cases}1,\ |\omega|\le(1-\gamma)\omega_n\\ \cos\left[\frac{\pi}{2}\beta\left(\frac{1}{2\gamma\omega_n}(|\omega|)-(1-\gamma)\omega_n\right)\right]\\ (1-\gamma)\omega_n\le|\omega|\le(1+\gamma)\omega_n\\ 0,\text{ otherwise}\end{cases} \quad 4.1$$

$$\psi_n(\omega)=\begin{cases}1,\ (1+\gamma)\omega_n\le|\omega|\le(1-\gamma)\omega_{n+1}\\ \cos\left[\frac{\pi}{2}\beta\left(\frac{1}{2\gamma\omega_{n+1}}(|\omega|-(1-\gamma)\omega_{n+1})\right)\right],\\ (1-\gamma)\omega_{n+1}\le|\omega|\le(1+\gamma)\omega_{n+1}\\ \text{Sin}\left[\frac{\pi}{2}\beta\left(\frac{1}{2\gamma\omega_n}(|\omega|-(1-\gamma)\omega_n)\right)\right],\\ (1-\gamma)\omega_n\le|\omega|\le(1+\gamma)\omega_n\\ 0,\text{ otherwise}\end{cases} \quad 4.2$$

Where the function $\beta(y)$ is defined as:

$$\beta(y)=\begin{cases}0,\ y\le 0\\ y^4\left(35-84y+70y^2-20y^3\right),\ 0<y<1\\ 1,\ y\ge 1\end{cases} \quad 4.3$$

For obtaining the tight frame $\varphi_n(\omega)$ and $\psi_n(\omega)$, the limiting condition of parameter γ is as follows:

$$\gamma=\min_n\left(\frac{\omega_{n+1}-\omega_n}{\omega_{n+1}+\omega_n}\right) \quad 4.4$$

Find the approximate coefficient $A_f\left(0,\ t\right)$ and details coefficients $D_f\left(n,\ t\right)$. The $A_f\left(0,\ t\right)$ is found by the inner product of the original signal and $\varphi_n(\omega)$ and the $D_f\left(n,\ t\right)$ obtained by inner product of original signal and $\psi_n(\omega)$. The mathematical formula is given as:

$$A_f\left(0,\ \mathrm{t}\right)=\int f\left(\tau\right)\overline{\varphi_1\left(\tau-t\right)}d\tau \qquad 4.5$$

$$D_f\left(n,\ \mathrm{t}\right)=\int f\left(\tau\right)\overline{\varphi_n\left(\tau-t\right)}d\tau \qquad 4.6$$

Calculate the sub-signals (empirical mode functions). The first sub-signal is denoted by $\mathrm{f}_1(\mathrm{t})$ and the nth sub-signal is denoted by $\mathrm{f}_n(\mathrm{t})$:

$$\mathrm{f}_1(\mathrm{t})=\mathrm{A}_f(0,\ \mathrm{t})*\varphi_1(t) \qquad 4.7$$

$$\mathrm{f}_n(\mathrm{t})=\mathrm{D}_f(n,\ \mathrm{t})*\varphi_n(t) \qquad 4.8$$

In this study, vibration signals are decomposed into six MF by EWT as shown in Figure 4.4.

4.4 Mode function selection method based on the energy ratio

To identify the MF that is most sensitive to fault information, an energy ratio-based approach is utilized to select the most informative MF. The MFs with a high energy ratio are preferred as they represent the dominant signal components. The energy ratio is calculated using Equation (4.9).

$$Energy\ ratio=\frac{\sum_{\mathrm{i}=1}^{\mathrm{N}}\mathrm{x}_\mathrm{i}^2}{\sum_{\mathrm{i}=1}^{\mathrm{N}}\mathrm{y}_\mathrm{i}^2} \qquad 4.9$$

where $\mathrm{y_i}$ represents the vibration signal, $\mathrm{x_i}$ represents a decomposed signal, and N is a number of modes.

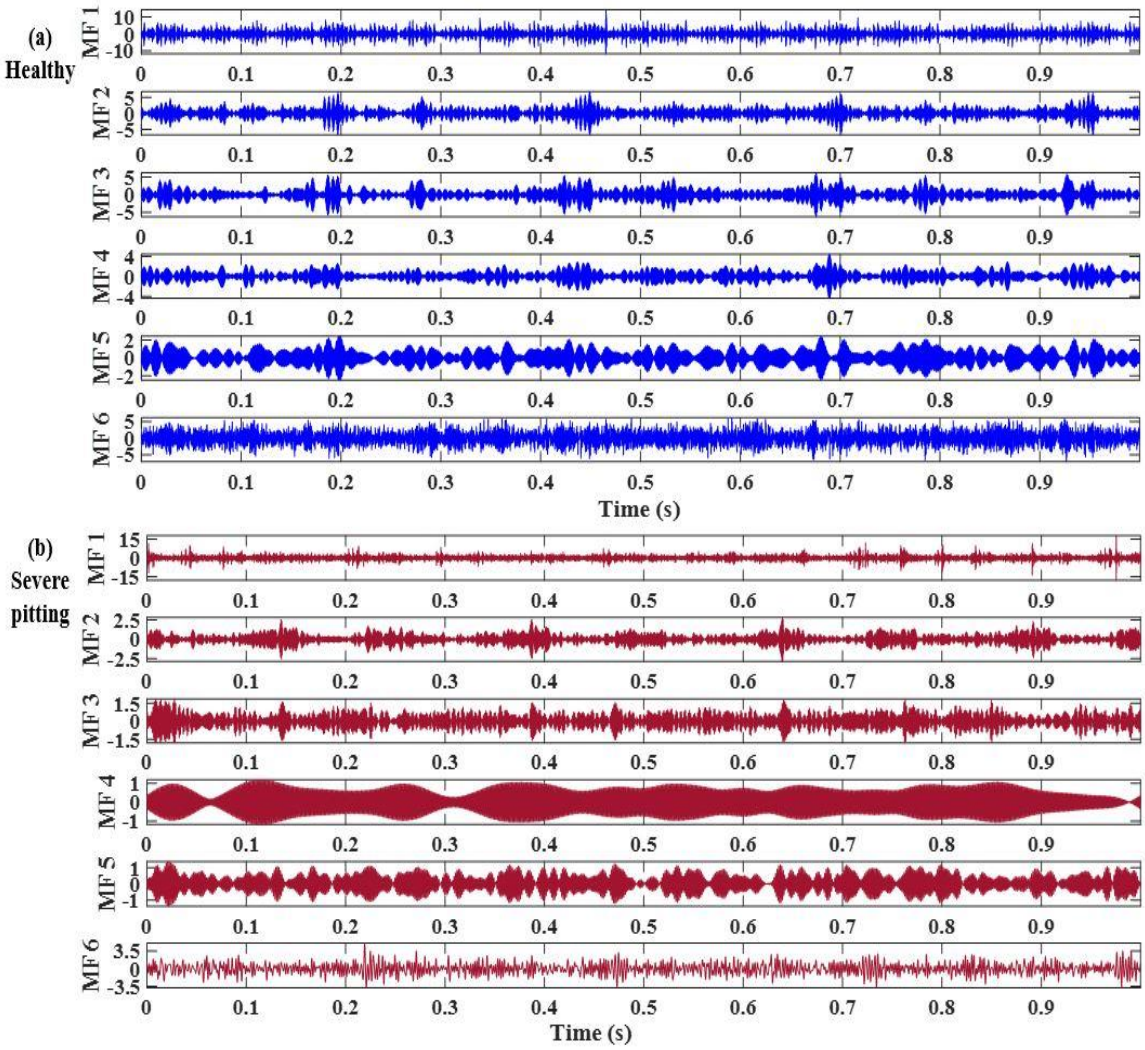

Figure 4.4 EWT-based MFs extracted from polymer gear vibration signal at 30 Hz speed and 3 Nm load condition.

Tables 4.1 and 4.2 present the energy ratio for each MF obtained through the EMD and EWT methods, respectively.

Table 4.1 Energy ratio of each MF decomposed by EMD at 30 Hz speed and 3 Nm torque condition.

Gear conditions	MF1	MF2	MF3	MF4	MF5	MF6
Healthy	0.923	0.059	0.036	0.015	0.005	0.002
Severe pitting	0.538	0.234	0.179	0.069	0.009	0.003

Table 4.2 Energy ratio of each MF decomposed by EWT at 30 Hz speed and 3 Nm torque condition.

Gear conditions	MF1	MF2	MF3	MF4	MF5	MF6
Healthy	0.348	0.129	0.132	0.057	0.04	0.225
Severe pitting	0.572	0.057	0.055	0.056	0.042	0.209

Based on the results from Tables 4.1 and Table 4.2, MF1 is identified as the most sensitive MF. The next step is to extract features from the selected MF for further analysis.

4.5 Feature extraction

This section focuses on detecting polymer gear faults using five relevant features, namely RMS, crest factor, shape factor, kurtosis, and Hjorth parameters [122]. While kurtosis and crest factor are well-defined in section 3.3, this section will discuss the shape factor and Hjorth parameters.

4.5.1 Shape factor

Shape factor: It is described by the ratio of RMS to the absolute mean of signal y_i and mathematically represented [123]:

$$SF=\frac{\sqrt{\frac{1}{N}\sum_{i=1}^{N}\left(y_i\right)^2}}{\frac{1}{N}\sum_{i=1}^{N}|y_i|} \tag{4.10}$$

4.5.2 Hjorth parameters

The HP, which were introduced by Hjorth [122], are commonly used for analyzing biological signals and measuring signal complexity in the time domain. The HP consist of three components: Activity, Mobility, and Complexity.

- $\text{Activity}=\text{Var}\left(y(t)\right)$

  4.11

- $\text{Mobility}=\sqrt{\frac{\text{Var}\left(\frac{dy(t)}{dt}\right)}{\text{Var}\left(y(t)\right)}}$ 4.12

- $\text{Complexity}=\frac{\text{Mobility}\left(\frac{dy(t)}{dt}\right)}{\text{Mobility}\left(y(t)\right)}$ 4.13

Where y(t) is the signal.

Activity quantifies the overall power or amplitude of the signal. It is calculated by computing the variance of the signal. Mobility reflects the changes in signal amplitude or frequency over time. It is calculated by dividing the standard deviation of the first derivative of the signal by the standard deviation of the signal. Complexity represents the changes in signal complexity or irregularity over time. It is calculated by dividing the mobility of the first derivative of the signal by the mobility of the signal.

4.6 Classification

The extracted features from the signal are utilized as input for the classification process, where three distinct classification methods are employed in this section: SVM, KNN, and LDA.

4.6.1 Support vector machine

SVM is a powerful machine learning algorithm that is commonly used for classification and regression tasks. The main goal of SVM is to find a hyperplane in the n-dimensional space, where n is the number of features, that separates the different classes of data points in the best way possible. In the context of classification, SVM is designed to find the hyperplane that

maximizes the margin between the closest points from each class, known as support vectors. This means that SVM tries to find the decision boundary that has the largest distance from the nearest data points from each class. By doing so, SVM can produce a clear and robust classification model that is less likely to overfit or underfit the data. SVM can be used for both binary and multi-class classification problems. For multi-class classification, SVM uses a one-against-one (OAO) or one-against -all (OAA) approach to train multiple binary classifiers and combine their outputs to make the final classification decision. In this study, the one-against-one (OAO) approach is utilized to create a multi-class classifier.

4.6.2 K-nearest neighbors

KNN is a supervised machine learning algorithm used for classification and regression problems. In the case of classification, given a new data point, the KNN algorithm searches for the K closest points in the training dataset and assigns a class to the new data point based on the majority class among its K neighbors. The value of K can be any positive integer and is typically chosen based on the characteristics of the dataset. The distance metric used to measure the distance between data points can vary, but Euclidean distance is the most commonly used. Once the K nearest neighbors are identified, the algorithm assigns the class label based on the majority class among the neighbors. The KNN algorithm is simple and easy to implement, and it can work well with a small dataset. However, it can be computationally expensive when dealing with large datasets, and it requires careful selection of the value of K to avoid underfitting or overfitting. In this study, K is set to 1.

4.6.3 Linear discriminant analysis

LDA is a versatile technique that performs both as a dimensionality reduction method and a robust supervised machine learning classifier [124]. It can also serve as a data visualization technique in some cases. As a dimensionality reduction method, LDA reduces the number of dimensions from

the original to j-1 features, where j represents the number of classes. The reduced features are then used to train a classifier to classify the data. As a classifier, LDA performs well on linearly separable data with high accuracy and less computation time. However, if the data is not linearly separable, LDA attempts to project it into another space with the maximum possible linear separability. In this study, LDA is chosen as the supervised machine learning classifier.

4.7 Results and discussion

In this study, the dataset consisted of 144 samples, which included healthy and three stages of pitting faults in polymer gear vibrations. To denoise the signals, two methods are compared, namely EMD and EWT, which decomposed the signals into sub-bands. The effectiveness of the decomposition methods was compared with no decomposition. The extracted features, including RMS, kurtosis, crest factor, shape factor, and Hjorth parameters, were then computed from selected MF after decomposition. The data were then classified into four classes namely, healthy, slight pitting, moderate pitting, and severe pitting using three classifiers: SVM, KNN, and LDA. The accuracy of these classifiers was evaluated using a 10-fold cross-validation method for data preparation. 10-fold cross-validation is a commonly used method in machine learning to evaluate the performance of a model. In this approach, the available data is divided into 10 equal subsets or folds. In each iteration, one of the subsets is used as the testing data, while the remaining 9 subsets are used as training data. This process is repeated 10 times, with each of the 10 subsets used once for testing. The results obtained from all 10 iterations are then averaged to give a final performance measure.

In this study, the performance of selected classifiers was evaluated to assess the potential of using HP as a novel feature for detecting faults in polymer gears. Three sets of features were considered for evaluation: the first set consisted of traditional features such as RMS, kurtosis, crest factor,

and shape factor; the second set included HP, while the third set was a combination of the first and second sets.

The classification results are evaluated using widely used standard metrics, accuracy. The accuracy is utilized to assess the performance of the classification model. Tables 4.3, Tables 4.4, and Tables 4.5 show the evaluation results for the first, second, and third feature sets, respectively, using three different classifiers and three decomposition strategies.

Table 4.3 indicates that the wavelet-based decomposition technique was found to perform better than other methods in differentiating between the four classes of polymer gear, while the non-decomposition mode resulted in the lowest accuracy. Furthermore, the KNN classifier performed better than LDA and SVM classifiers in the case of non-decomposition, EMD, and EWT-based decomposition modes.

Table 4.3 The results of different classifiers for fault detection using first feature sets.

	Accuracy (%)		
	KNN	SVM	LDA
No decomposition	88.2	84	59
EMD	92.4	91.7	65.2
EWT	97.2	97.2	69.4

Table 4.4 illustrates that the KNN classifier outperforms the other classifiers in differentiating the four classes of polymer gear using a second feature set i.e., HP in all signal decomposition and non-decomposition modes. The accuracy of various signal decomposition models and non-decomposition is compared, and the results reveal that the EWT-based decomposition mode achieves the highest accuracy in detecting faults in polymer gears. Table 4.5 reveals that the KNN classifier achieves higher accuracy than other classifiers in all signal decomposition and non-decomposition

modes when using the third feature set. In terms of signal decomposition, the EWT-based method is found to have the highest accuracy in detecting faults in polymer gears, compared to EMD and non-decomposition methods.

Table 4.4 The results of different classifiers for fault detection using second feature sets.

	Accuracy (%)		
	KNN	SVM	LDA
Raw signal	87.3	86.1	61.1
EMD	93.6	91.7	64.2
EWT	97.4	96.2	70.3

The comparison of results in Tables 4.3, 4.4, and 4.5 indicates that all classifiers perform better when HP is included as a feature, regardless of the decomposition mode. Among the three feature sets, the third one (combining traditional features and HP) results in the highest accuracy. The EWT-based decomposition mode with a KNN classifier achieves the best performance, with an accuracy of 99.3%.

Table 4.5 The third feature set of various classifiers with different signal decomposition methods.

	Accuracy (%)		
	KNN	SVM	LDA
Raw signal	93.4	93.1	67.4
EMD	97.2	94.4	69.4
EWT	99.3	98.6	75.7

The accuracy results for the KNN classifier and various decomposition techniques applied to the first, second, and third feature sets are depicted in

Figure 4.5. The x-axis represents different signal decomposition methods, while the y-axis represents the classification accuracy. The result indicate that the utilization of the EWT decomposition method with the third feature set and the KNN classifier demonstrates greater effectiveness in early detection of polymer gear faults. However, total classification accuracy does not provide a realistic view of the accuracy of each class.

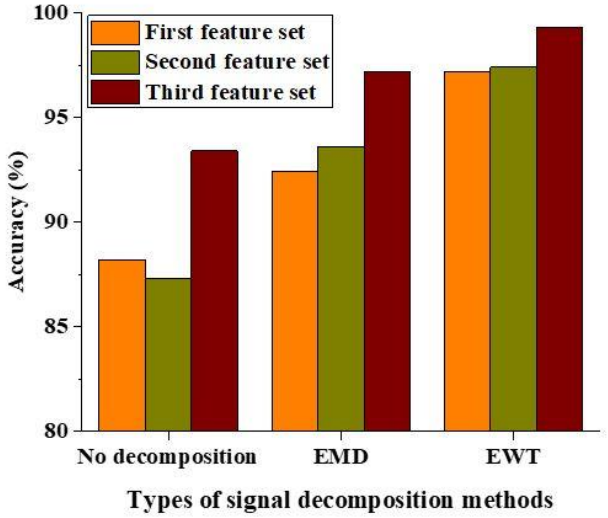

Figure 4.5 The accuracy of the different feature sets for polymer gear fault detection using KNN classifiers.

Additionally, the confusion matrices are analyzed for individual classes of gear fault. Figure 4.6 shows the confusion matrix of different classifiers trained using the third feature set with the EWT-based decomposition method. The number in each rectangle represents the number of tests. A blue rectangle in each confusion matrix indicates that the four health conditions of polymer gears, i.e., healthy (H), slight pitting (F1), moderate pitting (F2), and severe pitting (F3), are correctly identified. A dark purple rectangle indicates that at least one of the H, F1, F2, and F3 health categories is incorrectly identified. Figure 4.6 (a) illustrates the confusion matrix of the KNN classifiers, indicating that the F1 category achieved 35 correct predictions out of 36, while H, F2, and F3 achieved 36 accurate predictions out of 36. Similarly, Figure 4.6 (b) displays the confusion matrix of the SVM

classifiers, showing that the F1 and F2 fault categories are accurately classified at 97.23%, while H and F3 achieve a 100% accuracy rate. Furthermore, Figure 4.6 (c) presents the confusion matrix of the LDA classifiers, revealing accurate classifications of 67%, 69%, 83%, and 92% for F1, F2, F3, and H, respectively.

To assess the reliability of the proposed methodology, a comparative study is conducted between the proposed method and previous methods. Table 4.6 presents a summary of the proposed method and the previous methods. The results indicate that the proposed method outperforms the other studies in terms of fault detection effectiveness.

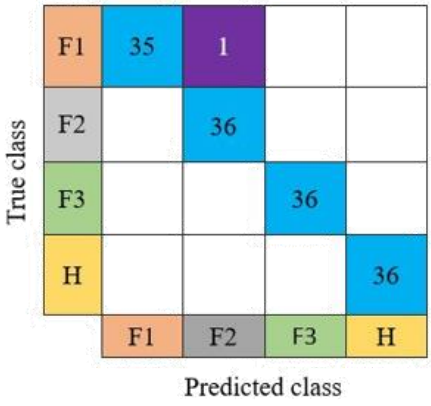

(a) KNN

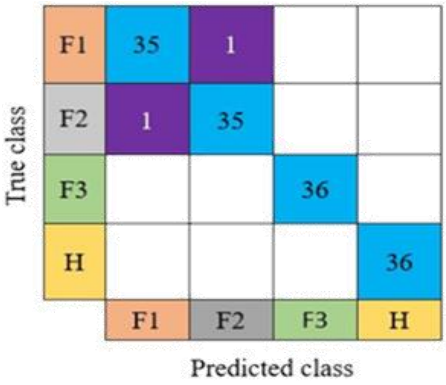

(b) SVM

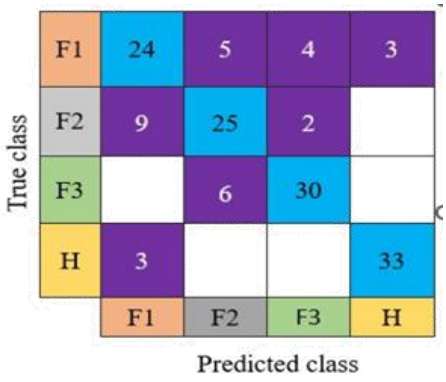

(c) LDA

Figure 4.6 Confusion matrix of different classifiers trained using third features set with EWT based decomposition method.

Table 4.6 Comparison of the results of the proposed work with other previously published work.

Proposed/Existing work	Features	Measured signal	Classifier	Accuracy (%)
Ramteke et. al. [125]	VMD based features	Vibration	Random forest	96..5
Li et al. [61]	10-time domain features	Vibration	KDA	95.59
Cherrez et al. [126]	Various Time domain, frequency domain, and time-frequency domain features	Vibration and acoustics	LDA	95.6
Proposed work	EWT based features	Vibration	KNN	99.3

4.8 Conclusions

Detecting faults in polymer gear at an early stage of pitting is a challenging task due to the non-stationary nature of the vibration signal and the good damping resistance of polymer gear. To address this issue, this experimental study employed three classifiers and three signal decomposition techniques to analyze polymer gear fault detection. Three different sets of features were used to train the classifiers. The following conclusions can be drawn from the study:

- The EWT-based signal decomposition method yielded the best fault detection accuracy, followed by EMD and raw signals. The KNN classifier achieved the highest accuracy among the three classifiers for all feature sets.

- The EWT-based decomposition with the KNN classifier achieved the highest accuracy (99.3%) when using the third feature set, while the lowest accuracy (97.2%) was achieved when using the first feature set.
- Among all the combinations of decomposition methods, classifiers, and feature sets, raw signals with LDA had the lowest accuracy of 59%.
- The proposed method demonstrated a significant improvement in accuracy compared to previous works.

Chapter 5

Classification of polymer gear pitting faults using double decomposition and Hjorth parameters

5.1 Introduction

Several techniques have been proposed in the literature [50,127–129] for identifying gear faults from non-stationary vibration signals. Another powerful tool for condition monitoring and fault diagnosis is wavelet transform. It effectively represents various transient patterns present in vibration signals associated with gearbox faults. The key advantage of wavelet transform in signal analysis lies in its ability to provide multi-resolution localization of short-time components, allowing for the detection of diverse gear faults using a single time-scale distribution derived from the transform. Wang et. al. [130] have outlined the utilization of wavelet transforms for analyzing both distributed and localized faults in helicopter gearboxes.

This study utilizes a double decomposition method to extract the most sensitive signal. The process begins with the application EMD on the acquired vibration signal, resulting in a decomposition into a set of IMFs with specific frequencies. Next, IMFs with higher correlation coefficients undergoes Discrete Wavelet Transform (DWT), generating DWT sub-bands. The energy ratio estimation technique is then employed on these decomposed sub-bands to identify the most sensitive vibration signals and create a feature vector. This feature vector is subsequently used as input for training and testing classifiers.

To evaluate the effectiveness of the proposed methodology, a comparison is conducted with ordinary EMD and DWT techniques. The

classification of pitting faults in polymer gears using the double decomposition method is depicted in Figure 5.1.

Moreover, this study focuses on the utilization of MC901 material-based polymer gears. Detailed information regarding the material properties and specifications can be found in Table 2.1 and Table 2.2.

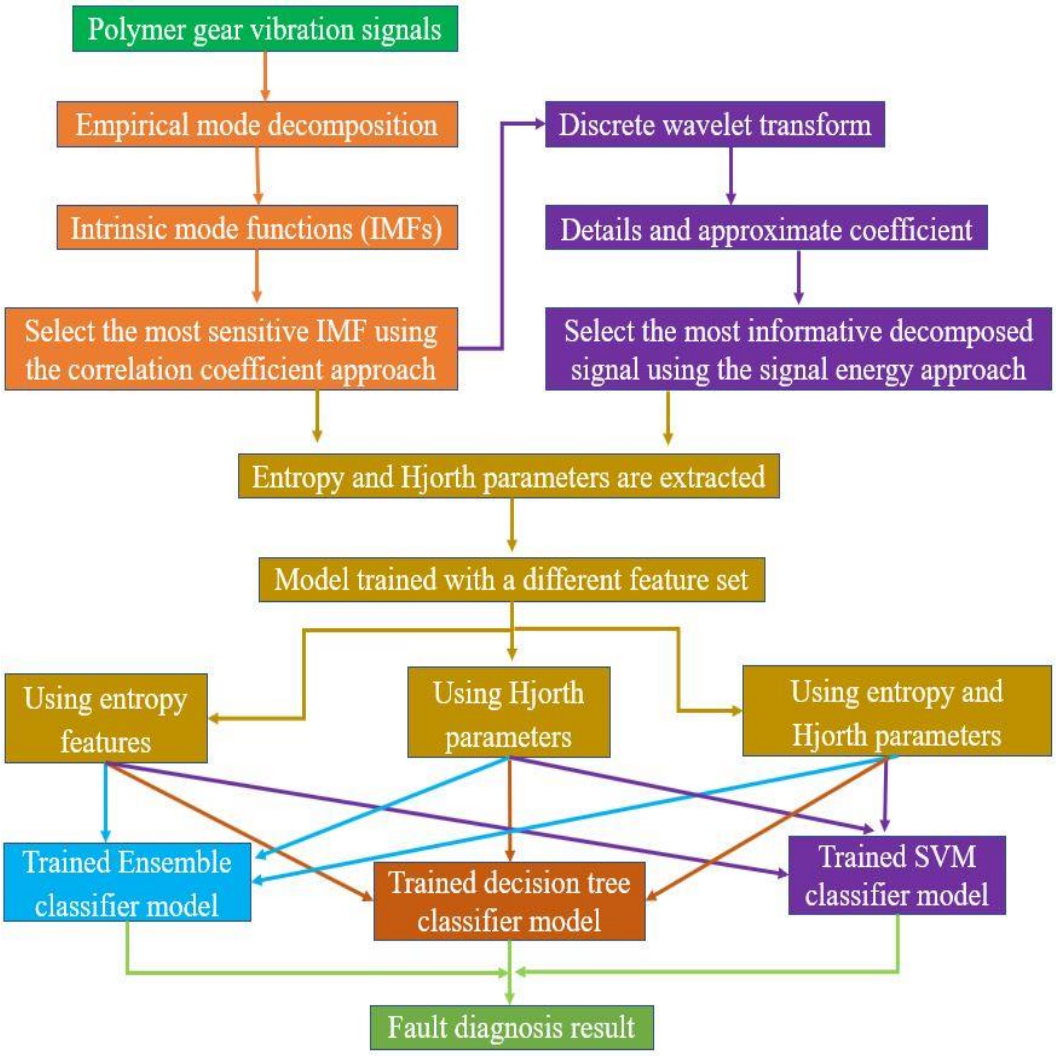

Figure 5.1 Flow chart of the proposed polymer gear fault classification method.

5.2 Experimental study

The experimental setup depicted in Figure 5.2 is utilized in this study to capture vibration signals from different polymer gear pitting faults under various experimental conditions.

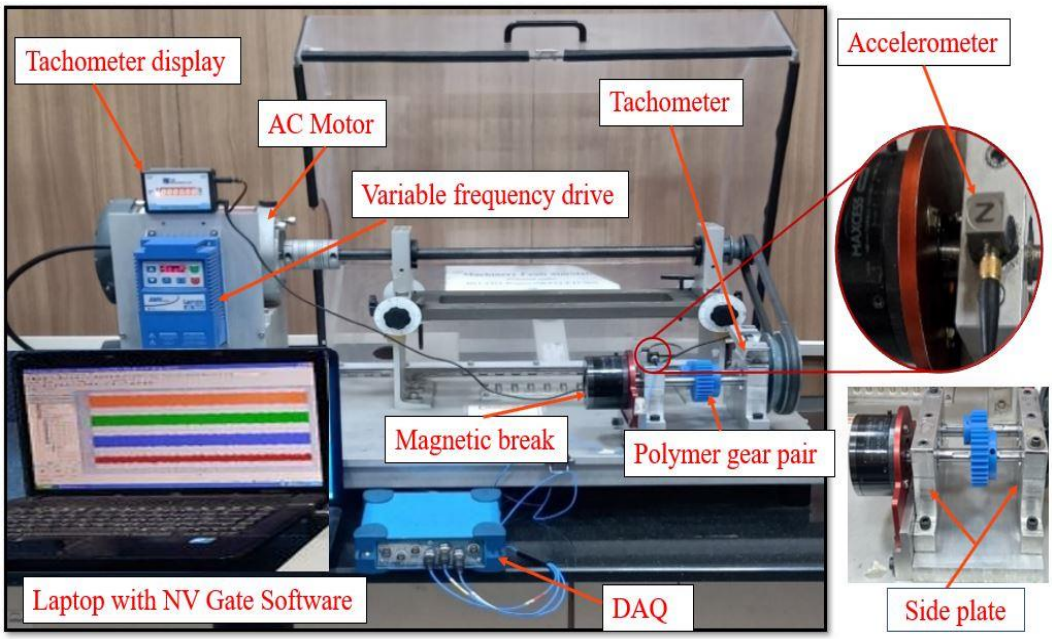

Figure 5.2 Experimental setup.

A total of five gear pairs are analyzed: gear in healthy condition, and pinion with various simulated pitting faults namely Fault 1, Fault 2, Fault 3, Fault 4, and Fault 5. The simulated pits were created on the pinion gear tooth surface using a micro-milling machine, with a pit depth of 0.2 mm and a diameter of 2 mm. In the case of the healthy gear, there were no pits present on the tooth surface. However, in the case of Fault 1 through Fault 5, the number of pits on the tooth surface ranged from one to five. The simulated tooth pitting on the polymer gears is depicted in Figure 5.3. Vibration signals were captured from each gear at four different speeds (10 Hz, 20 Hz, 30 Hz, and 40 Hz) while at a constant torque of 3 Nm. Each acquired signal had a length of 20 seconds and was sampled at a frequency of 12.8 kHz.

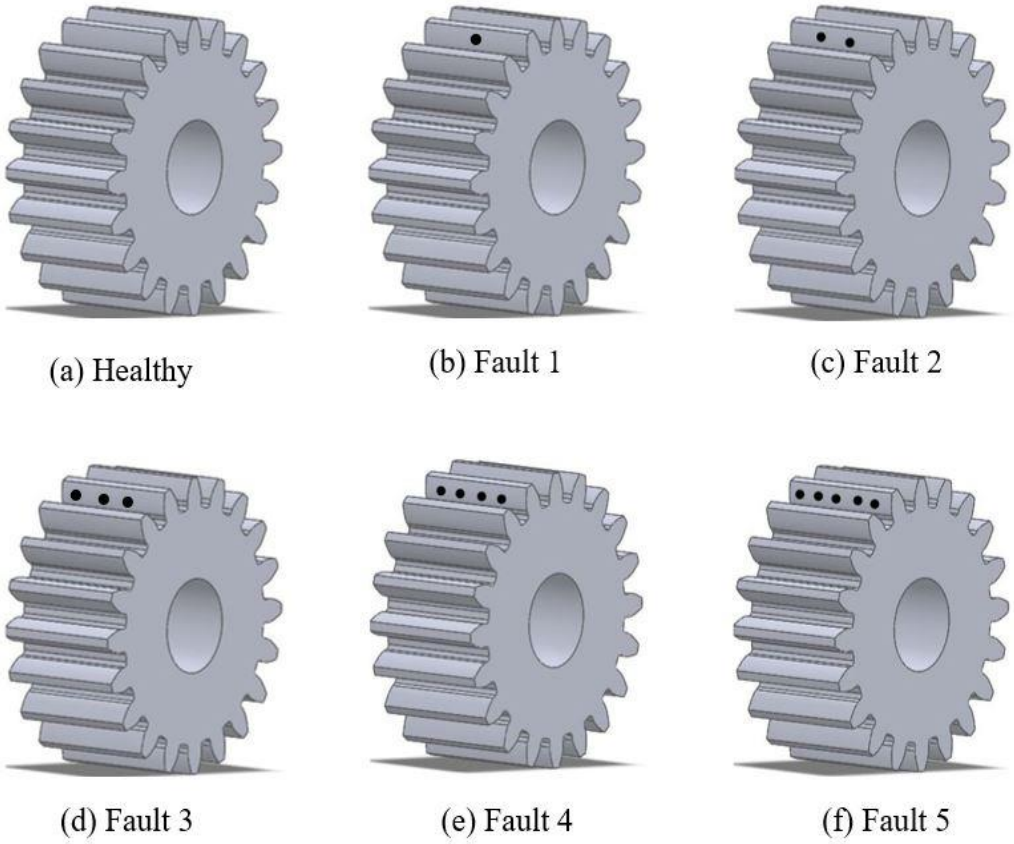

Figure 5.3 Simulated tooth pitting on polymer gears.

5.3 Features extraction

To train the classifier for fault classification, this study utilizes entropy and Hjorth parameters-based features. The extracted features consist of log energy entropy, threshold entropy, sure entropy, norm entropy, Shannon entropy, and HPs. Entropy is used to measure the degree of disorder present in the system. Sharma et al. [131] have described the use of entropy-based features for fault detection. These features are defined as follows:

5.3.1 Log energy entropy (E_{Le})

The level of complexity in gear signals is calculated by E_{Le}. Mathematically it can be written as.

$$E_{le} = \sum_{i=1}^{N} \log(y_i)^2 \qquad 5.1$$

where N is the length of the signal and y_i is the *i*th signal sample.

5.3.2 Threshold entropy (E_{th})

The signals threshold entropy is defined as,

$$E_{th} = \begin{cases} 1, if \left| y_i \right| \rangle v, and \\ 0, elsewhere \end{cases} \quad 5.2$$

where v is the threshold.

5.3.3 Sure entropy (E_{sure})

It is a common measuring tool for quantifying properties related to information for a perfect representation of a signal. E_{sure} of a signal is mathematically expressed as

$$E_{sure} = N - \neq \left\{ i \ \ such \ \ that \ \ \left| y_i \right| £ v \right\} + \sum_{i=1}^{N} \min\left(y_i^2, v^2 \right) \quad 5.3$$

where, ε is a positive threshold value. In this study, *ε is 0.2.*

5.3.4 Norm entropy (E_{ne})

The power and energy content of a signal is provided by norm entropy. It can be calculated as,

$$E_{ne} = \left| y_i \right|^v \quad 5.4$$

5.3.5 Shannon entropy (E_{sha})

Shannon entropy is utilized to assess the level of uncertainty associated with an event. It analyzes the information and the probability distribution of data, with higher entropy values indicating a greater degree of uncertainty. Conversely, data with a narrow and peaked distribution exhibit low entropy value. E_{sha} can be mathematically expressed as:

$$E_{sha} = - \sum_{i=1}^{N} y_i^2 \log \left(y_i \right)^2 \quad 5.5$$

5.3.6 Hjorth parameters

The HPs are explicitly defined in section 4.5.2 of this thesis, providing clear explanations and descriptions of their characteristics and calculations.

5.4 Feature extraction process

This section discusses the different techniques for feature extraction. Specifically, decomposition techniques such as EMD, DWT, and the double decomposition method i.e., EMD-DWT are utilized for feature extraction.

5.4.1 Feature extraction using the EMD approach

Section 3.2.1 provides detailed information about EMD and its shifting process. In this study, acquired vibration signals are decomposed into ten IMFs. Figure 5.4 depicts the first five IMFs of healthy and Fault 1 gear signal at 40 Hz speed and 3 Nm torque conditions. The first column indicates the healthy gear vibration signals and their IMFs, similarly second column indicates the Fault 1 gear vibration signals and their IMFs. The X-axis represents the number of samples, and the Y-axis represents the signal amplitude in m/s^2. Similarly, other signals are also decomposed.

Selecting the most sensitive IMF after decomposing the raw signal and obtaining all the IMFs is a crucial task that captures the most sensitive fault information. Several methods have been developed by researchers to select the sensitive IMF. This study employs the correlation coefficient-based method to select the sensitive IMF, which measures the similarity between IMFs and the raw signal. Zheng et al. [49] define a correlation coefficient (CC) as a measure of the similarity between two signals. The mathematical expression for CC is given by equation 5.6.

$$CC = \frac{\sum_{i=1}^{N} (y_i - \bar{y})\,(c_{ji} - \bar{c}_j)}{\sqrt{\sum_{i=1}^{N} (y_i - \bar{y})^2}\ \sqrt{\sum_{i=1}^{N} (c_{ji} - \bar{c}_j)^2}} \qquad 5.6$$

where, CC is the correlation coefficient, y represents the raw signal, $\bar{y}$ is mean of the raw signal, c_j is the j_{th} IMF and $\overline{c_j}$ is the mean of j_{th} IMF.

The correlation coefficient value for the healthy and five faulty conditions at 40 Hz speed and 3 Nm torque condition is presented in Table 5.1. Based on this, the IMF with the highest correlation coefficient value is chosen as the dominant IMF, and IMF 1 is selected as the dominating IMF. The entropy and Hjorth parameters are then extracted from this dominated IMF. This same methodology is applied to other gear fault and experimental conditions.

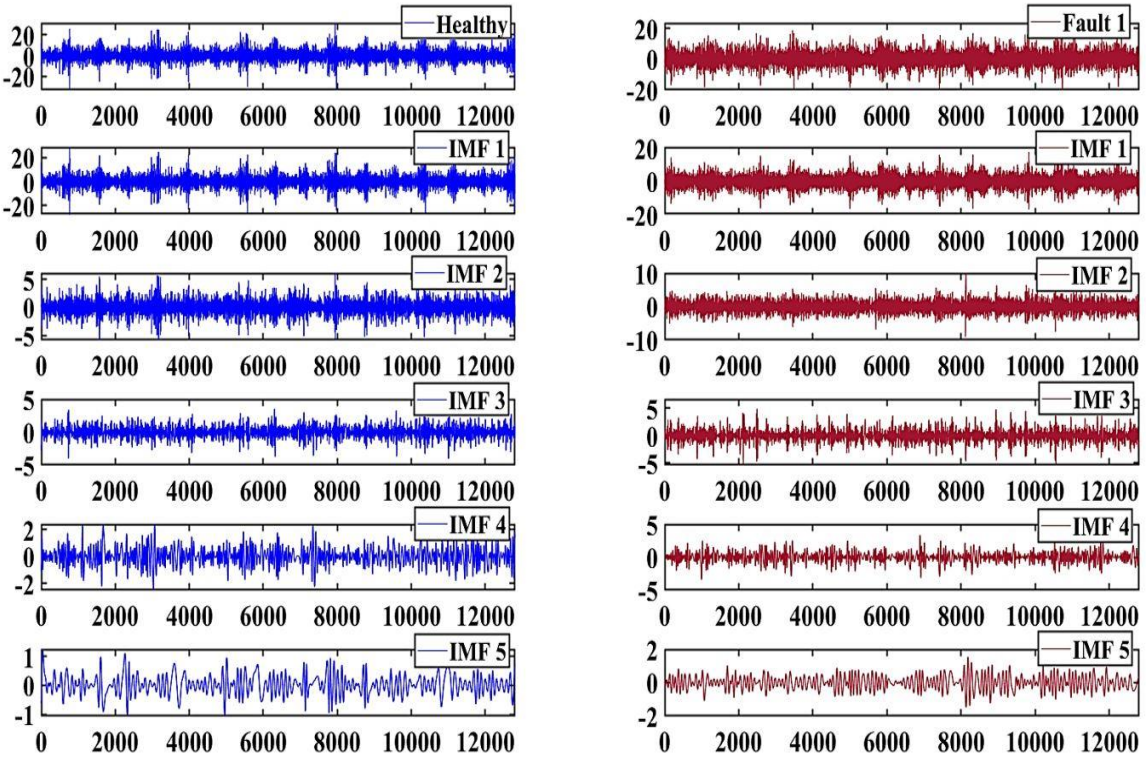

Figure 5.4 IMFs of healthy and fault 1 gear signal at 40Hz speed and 3 Nm torque condition.

Table 5.1 The correlation coefficient of the first 5 IMFs of healthy and five Faulty conditions at 40 Hz speed and at 3 Nm torque condition.

Gear health	IMFs				
	IMF 1	IMF 2	IMF 3	IMF 4	IMF 5
Healthy	0.928	0.218	0.137	0.097	0.048
Fault 1	0.952	0.152	0.091	0.056	0.040
Fault 2	0.843	0.343	0.244	0.174	0.082
Fault 3	0.904	0.287	0.167	0.114	0.056
Fault 4	0.868	0.292	0.253	0.163	0.059
Fault 5	0.779	0.411	0.351	0.206	0.067

5.4.2 Feature extraction using discrete wavelet transform approach

DWT [132] has been one of the most useful techniques in non-stationary signal analysis. This technique has emerged as one of the most essential tools in non-stationary signal analysis because it can extract localization information from time-domain signals at the local time and frequency. During the DWT process, the raw signal is analyzed by decomposed into an approximation and detailed coefficients [132]. Mathematically, approximation ($a_{i,j}$) and details coefficient ($d_{i,j}$) can be expressed as follows:

$$a_{i,j} = \left\langle g(t), \phi_{i,j}(t) \right\rangle = \int_R g(t) 2^{(-i/2)} \overline{\phi(2^{-i}t - j)dt} \quad 5.7$$

$$d_{i,j} = \left\langle g(t), \psi_{i,j}(t) \right\rangle = \int_R g(t) 2^{(-i/2)} \overline{\psi(2^{-i}t - j)dt} \quad 5.8$$

where, $\psi(t)$ represent the mother wavelet, $\phi(t)$ represent basic scaling, i represent the scale index and j represents the translation parameter. The inverse DWT is provided by:

$$g(t) = \sum_j a_{i,j} 2^{(-i/2)\phi(2^{-i}t-j)} + \sum_j d_{i,j} 2^{(-i/2)\psi(2^{-i}t-j)} \quad 5.9$$

To extract features from the acquired vibration signal in this section, the DWT technique is utilized. To achieve this, the signal was decomposed into 6 levels to obtain sub-band signals. The DWT decomposition was performed using Daubechies-4 (db4) as the mother wavelet due to its orthogonality, low computational effort, and compact time-domain support Daubechies et al [133].

Figure 5.4 illustrates the six levels of decomposition obtained from the vibration signals of healthy and Fault 1 gear under 40 Hz speed and 3 Nm torque conditions. The leftmost column corresponds to the vibration signals and their corresponding IMFs for the healthy gear, while the second column represents the same for the Fault 1 gear. The X-axis denotes the number of samples, and the Y-axis indicates the signal amplitude measured in m/s^2. This decomposition process is similarly applied to other acquired signals as well.

Once the sub-bands of the polymer gear signal were obtained using DWT, the most sensitive sub-band was selected to reduce computational time for further data analysis. It was observed that level 1 of the decomposed signal corresponds to higher frequency categories and contains sensitive fault information about the polymer gear system. This observation is supported by the calculation of the energy ratio of all decomposed levels by Sharma et al. [134]. A detailed discussion about the energy ratio can be found in section 4.4. Table 5.2 displays the energy ratio values for the healthy condition and five different faulty conditions observed at 40 Hz speed and 3 Nm torque conditions. Based on the results presented in Table 5.2, it is apparent that level 1 exhibits the highest energy ratio value, indicating its greater sensitivity as a sub-band for further analysis. From this specific sub-band, entropy and HPs were extracted. The same methodology was applied to the analysis of other experimental conditions.

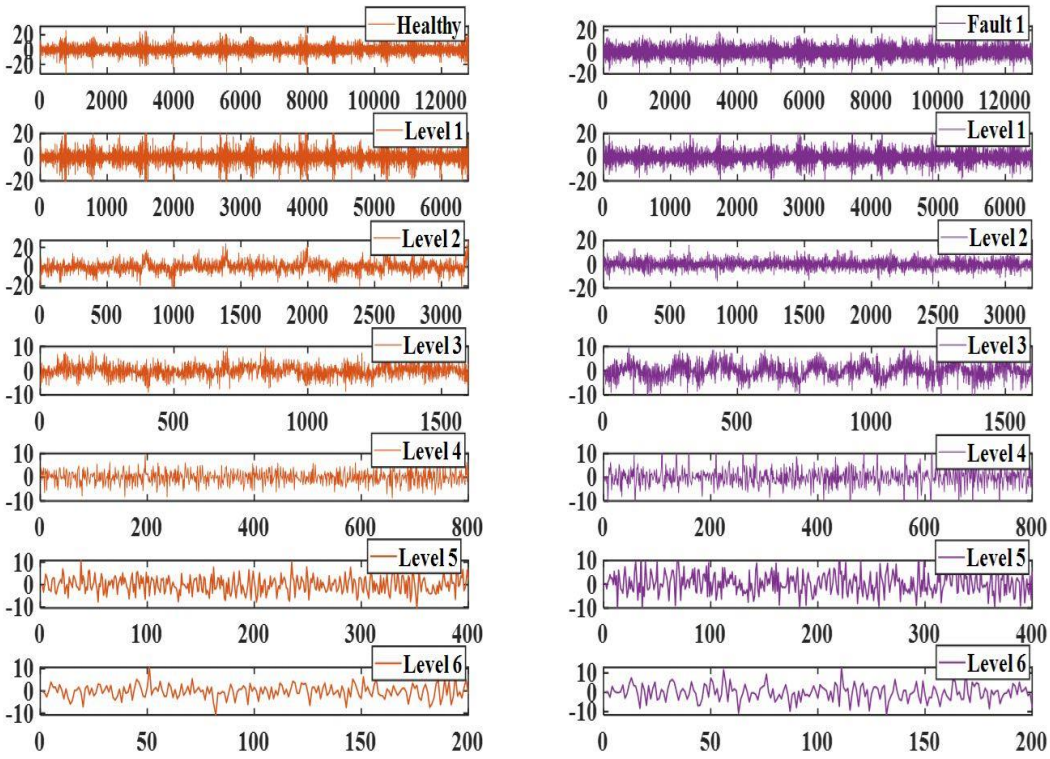

Figure 5.5 Healthy and Fault 1 vibration signal and its DWT based sub-band at 40 Hz speed and 3 Nm torque.

Table 5.2 DWT sub-bands and their energy ratio with respect to the raw signal at 40 Hz under 3 Nm torque.

Gear Health	Sub-bands					
	Level 1	Level 2	Level 3	Level 4	Level 5	Level 6
Healthy	0.565	0.342	0.042	0.022	0.019	0.007
Fault 1	0.603	0.195	0.084	0.052	0.038	0.017
Fault 2	0.643	0.224	0.059	0.032	0.024	0.005
Fault 3	0.605	0.216	0.063	0.053	0.048	0.008
Fault 4	0.431	0.223	0.108	0.12	0.088	0.018
Fault 5	0.566	0.343	0.042	0.022	0.018	0.007

5.4.3 Feature extraction using the EMD-DWT

Exploring the ability of features to classify polymer gear faults using double decomposition techniques i.e., combined EMD-DWT would be of interest. The motivation behind this approach stems from the success of classifying various types of non-stationary signals, such as ECG and EEG, using features extracted from hybrid time-frequency techniques. In this section, the decomposition of the polymer gear vibration signal was carried out in two steps. In the first step, the signal was decomposed into its constituent components using EMD. Subsequently, in the second step, the dominant IMF obtained from the decomposition was further decomposed into sub-bands using DWT. Following the decomposition, the sub-band with the highest information content was selected based on the energy ratio criteria. This chosen sub-band was then utilized for feature extraction purposes.

Figure 5.6 displays the dominant IMF and six levels of DWT decomposition of healthy and Fault 1 gear signals at 40 Hz speed and 3 Nm torque conditions. The dominant IMF is obtained by analyzing the set of IMFs using the correlation coefficient. The horizontal axis of Figure 5.6 represents the sample numbers, while the vertical axis represents the signal amplitude measured in m/s^2. Upon obtaining the different levels of Discrete Wavelet Transform (DWT), the energy ratio is computed for each of these obtained signal levels. Table 5.3 displays the energy ratio values for the sub-bands. The results from the analysis indicate that the Level 1 decomposition exhibits the highest energy ratio value. As a result, Level 1 is chosen as the most sensitive sub-band for subsequent analysis and feature extraction. From this selected sub-band, entropy features and HPs are extracted. The same methodology is also applied to experimental conditions involving frequencies of 10 Hz, 20 Hz, and 30 Hz while keeping the torque constant.

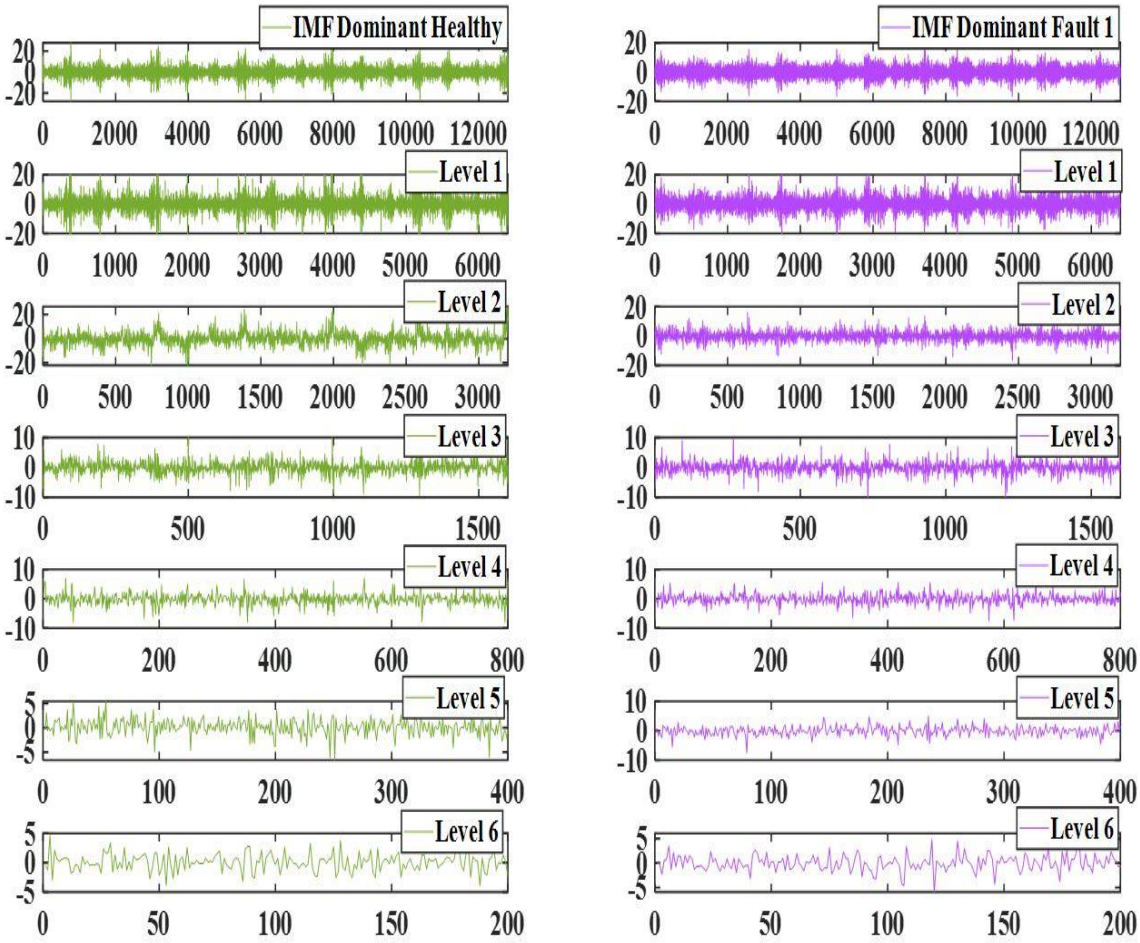

Figure 5.6 The dominant IMF with the DWT coefficients of faulty5 gear condition at 40 Hz and 3 Nm torque condition

Table 5.3 EMD-DWT sub-bands and their energy ratio with respect to dominant IMF at 40 Hz and 3 Nm torque condition.

Gear Health	Sub-band name					
	Level1	Level 2	Level 3	Level 4	Level 5	Level 6
Healthy	0.606	0.351	0.027	0.012	0.004	0.002
Fault 1	0.763	0.177	0.035	0.013	0.006	0.003

5.5 Machine learning models

In this study, three distinct machine learning models are employed to predict faults in PGs using three different feature sets. The feature matrices are constructed by considering a splitting ratio of 10-fold cross-validation for the dataset. The details of the different machine learning models utilized in this study will be elaborated upon in the subsequent section.

5.5.1 Ensemble learning classifier (Bagged tree)

The Bagged tree classifier, which is an ensemble learning technique, is employed in this study. The goal of bagging is to create multiple subsets of data randomly selected from the training sample. Each subset is used to train a separate decision tree. These decision trees denoted as B_1, B_2, B_3, ..., B_n, are derived from constructing base classifiers using bootstrap samples J_1, J_2, J_3, ..., J_n, respectively, with replacement from the defined data set J. The resulting bagged tree model consists of a collection of all the constructed base classifiers, and the final prediction is determined based on majority voting. The ensemble model combines predictions from different decision trees, resulting in a more robust classifier compared to a single decision tree. In this study, the parameters of the Bagged tree classifier were tuned. The maximum number of splits was set to 239, and the number of learners (decision trees) was set to 30.

5.5.2 Decision tree classifier

The Decision tree classifier is a popular supervised machine learning algorithm used for classification tasks. It represents a tree-like structure where each internal node represents a feature or attribute, and each branch represents a decision rule based on that attribute. The leaves of the tree represent the class labels or outcomes. The decision tree algorithm works by recursively partitioning the data based on different features, aiming to create homogeneous subsets at each step. The splitting criterion, such as the Gini index or entropy, is used to determine the best attribute to split the data. The selection of splits is the most crucial element [135]. In this study, the fine

tree method is used with a maximum number of the split is 100 and Gini's diversity index is used for the split criterion.

5.5.3 Support vector machine

For a comprehensive understanding of SVM, refer to section 4.6.1, which provides detailed explanations about SVM and its functioning.

5.6 Results and discussion

This section explains the classification of polymer gear faults by analyzing the vibration signals obtained under different experimental conditions for various gear fault scenarios. To analyze polymer gear signals, three methods are used for signal decomposition: (a) EMD, (b) DWT, and (c) EMD-DWT. The most informative signal is selected after decomposition, and features are extracted from it. These features are then used to train various classifiers for the classification of polymer gear faults. To prevent overfitting and provides a more reliable estimate of the model's performance, the classification process is carried out using a 10-fold cross-validation approach. Accuracy is the most commonly used measure for evaluating classification performance, and it can be computed using the following equation:

$$Accuracy = \frac{TP + TN}{TP + TN + FP + FN} \tag{5.10}$$

where TP represents true positives (the number of correctly predicted positive cases), TN denotes true negatives (the number of correctly predicted negative cases), FP refers to false positives (the number of incorrectly predicted positive cases), and FN represents false negatives (the number of incorrectly predicted negative cases).

Additionally, the effectiveness of the ensemble learning classifier, decision trees classifier, and SVM is assessed using three sets of features. The first feature set comprises entropy features, such as log energy entropy, threshold entropy, sure entropy, norm entropy, and Shannon entropy. The second feature set consists of the Hjorth parameters. Finally, in the third

feature set, both the first and second feature sets are employed together in training the classifiers for fault classifications.

The results of the evaluation of the three types of decomposition coupled with three classifiers utilizing the first, second, and third feature sets are presented in Tables 5.4, Table 5.5, and Table 5.6, respectively.

Based on the results presented in Table 5.4, all classifiers were trained using the first feature set. The findings demonstrate that the fine tree classifier yielded the highest accuracy, reaching 90%, as compared to the SVM and bagged tree classifiers when coupled with the EMD-DWT decomposition method. The bagged tree classifier achieved the maximum accuracy of 92.9% when coupled with DWT and attained the highest accuracy of 90% when using EMD. However, SVM with EMD obtained the lowest accuracy 26.2% among all classifiers.

Table 5.4 Accuracy of classifiers for fault detection using first feature sets.

	Accuracy (%)		
	Bagged tree	Fine tree	SVM
EMD	90	85.4	26.2
DWT	92.9	87.9	35.4
EMD-DWT	89.6	90	35.8

Table 5.5 shows the evaluation results for the second feature set. The bagged tree classifier coupled with EMD-DWT achieved the highest accuracy of 93.3% for classifying the polymer gear faults. On the other hand, SVM classifiers had lower accuracy compared to other classifiers. When using EMD and DWT separately, the bagged tree achieved 92.5% accuracy in both cases. However, the SVM classifier with the DWT decomposition method trained by Hjorth parameters showed the lowest accuracy among all classifiers and decomposition techniques.

Table 5.5 Accuracy of different classifiers for fault detection using second feature sets.

	Accuracy (%)		
	Bagged tree	Fine tree	SVM
EMD	92.5	88.8	62.5
DWT	92.5	92.1	56.7
EMD-DWT	93.3	85.8	65

Table 5.6 presents the results of evaluating the third feature set. The bagged tree classifier coupled with EMD-DWT achieved the highest accuracy of 99.2% for identifying polymer gear faults. However, SVM classifiers had a lower accuracy of 84.6% compared to other classifiers. When using EMD and DWT separately, the bagged tree achieved 97.5% and 97.9% accuracy, respectively. In contrast, the SVM classifier with the DWT decomposition method trained by the third feature set showed the lowest accuracy of 71.7% among all classifiers and decomposition techniques.

Table 5.6 Accuracy of different classifiers for fault detection using third feature sets.

	Accuracy (%)		
	Bagged tree	Fine tree	SVM
EMD	97.5	88.3	75
DWT	97.9	88.8	71.7
EMD-DWT	99.2	90	84.6

After analyzing the results presented in Tables 5.4, 5.5, and 5.6, it becomes evident that the most effective approach for polymer gear fault detection is through the utilization of the double decomposition method coupled with the bagged tree classifier. The highest accuracy of 99.2% is attained when combining this method with the third feature set.

Figure 5.7 illustrates the confusion matrix obtained from various classifiers trained using the third feature set and utilizes the EMD-DWT signal decomposition method. In Figure 5.10 (a), the identification rate for healthy, Fault 1 (F1), Fault 2 (F2), Fault 3 (F3), and Fault 4 (F4) is 100%, indicating accurate classification for these conditions. Furthermore, the recognition rate for Fault 5 (F5) gear pitting exceeds 95%.

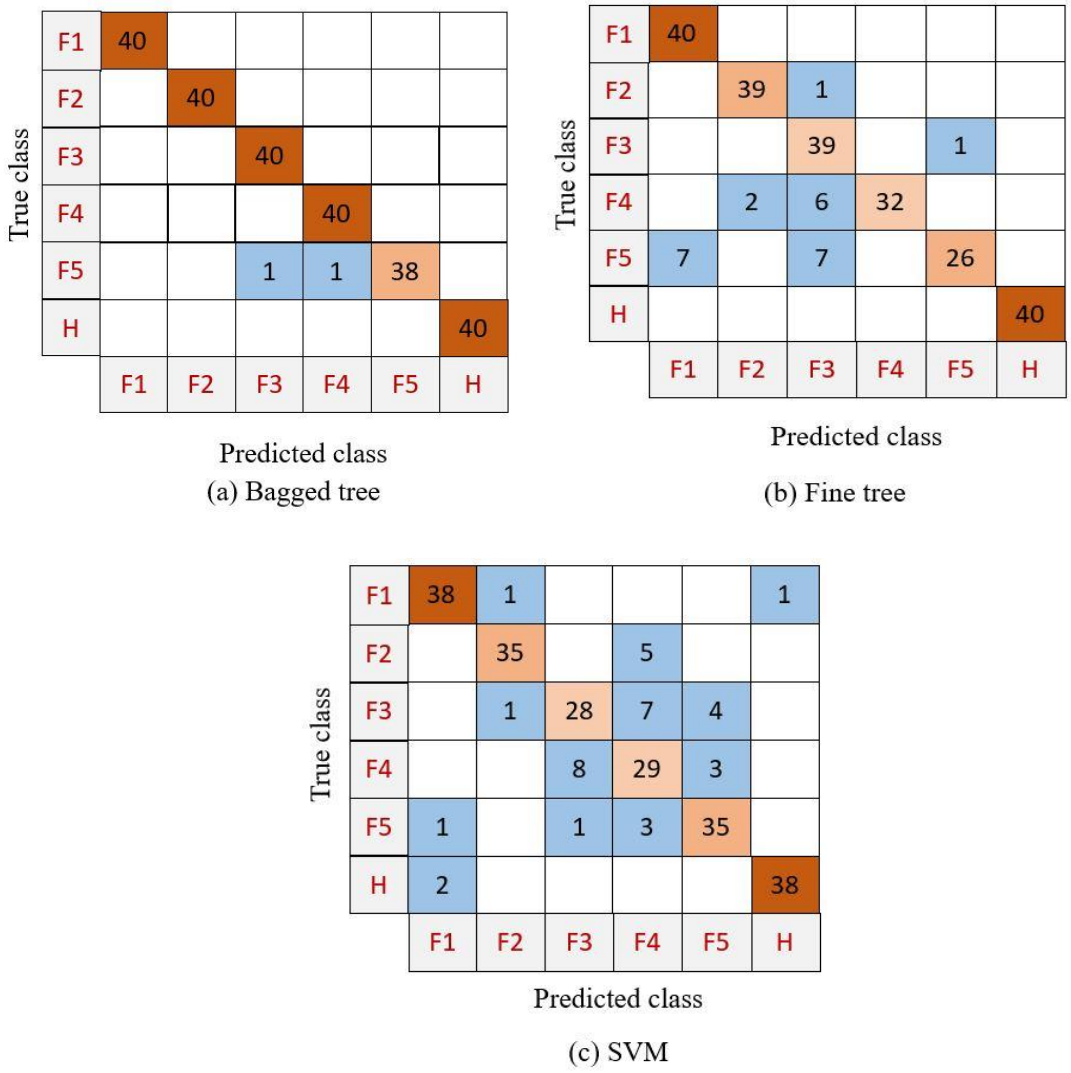

Figure 5.7 Confusion matrix of different classifiers trained by third feature set using EMD-DWT signal decomposition method.

Examining Figure 5.10 (b), it becomes evident that the classification accuracy for healthy and F1 gear conditions is 100%. However, for pitting conditions F2 and F3, approximately 2.5% of instances are misclassified. Similarly, for F4 and F5 fault conditions, approximately 20% and 35% of instances are misclassified, respectively. Figure 5.10 (c) shows the SVM accuracy of each class.

5.7 Conclusion

This study aims to develop a novel polymer ger fault classification method. For this, a double decomposition method i.e., EMD-DWT has been developed. The proposed method helps in the detection of early pitting defects in polymer gears. In this study, a total of six classes (one is healthy and the remaining faulty) of polymer gears have been studied for fault classification. The well-known EMD and DWT decomposition techniques are selected and developed as an EMD-DWT-based decomposition technique, for extracting highly discriminatory features. Three sets of features are extracted i.e., the first feature set (entropy-based feature), the second feature set (Hjorth parameters), and the third feature set which is a combination of the first and second feature sets. These feature sets are used to train three different classifiers: the bagged tree, fine tree, and SVM.

The proposed method has been shown more effective for polymer gear fault detection, and this demonstrates that the decomposition of polymer gear vibration signals through EMD-DWT before the feature extraction step is efficiently better than only EMD and DWT decomposition. Moreover, in most cases, the accuracy is increased when using a combination of entropy and Hjorth parameters as a feature for training the classifiers. It is found that using bagged tree classifiers, the data can be classified more effectively, and the classifier achieved 99.2 % accuracy.

Chapter 6

Hybrid deep learning model for polymer gear multiclass fault classification

6.1 Introduction

To overcome EMD mode mixing limitations, a new method, ensemble EMD (EEMD), is introduced Zhaohua [136]. The EEMD adds different series of white noise in multiple trials into the signal. While EEMD performs well in signal processing, calculating the large ensemble mean can be time-consuming. To address this issue, Yeh et al. [137] developed a new novel noise-enhanced technique known as the complete EEMD (CEEMD).

Furthermore, Torres et al. [138] introduced complete ensemble empirical mode decomposition with adaptive noise (CEEMDAN), a noise-enhanced data processing method that uses adaptive noise. CEEMDAN can significantly reduce unwanted noise in the signal.

In recent years, deep learning has become increasingly prevalent. Deep learning has been used to address the limitations of traditional methods for identifying mechanical faults. Zhang et al. [139] proposed a failure detection approach for rolling bearings using deep convolution neural networks (CNN) that eliminated the need for human feature extraction and achieved automatic feature learning. Liu et al. [140] proposed a bearing fault detection approach based on a recurrent neural network (RNN) in the form of an autoencoder. However, the ordinary RNN has a limitation that it cannot store long-term data [141]. This problem has been solved by the introduction of LSTM and GRU classifiers, which use gate mechanics to store and remove relevant information. Compared to the traditional RNN, LSTM performs better. Li et al. [80] demonstrated a GRU network for detecting gear pitting faults. The approach also has the ability to train on a limited

number of samples and still attain accuracy levels above 98%. Haj et al. [142] studied multiclass gear fault detection using a hybrid CNN-LSTM network, and the accuracy of this network is more than 97%. Li et al. [77] proposed a Bidirectional LSTM (BiLSTM) model to gear pitting fault detection using vibration signals. The overall accuracy of this proposed model is more than 96%, which is 4% higher than the LSTM model.

After reviewing the literature, it is evident that DNN networks, such as CNN or RNN, are commonly used to extract features directly from signals. To enhance the training efficiency of RNNs, the data's dimensionality and variability are reduced using feature extraction techniques or dimensionality reduction. However, this study aims to explore the use of deep learning for polymer gears' multiclass fault detection while minimizing computational complexity. This study proposes a novel method that combines the hybrid LSTM-GRU classifier model with CEEMDAN for polymer gear fault diagnosis.

6.2 Experimental setup and data collection

This experimental study involves examining various simulated faults in polymer gears at different rotating speeds and constant torque, using a test rig developed in-house, as depicted in Figure 6.1. The test setup is described in detail in section 2.3.1, while the material properties and specifications of the test polymer gears can be found in Table 2.1 and 2.2 respectively. This experimental study investigates the effects of different faults on four polymer pinion gears. One gear is a healthy gear (H), assumed to be defect-free, while the other three gears have different types of faults: slight abrasive wear (SW), moderate abrasive wear (MW), and pitting gear (PT). These four gear conditions are shown in Figure 6.2. The SW and MW faults are manually created using wide-grain sandpaper, and the degree of wear is measured by weight loss, which is the difference between the initial and final weight of the gear. In the case of PT, a circular pit is created using a micro-milling machine, with the diameter and depth of the pit being

approximately 2 mm and 0.2 mm, respectively. Table 6.1 provides a detailed description of the faults present in the PGs.

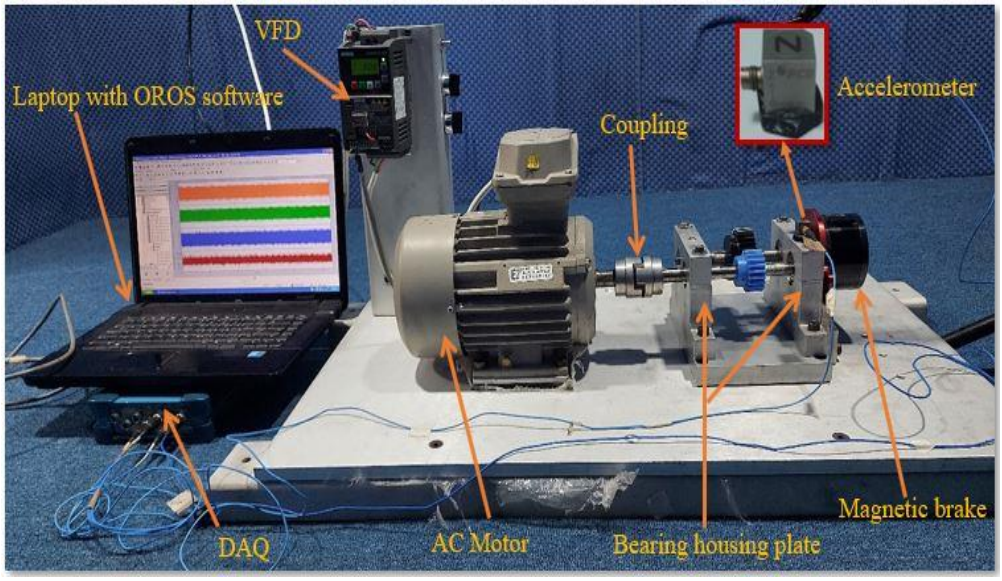

Figure 6.1 Picture of the experimental setup.

The PG vibration signals were captured in this experimental study using a tri-axial accelerometer (PCB-Piezotronics 355339), which was directly mounted on the top of the bearing housing, while the gears were rotated at three different speeds (500 rpm, 800 rpm, and 1100 rpm) and a constant torque of 2 Nm. The vibration data were collected using an OROS-OR34 data acquisition system (DAQ) and visualized on a laptop with NV Gate software. A 20-second vibration signature was captured from each of the healthy and three faulty gears at different speeds and constant torque, with a sampling frequency of 12.8 kHz. To analyze the captured signal, a sliding window approach with a duration of 0.1 seconds was employed, with no overlap in the signal segments.

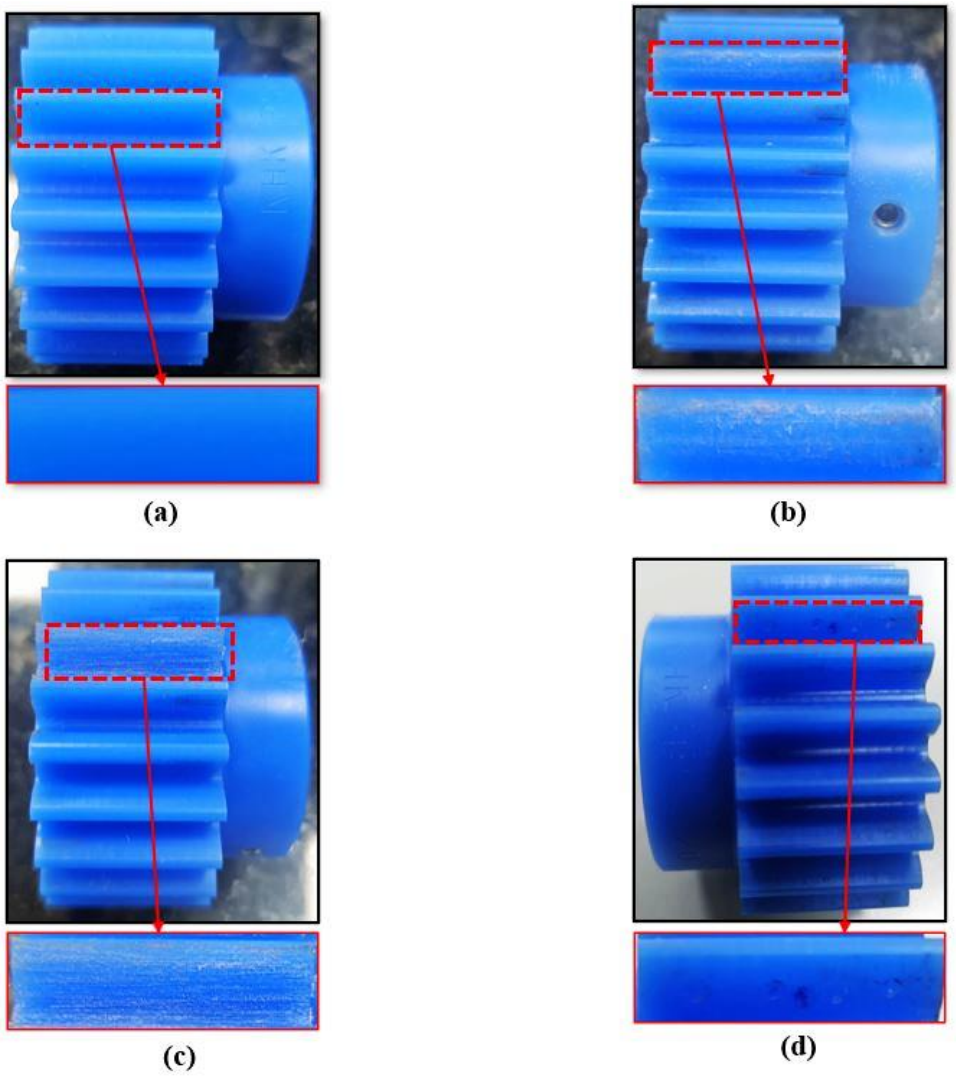

Figure 6.2 Polymer test gears (a) H, (b) SW, (c) MW, and (d) PT.

Table 6.1 Gear fault type.

Component	Type	Description
Polymer gear	H	Free from defects
	SW	weight loss (0.019g) from a single tooth
	MW	weight loss (0.029g) from a single tooth
	PT	Four pits on a single tooth

6.3 Proposed method

To identify the polymer gear faults, in this proposed method. A LSTM-GRU model is designed and trained by various features extracted from the enhanced signal obtained by CEEMDAN. The main steps of the proposed method are illustrated in Fig. 6.3, while the detailed explanation of each step is presented in the following sections.

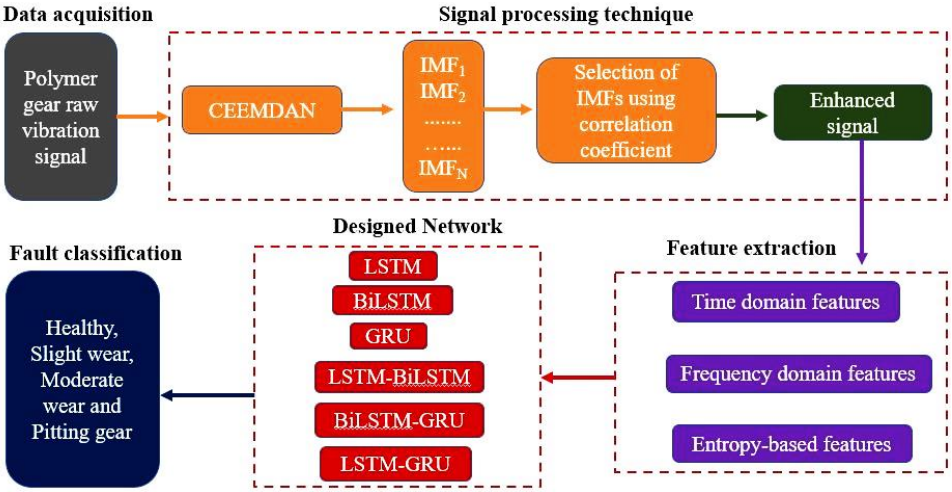

Figure 6.3 Flow diagram of the proposed method.

6.3.1 Decomposition of vibration signal using CEEMDAN

CEEMDAN is an effective algorithm for analyzing non-stable and nonlinear signals like gear signals because it is data-driven, has a low computational cost, and does not require a prior basis function [143]. CEEMDAN enhances the EEMD method by eliminating the residual noise produced in the reconstructed signal. To increase the effectiveness of the signal decomposition, an adaptive white noise has been included with the residual at each stage. Using the CEEMDAN approach, the initial decomposition of the raw signal $y(t)$ is decomposed into a finite set (k = 1,2,.., K) of IMFs or modes $M_k^l(t)$. Each signal component $y(t)$ is added with a white noise realization of zero mean and unit variance, $j^l(t)$ where l = 1,2,…, N, and the noise added signal are characterized by equation (6.1).

$$y^l(t) = y[t] + \varphi_0 j^l(t) \quad 6.1$$

where φ_0 represents the standard deviation of white noise.

After that, conventional EMD is used to decompose $y^l(t)$ until the first mode is reached. The first IMF is obtained by taking the mean of corresponding modes $M_k^l(t)$,

$$\tilde{M}_1[t] = \frac{1}{N}\sum_{i=1}^{N} M_1^l[t] \quad 6.2$$

Equation (6.3) is used to determine the residue for the first mode,

$$r_1[t] = y[t] - \tilde{M}_1[t] \quad 6.3$$

After the first mode has been evaluated, the remaining modes are recovered by introducing noise with various realizations to the current residue. The operator $B_j(\bullet)$ used EMD to produce p^{th} modes. As a result, the noise-added residue $r_1[t] + \varphi_1 B_1\left(j^l[t]\right)$ is decomposed, and equation (6.4) is used to compute the second CEEMDAN mode.

$$\tilde{M}_2[t] = \frac{1}{N}\sum_{i=1}^{N} B_1\left(r_1[t] + \varphi_1 B_1\left(j^l[t]\right)\right) \quad 6.4$$

The residue is measured as $r_k[t] = r_{(k-1)}[t] - \tilde{M}_k[t]$, for the subsequent stages, where $k = 2,\ldots, K$. Similarly, the k^{th} residue added with a noise realization, $r_k[t] + \varphi_k B_k\left(g^l[t]\right)$, are decomposed and $(k + 1)^{\text{th}}$ mode has been obtained by equation (6.5),

$$\tilde{M}_{(k+1)} = \frac{1}{N}\sum_{i=1}^{N} B_1\left(r_k[t] + \varphi_k B_k\left(g^l[t]\right)\right) \quad 6.5$$

When the computed residue becomes monotone, further decomposition of the mode functions is not possible.

6.3.2 Selection of IMFs

The experiment involves the acquisition of vibration signals of different gear faults at various speed and at a constant torque. Figure 6.4 shows the

raw signals of the gear along its z-axis. Each row in the figure displays the vibration signal of different gear fault conditions, and each column corresponds to the same gear fault condition but at different rotational speeds. As shown in Figure 6.4, the gear's raw vibration signal amplitude increases with the rotational speed. Additionally, the amplitude of the healthy gear is higher than that of the pitting gear signal, which may be due to background noise in the raw signals. Therefore, it is necessary to denoise the signals before extracting fault features. The denoising process is carried out in the subsequent step.

The CEEMDAN algorithm is employed to adaptively decompose the signal into 12 IMF components. However, all these IMFs are not equally sensitive for fault identification. Select the most informative IMFs, by using the correlation coefficient and threshold value. The correlation coefficient between each IMF_i (i=1,2,…,12) component and the raw signal is calculated using Equation 6.6.

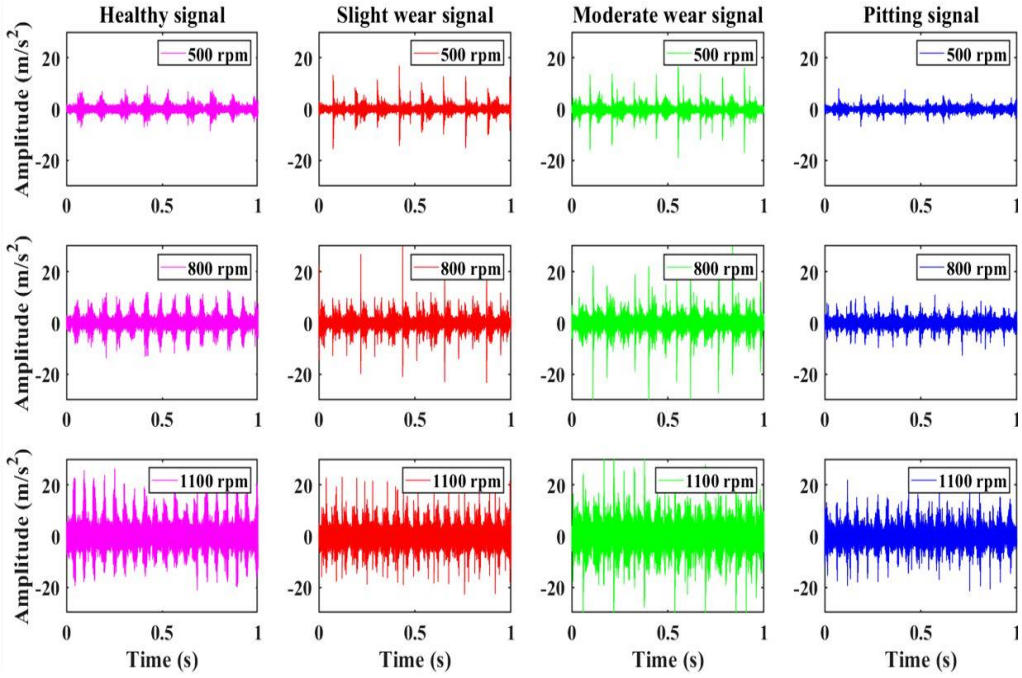

Figure 6.4 Raw signal waveforms of healthy and faulty polymer gears.

$$CC=\frac{\sum_{i=1}^{N}\left(y(i)-\bar{y}\right)\left(m_j(i)-\overline{m_j}\right)}{\left[\sum_{i=1}^{N}\left(y(i)-\bar{y}\right)^2\sum_{i=1}^{N}\left(m_j(i)-\overline{m_j}\right)^2\right]^{1/2}} \quad 6.6$$

Where, y_i and $m_j(i)$ represent raw signal and the IMFs signal respectively, and $\bar{y}$, $\overline{m_j}$ represent the mean of raw and IMFs signal. The IMF is selected by the threshold value, which is determined by equation (6.7).

$$\mu_{th}=\frac{\max(CC)}{10\times\max(CC)-3} \quad 6.7$$

The IMFs are kept and treated as the most informative IMF component if the correlation coefficient is higher than the threshold μ_{th}. If not, it is eliminated as a false component. For all experimental settings, the correlation coefficient and threshold calculation results are displayed in Figure 6.5. The correlation coefficients of the IMF9-IMF12 components are not presented in Figure 6.5, since they are nearly close to zero. Using the IMFs selection criteria discussed earlier in this section, IMF1 to IMF6 for H, SW, and PT at 800 rpm is chosen as the most informative IMFs because their correlation coefficients exceed the threshold value of 0.21437. IMF1 to IMF5 for MW at 800 rpm is selected as the most informative IMF. Similarly, the IMF1 to IMF 4 for H under 800 rpm are sensitive IMFs and IMF1-IMF5 for SW, MW, and PT are the most informative IMFs. At 1100 rpm, IMF1 to IMF 4 for H are the most informative IMFs, and IMF1-IMF5 for SW, MW, and PT are the most informative IMFs.

Subsequently, the selected IMF components are summed, resulting in the generation of the enhanced signal for each gear class at various rotational speeds, including 500 rpm, 800 rpm, and 1100 rpm.

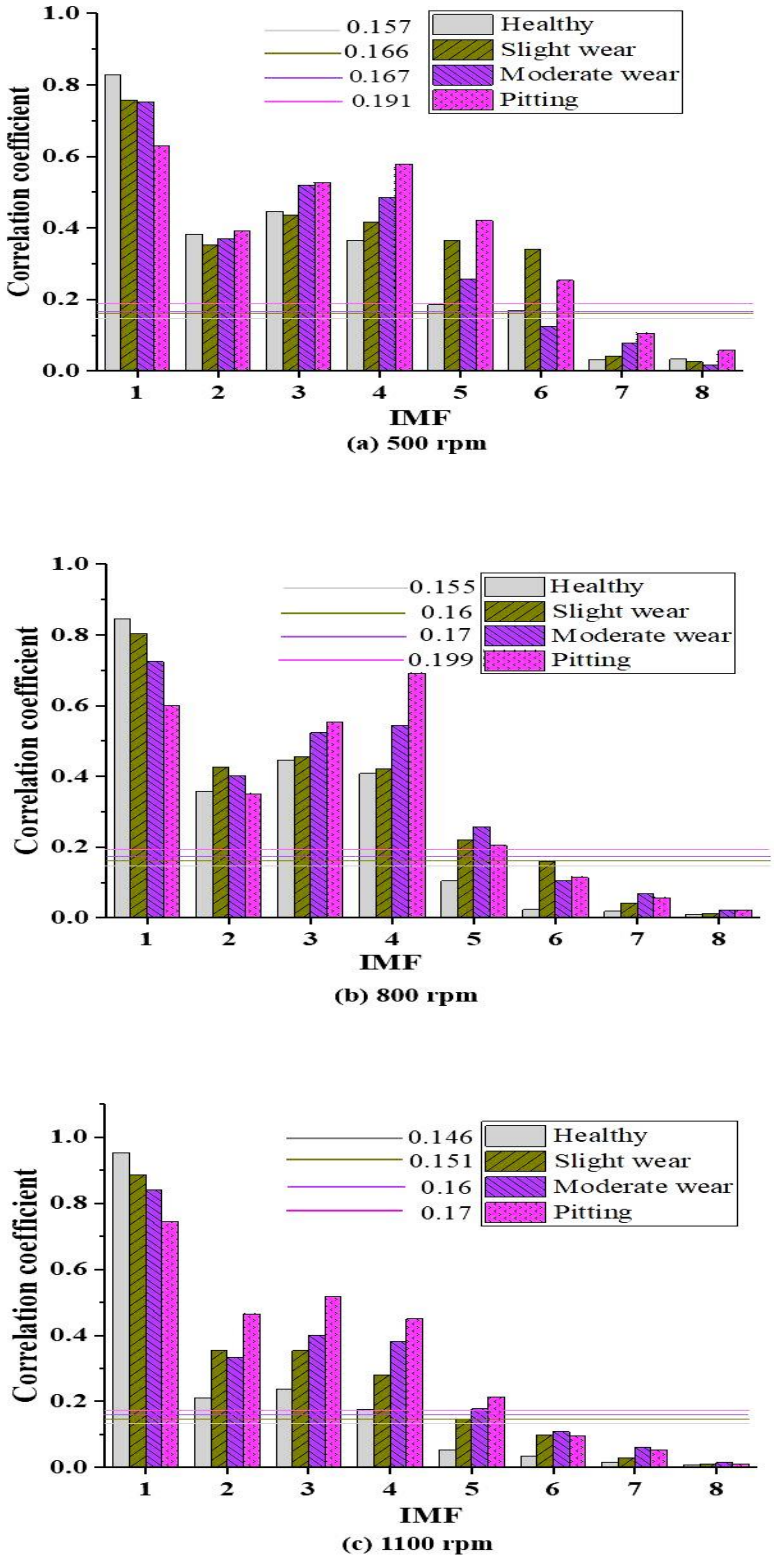

Figure 6.5 The correlation coefficient of each IMF component and the correlation coefficient threshold for different gear fault conditions.

6.3.3 Feature extraction

Feature extraction is a crucial step in machine learning, as it directly impacts the success of the trained model. In this experimental study, eleven features are extracted from the filtered vibration signal. Seven of these features are standard time-domain-based features, including RMS, kurtosis, crest factor, shape factor, standard deviation, impulse indicator, and clearance factor. These features are well-documented in Sharma and Parey [109]. Two frequency domain-based features namely mean frequency, and median frequency. The remaining two features are multiscale-based entropy features, including refined composite multiscale dispersion entropy (RCMDE), and refined composite multiscale fuzzy entropy (RCMFE).

RMS, crest factor, shape factor, and kurtosis are well defined in the previous chapter. This section only describes the rest of the features.

6.3.3.1 Standard deviation

$$\text{Standard deviation} = \left[\frac{1}{N-1} \sum_{i=1}^{N} \left(y_i - \bar{y} \right)^2 \right]^{1/2} \tag{6.8}$$

6.3.3.2 Impulse indicator

$$\text{Impulse indicator} = \frac{y_{\max}}{\bar{y}} \tag{6.9}$$

6.3.3.3 Clearance factor

$$\text{Clearance factor} = \frac{\max\left(|y_i|\right)}{\left(\frac{1}{N} \sum_{i=1}^{N} \sqrt{|y_i|} \right)^2} \tag{6.10}$$

6.3.3.4 Mean frequency

The mean frequency refers to the average frequency present in the signal and is calculated by summing the product of the power spectrum with the

corresponding frequency and dividing it by the total sum of the power intensity. The mathematical expression for mean frequency is given by [144]

$$\text{Mean frequency} = \sum_{i=1}^{M} f_i p_i \Big/ p_i \tag{6.11}$$

where P_i is the power spectrum at frequency i, M is the length of frequency and f_i is a frequency value at a frequency i.

6.3.3.5 Median frequency

The median frequency is defined as the frequency value at which the power spectrum of a signal is divided into two regions with equal integrated power. Mathematically, it can be expressed as [144]

$$\sum_{i=1}^{MDF} p_i = \sum_{i=MDF}^{M} p_i = \frac{1}{2} \sum_{i=1}^{M} p_i \tag{6.12}$$

6.3.3.6 Refined composite multiscale fuzzy entropy

The uncertainty in a system is measured by Entropy. it is particularly valuable for analyzing systems with nonlinear characteristics. Fuzzy entropy is a type of entropy commonly employed in fault diagnosis. The mathematical expression representing fuzzy entropy is written as [145]

$$\text{Fuzzy entropy} = \ln \varphi^m - \ln \varphi^{m+1} \tag{6.13}$$

$$\varphi = \frac{1}{N-m} \sum_{i=1}^{N-m} \left(\frac{1}{N-m-1} \sum_{j=1, j \neq i}^{N-m} e^{-\left(\frac{D_{ij}^n}{r}\right)} \right) \tag{6.14}$$

where N is the data in a sample, m is the embedded dimension, n is the power of fuzzy entropy, r is the tolerance, and D_{ij} is the degree of similarity calculated using a fuzzy function.

The fundamental concept underlying the application of multiscale entropy involves creating progressively coarser time series by downsampling the

original time series [145]. RCMFE is calculated based on the standard deviation (σ) and is given by [145]

$$RCMFE\left(x,m,c,d,\tau\right)=-\ln\left[\frac{\varphi_{\tau}^{1-m}}{\varphi_{\tau}^{-m}}\right] \quad 6.15$$

where embedding dimension *m*, category *c*, time delay *d*, and scale factor τ .

The specific values assigned to the parameters m, c, d, and τ are 2, 2, 1, and 0.15, respectively [145].

6.3.3.7 Refined composite multiscale dispersion entropy

RCMDE is a significantly faster entropy measure compared to other entropies such as refined composite multiscale sample entropy when it comes to quantifying the complexity of a signal. Mathematically, RCMDE is defined as follows [145]:

$$RCMDE\left(x,m,c,d,\tau\right)=-\sum_{i=1}^{c^m}\bar{p}\left(\pi_{\upsilon_0,\upsilon_1,.....\upsilon_{m-1}}\right)\cdot\ln\left(\bar{p}\left(\pi_{\upsilon_0,\upsilon_1,.....\upsilon_{m-1}}\right)\right) \quad 6.16$$

Where $\bar{p}\left(\pi_{\upsilon_0,\upsilon_1,.....\upsilon_{m-1}}\right)$ represents the mean probability that each coarse-grained sequence will exhibit a fluctuation dispersion pattern.

6.4 Deep learning models

To classify the faults, a variety of machine learning (ML) methods are used. One type of ML is deep learning. Deep learning is based on ANN that uses numerous layers of processing to extract progressively higher-level features from input. Deep learning models may be RNN, LSTM, BiLSTM, and GRU. In this present study, a novel design hybrid model LSTM-GRU is used as a classifier and compared with different designed models namely,

LSTM model, BiLSTM model, GRU model, hybrid LSTM-BiLSTM model, and BiLSTM-GRU model.

6.4.1 Long short-term memory

LSTM has been proposed by Hochreiter and Schmidhuber [146]. The main feature of LSTM is its cell state which saves and transforms the input cell memory into the output cell memory. LSTM consists of three different gates: forget gate (f_t), input gate (i_t), and output gate (o_t), which control the path of information transmission, illustrate in Figure 6.6.

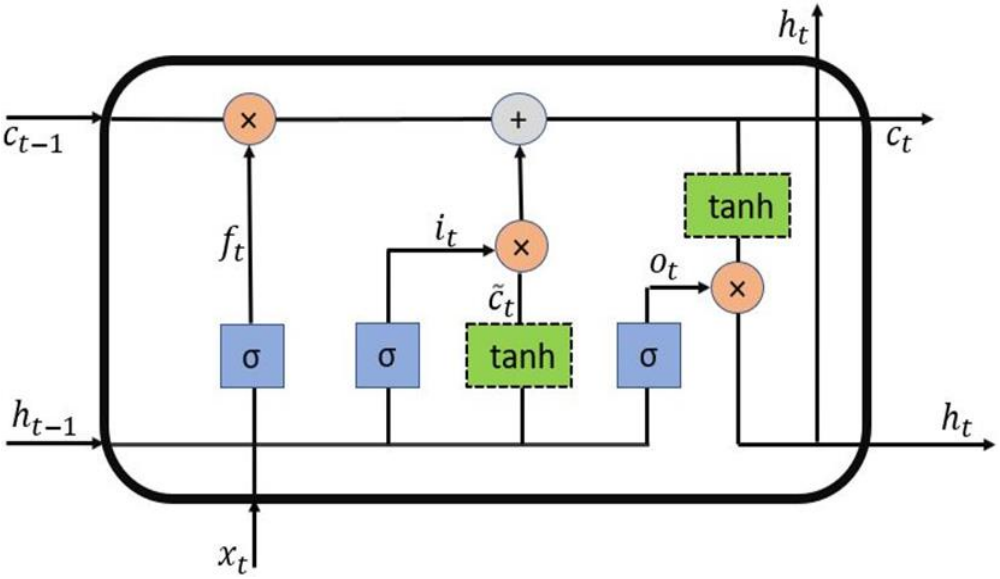

Figure 6.6 Basic structure of LSTM.

The initial stage in LSTM design should identify what data to eliminate using the data x_t and h_{t-1} as input. The activation function for these processes is the sigmoid (σ), which is employed in equation (6.17) in the forget gate layer (f_t).

$$f_t = \sigma\left(W_f * \left[h_{t-1}, x_t\right] + b_f\right) \tag{6.17}$$

In the second step, the input gate i_t is used to determine how much data must be stored at present and i_t is determined by equation (6.18). Then

the tanh function determines the information about the candidates that will make up the new information given by equation (6.19).

$$i_t = \sigma\left(W_i * \left[h_{t-1}, x_t\right] + b_i\right) \tag{6.18}$$

$$\tilde{c}_t = \tanh\left(W_c * \left[h_{t-1}, x_t\right] + b_c\right) \tag{6.19}$$

The internal variable of LSTM is c_t, which keeps track of information going back to the present, determined by the equation (6.20).

$$c_t = f_t * c_{t-1} + i_t * \tanh\left(\tilde{c}_t\right) \tag{6.20}$$

Finally, Equations (6.21) and (6.22) are used to produce the output data.

$$o_t = \sigma\left(W_o * \left[h_{t-1}, x_t\right] + b_o\right) \tag{6.21}$$

$$h_t = o_t * \tanh\left(c_t\right) \tag{6.22}$$

where the weight matrix is represented by $W_{(.)}$, and $b_{(.)}$ represents the bias term.

6.4.2 Bidirectional LSTM

The LSTM network retains only forward direction information. When processing data just in one way, there is a chance of removing important information. To address this issue BiLSTM method is used. An improved form of the LSTM network is called BiLSTM. The BiLSTM algorithm allows inputs to be processed simultaneously in two directions (forward and backward), one from the past to the future and the other from the future to the previous. Two LSTMs outputs are combined to produce the final result. Figure 6.7 depicts the BiLSTM network's organizational structure. The BiLSTM layer produces an output vector $y_{(t)}$, which is as follows:

$$h_t = \sigma_h\left(W_{t\vec{h}} x_t + W_{\vec{h}\vec{h}} \vec{h}_{t-1} + b_{\vec{h}}\right) \tag{6.23}$$

$$h_t = \sigma_h\left(W_{t\overleftarrow{h}}x_t + W_{\overleftarrow{h}\overleftarrow{h}}\overleftarrow{h}_{t-1} + b_{\overleftarrow{h}}\right) \quad 6.24$$

$$y_t = W_{\overrightarrow{t}y}\overrightarrow{h}_t + W_{\overleftarrow{t}y}\overleftarrow{h}_t + b_0 \quad 6.25$$

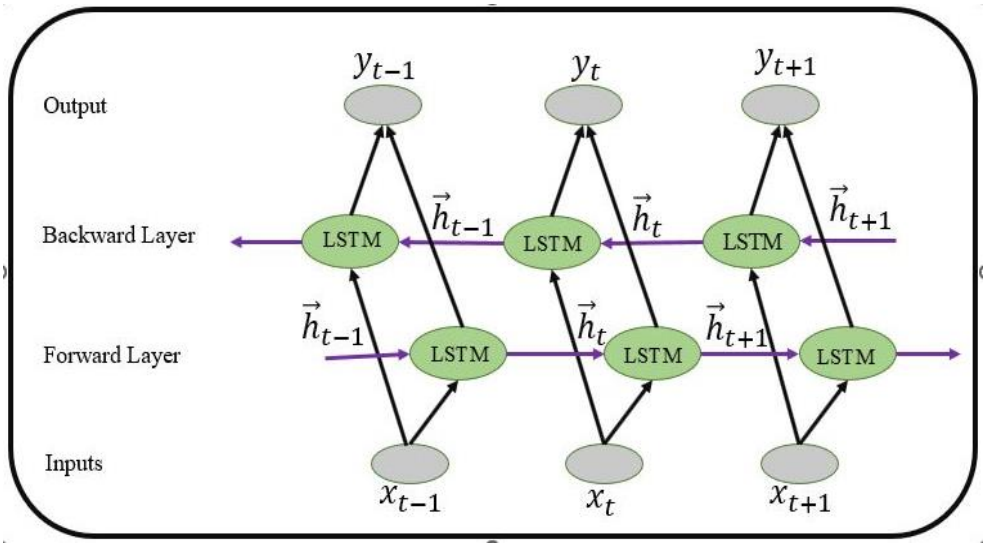

Figure 6.7 Basic structure of BiLSTM.

6.4.3 Gated recurrent unit

GRU [147] is a simplified form of the LSTM depicted in Fig. 6.8. It takes less training time and enhances network performance. The function of GRU and LSTM are similar in operation, but the architecture of GRU is different. The update gate in the GRU design combines the input gate and forget gate into one gate. GRU consists of two gates, i.e., the update gate and the reset gate. The hidden state of the GRU is represented by the equation (6.26):

$$h_t = \left(1 - z_t\right) * h_{t-1} + z_t * h_t \quad 6.26$$

The update gate, which governs how much of the GRU unit is updated, is represented by the equation (6.27):

$$z_t = \sigma\left(W_z * \left[h_{t-1}, x_t\right]\right) \quad 6.27$$

The reset gate is determined by equation (6.28):

$$r_t = \sigma\left(W_r * \left[h_{t-1}, x_t\right]\right) \quad 6.28$$

The hyperbolic tangent function of the reset gate is the new remember a gate, which is determined by Equation (6.29).

$$h_t = \tanh\left(W * \left[r_t * h_{t-1}, x_t\right]\right) \quad 6.29$$

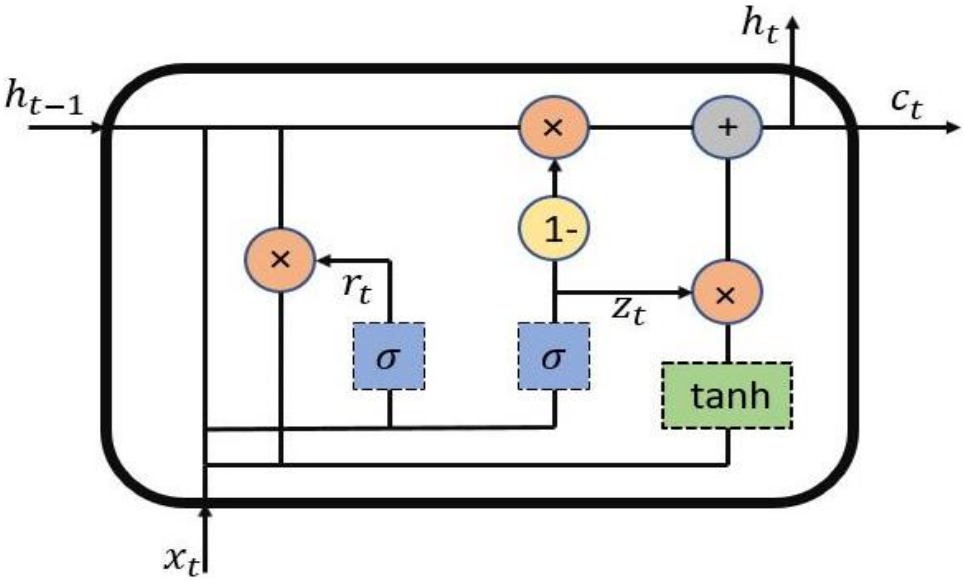

Figure 6.8 Basic structure of GRU.

6.5 Proposed LSTM-GRU model.

This study introduces a hybrid model based on LSTM-GRU for the identification of multiclass faults in polymer gears. The layout of the proposed model is depicted in Figure 6.9. The process begins by acquiring vibration signals at various speeds and at a constant torque of 2 Nm, which are then decomposed using CEEMDAN to generate multiple IMFs representing the acquired signal. In the next step, the IMFs are selected based correlation coefficient and its threshold limit and get the enhanced signal. Subsequently, features are extracted from the enhanced signal, and these feature vectors are utilized to train the classifiers. The proposed LSTM-GRU classifier (referred to as model VI) is presented in Figure 6.9.

Model VI is constructed by incorporating a single layer of the LSTM classifier and a single layer of the GRU classifier. The decision to limit the number of layers is based on the observation that increasing the layer count unnecessarily leads to complex networks that are prone to overfitting. A dropout layer with a rate of 20 percent is inserted before the second layer to mitigate overfitting risks. Within the network, the fully connected layer is connected to a hidden layer using the SoftMax activation function, facilitating the classification process. The cross-entropy loss, calculated by the classification layer, is employed in the optimization process to update the network weights. For optimization, the adaptive moment estimation (Adam) optimizer is selected with a learning rate of 0.001. Adam adjusts the learning rate for each weight parameter individually, which helps in faster convergence and better generalization. The proposed classifier's performance is evaluated by comparing it with other designed networks, specifically models I, II, III, IV, and V, as depicted in Figure 6.9.

The network is built using the deep network designer tool in MATLAB 2022b. Additionally, a comparative study is carried out for fault classification at different rotational speeds: 500 rpm, 800 rpm, 1100 rpm, and fused conditions. Fused conditions refer to a scenario in which the model was trained using combined feature sets extracted from all speeds, namely 500 rpm, 800 rpm, and 1100 rpm.

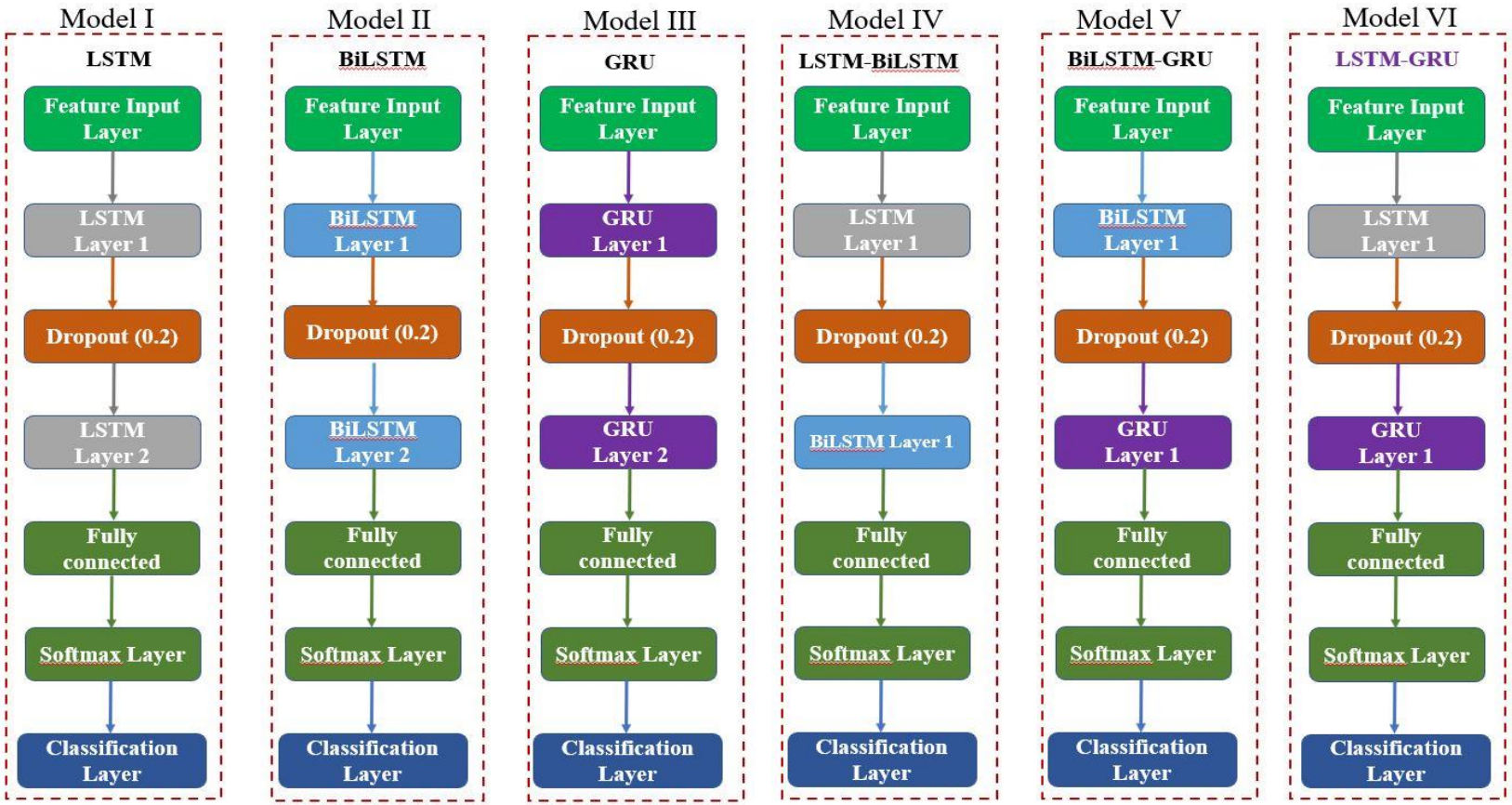

Figure 6.9 Various design models for deep learning for fault detection of polymer gears.

6.6 Results and discussion

The main objective of this study is to identify the optimal model for accurately and efficiently detecting PG faults. To assess the models performance, a confusion matrix is employed as the standard decision-making tool. Various metrics, including accuracy, F1 score, and Kappa, are extracted from the confusion matrix to evaluate the models performance [148]. Equations (6.30) to (6.34) describe these metrics in detail. Accuracy reflects the proximity of the predicted values to the actual values during multiple iterations over the same dataset, without any errors. The F1 score represents the harmonic mean of recall and precision, striking a balance between the two. Recall, also known as the true positive rate, quantifies the proportion of correctly classified instances (TP) to the total number of instances (TP + FN) within the same class. Precision calculates the ratio of correctly predicted samples to the total number of predicted samples for a particular class. Kappa is a measure of the agreement between predicted and actual class labels in a confusion matrix.

$$Accuracy = \frac{TP+TN}{TP+TN+FP+FN} \tag{6.30}$$

$$F1\,Score = 2\times\left(\frac{Precision\times Recall}{Precision+Recall}\right) \tag{6.31}$$

$$Precision = \frac{TP}{TP+FP} \tag{6.32}$$

$$\mathrm{Re}call = \frac{TP}{TP+FN} \tag{6.33}$$

$$Kappa = \frac{\frac{TP+TN}{TP+TN+FP+FN} - \frac{(TP+FP)(TN+FN)+(FN+TP)(FP+TP)}{(TP+TN+FP+FN)^2}}{1-\frac{(TP+FP)(TN+FN)+(FN+TP)(FP+TP)}{(TP+TN+FP+FN)^2}} \tag{6.34}$$

where FP represents false positives (incorrectly anticipated positive instances), FN stands for false negatives (incorrectly forecasted negative cases), TP stands for true positive (correctly predicted positive cases), and TN is for true negative (correctly predicted negative cases) (incorrectly predicted negative cases)

In this study, multiple models were trained using feature vectors extracted from different speed conditions and at a constant torque of 2 Nm. The dimension of the feature vector for 500 rpm, 800 rpm, and 1100 rpm is 800×11 separately, while the dimension for the fused condition is 2400×11. The feature vector is then randomly split, with 70% of the datasheet being used for training and 30% for testing. To ensure a fair comparison, constant hyperparameter values were maintained across all six classifiers during training. The hyperparameter values are presented in Table 6.2.

Table 6.2 Configuration of the hyperparameters.

Parameter	Value
Optimizer	Adam
Number of epochs	100
Minibatch size	16
Learning rate	0.001

6.6.1 Analysis of the various designed models under different speeds and at a constant torque condition

Table 6.3 presents the experimental results and performance comparison of the proposed model and different design models at 500 rpm speed and 2 Nm torque. Figure 6.10 provides a visual representation of these results. The hybrid model LSTM-GRU exhibited the highest performance parameter value compared to other design models, as demonstrated in Figure 6.10 (a). Models I, II, and III had lower accuracy than hybrid models IV, V, and VI. The proposed model achieved a maximum accuracy of 99.6%, which is

3.53% higher than the LSTM model, 2.15% higher than the BiLSTM model, and 2.57% higher than the GRU model. Figure 6.10 (a) also demonstrates that the BiLSTM-based model performs significantly better than the LSTM-based model. This is because the BiLSTM utilizes information in two ways, both from past to feature and from feature to past, whereas the LSTM only relies on information from previous inputs. On the other hand, the BiLSTM model consumes the maximum computational time for fault classification.

The experimental outcomes of the proposed model and other designed models at 800 rpm speed and 2 Nm torque are summarized in Table 6.4, while the performance comparison is presented in Figure 6.11. In Figure 6.11 (a), it is evident that the proposed hybrid model LSTM-GRU achieves higher accuracy (99.58%), F1 Score (99.6), and Kappa (98.89%) values compared to the other designed networks.

The proposed LSTM-GRU model demonstrates a maximum accuracy of 99.6%, which is 1.7% higher than that of the LSTM model, 0.8% higher than that of the BiLSTM model, and 1.26% higher than that of the GRU model. The computational time for training the different designed networks is displayed in Figure 6.11(b).

Table 6.3 The values of classifiers' performance parameters and computational time at 500 rpm speed and 2 Nm torque.

Model	Accuracy (%)	F1 Score (%)	Kappa (%)	Computational time (s)
I (LSTM)	96.2	96.3	90	27
II (BiLSTM)	97.5	97.4	93.33	48
III (GRU)	97.1	97	92.2	26
IV (LSTM-BiLSTM)	98.8	98.7	96.67	33
V (BiLSTM-GRU)	97.91	97.9	94.5	31
VI (LSTM-GRU)	99.6	99.6	98.89	24

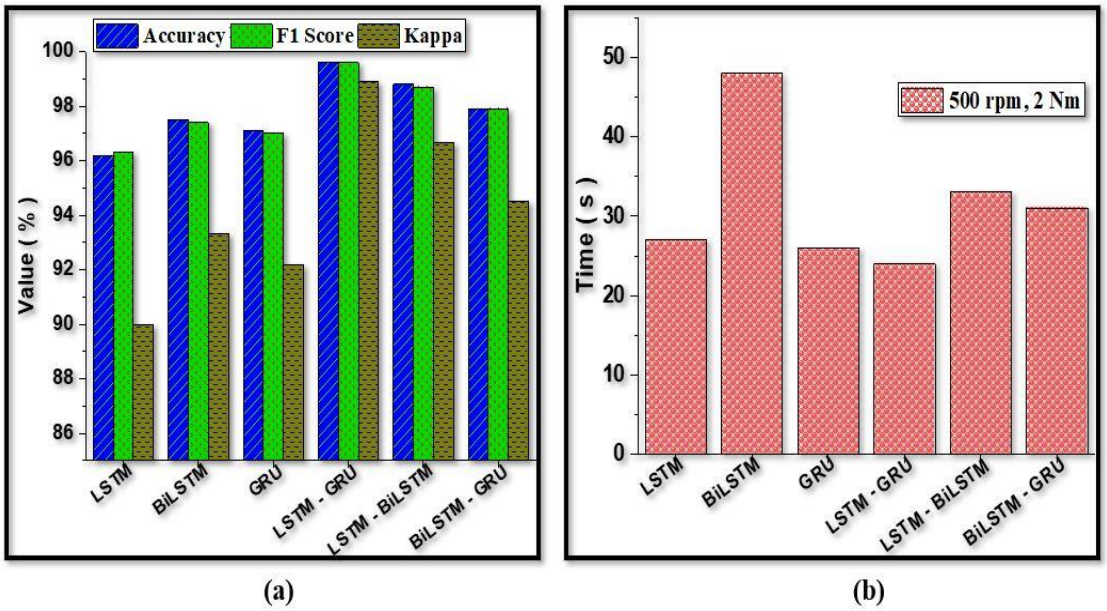

Figure 6.10 Comparison between different classifiers at 500 rpm speed and 2 Nm torque, (a) performance, and (b) computational time.

As depicted, the proposed model requires less computing time compared to other designed models. This indicates its efficiency in the training process. Table 6.5 presents the experimental results of the proposed LSTM-GRU approach and a performance comparison with alternative design models at a rotational speed of 1100 rpm and a torque of 2 Nm. The corresponding performance comparison is illustrated in Figure 6.12. Figure 6.12 (a) reveals that the hybrid LSTM-GRU model outperforms the other designed models. In terms of accuracy, the suggested LSTM-GRU model achieves the highest value of 99.16% compared to the other design models. Similarly, it demonstrates superior performance in terms of F1 Score (99.19%) and Kappa (97.8%) compared to alternative design models. Figure 6.12 (b) displays the computational time comparisons between different classifiers. It provides insights into the relative efficiency of each classifier in terms of computational time.

Table 6.4 The values of classifiers' performance parameters and computational time under 800 rpm speed and 2 Nm torque.

Model	Accuracy (%)	F1 Score (%)	Kappa (%)	Computational time (s)
LSTM	97.92	97.9	94.5	28
BiLSTM	98.78	98.8	96.67	43
GRU	98.34	98.36	95.56	28
LSTM-BiLSTM	99.16	99.16	97.8	32
BiLSTM-GRU	98.75	98.8	96.67	31
LSTM-GRU	99.58	99.6	98.89	27

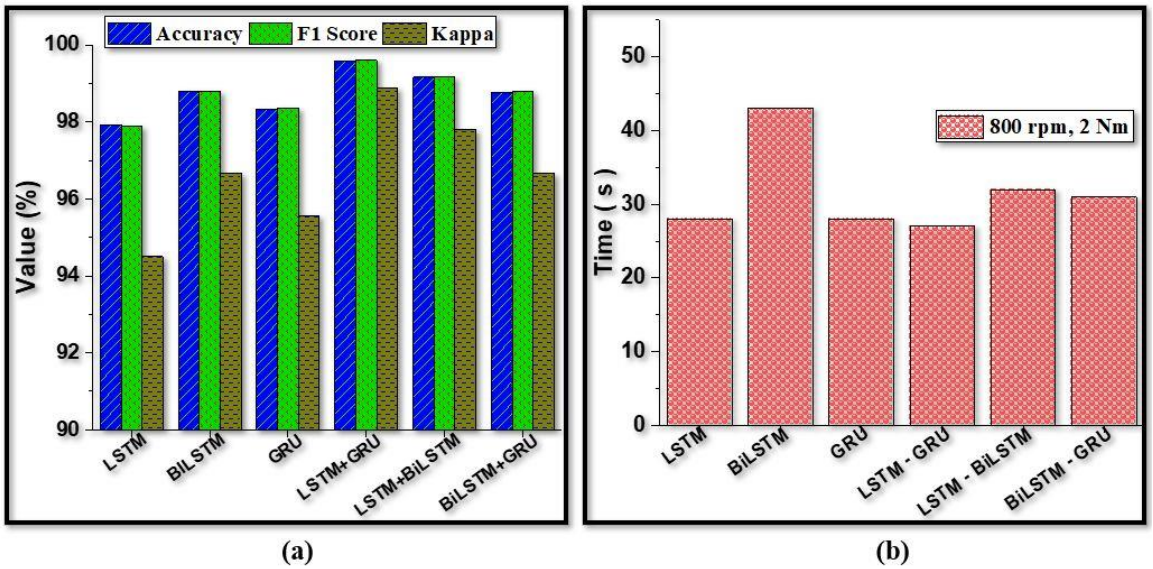

Figure 6.11 Comparison between different classifiers at 800 rpm speed and 2 Nm torque, (a) performance and (b) computational time

Overall, the experimental results and performance comparisons highlight the superiority of the proposed LSTM-GRU approach in terms of accuracy, F1-Score, and Kappa, as well as its lower computational efficiency.

Table 6.5 The values of classifiers' performance parameters and computational time at 1100 rpm speed and 2 Nm torque.

Model	Accuracy (%)	F1 Score (%)	Kappa (%)	Computational time (s)
LSTM	97.5	97.2	93.34	26
BiLSTM	98.33	98.31	95.6	44
GRU	97.92	97.91	94.5	25
LSTM-BiLSTM	98.75	98.7	96.7	31
BiLSTM-GRU	98.34	98.3	95.56	31
LSTM-GRU	99.16	99.19	97.8	24

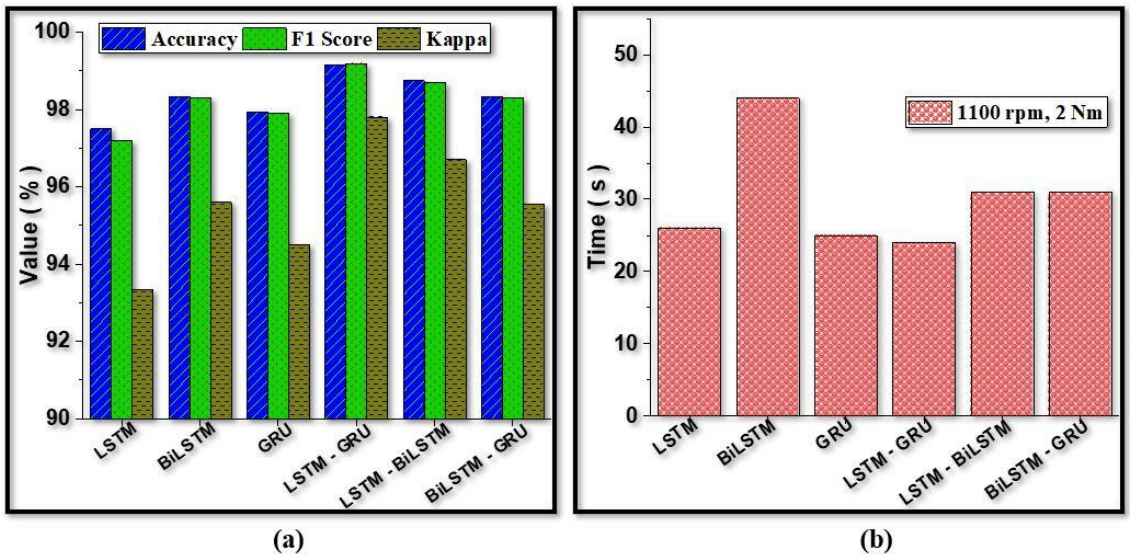

Figure 6.12 Comparison between different classifiers at 1100 rpm speed and 2 Nm torque, (a) performance and (b) computational time

To develop a speed-independent diagnosis model, the recorded vibration signals from different speeds are fused in a consolidated manner and utilized for model training. The experimental results, including accuracy, F1-Score, and Kappa, of the proposed LSTM-GRU model and a performance comparison with other design models, are presented in Table 6.6. These findings are also visualized in Figure 6.13.

Table 6.6 The values of classifiers' performance parameters and computational time under fused conditions.

Model	Accuracy (%)	F1 Score (%)	Kappa (%)	Computational time (s)
LSTM	94.8	94.8	86.3	69
BiLSTM	95.8	95.8	88.9	149
GRU	95.6	95.7	88.5	84
LSTM-BiLSTM	96.52	96.54	90.1	104
BiLSTM-GRU	96.11	96	89.6	98
LSTM-GRU	97.9	97.9	94.4	77

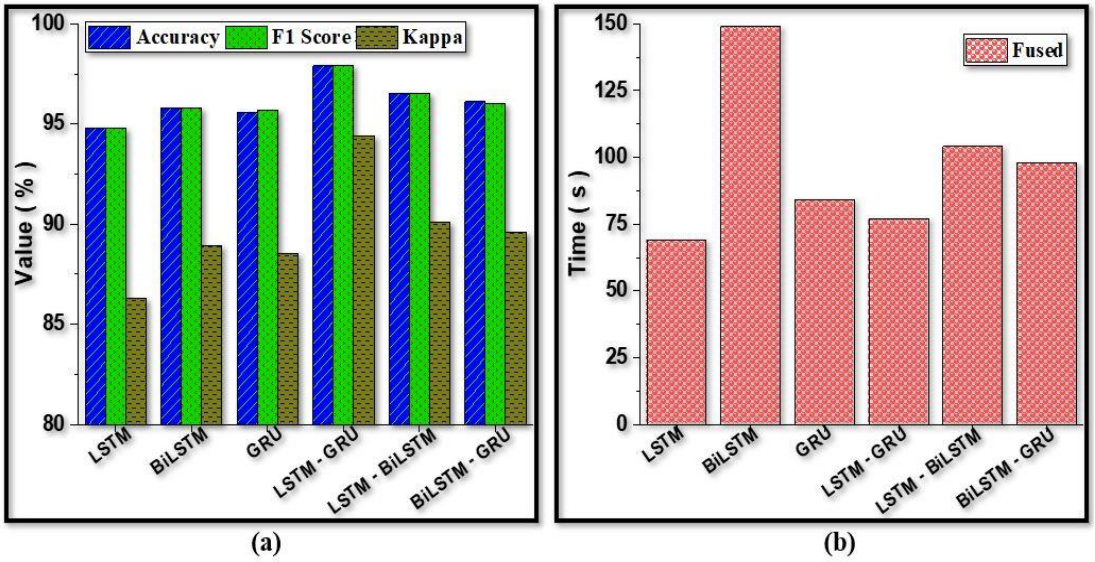

Figure 6.13 Comparison between different classifiers under fused condition, (a) performance and (b) computational time

The accuracy and F1 Score values are relatively consistent among the designed models, with the proposed model attaining a maximum accuracy and F1-Score of 97.9%. The LSTM model exhibits the lowest accuracy of 94.8%. Moreover, the Kappa value of the proposed model (94.4) is higher than that of the LSTM (9.38%), BiLSTM (6.2%), GRU (6.7%), LSTM-

BiLSTM (4.8%), and BiLSTM-GRU (5.3%) models. Figure 6.13 (b) presents the computational time of all designed networks. The BiLSTM network requires the highest computational time of 2 minutes and 48 seconds, while the proposed LSTM-GRU network exhibits the minimum computational time of 1 minute and 28 seconds. All experiments were conducted on a Dell desktop equipped with an Intel (R) Core (TM) i7-10700 processor with a clock rate of 2.90 GHz and 128 gigabytes of RAM.

The total classification accuracy does not give a more realistic view of the accuracy of each class. As a result, the confusion matrices are examined. Figure 6.14 illustrates the four confusion matrices for the proposed LSTM-GRU model at different rotational speeds. In each confusion matrix, the numbers within the rectangles indicate the number of tests. A blue rectangle indicates the correct identification of the four health conditions of polymer gears, namely H, SW, MW, and PT faults. A light blue rectangle indicates incorrect identification of at least one of these health categories. Figure 6.14 (a) reveals that out of 240 tests, 239 (99.58%) are accurately classified. The H, SW, and MW fault classes are correctly identified, while there is one misclassification (0.42%) for the PT fault class. In the second case (800 rpm at 2 Nm), as shown in Figure 6.14 (b), 239 out of 240 tests (99.58%) are correctly classified. The H, SW, and PT fault classes are accurately identified, while the MW fault class is misclassified. For the third case (1100 rpm at 2 Nm), depicted in Figure 6.14 (c), 238 out of 240 tests (99.16%) are classified correctly. The MW and PT fault classes are correctly identified, but there are misclassifications for 2 tests (0.84%) in the H and MW fault classes. Regarding the fused class, as presented in Figure 6.14 (d), 705 out of 720 tests (97.9%) are accurately classified.

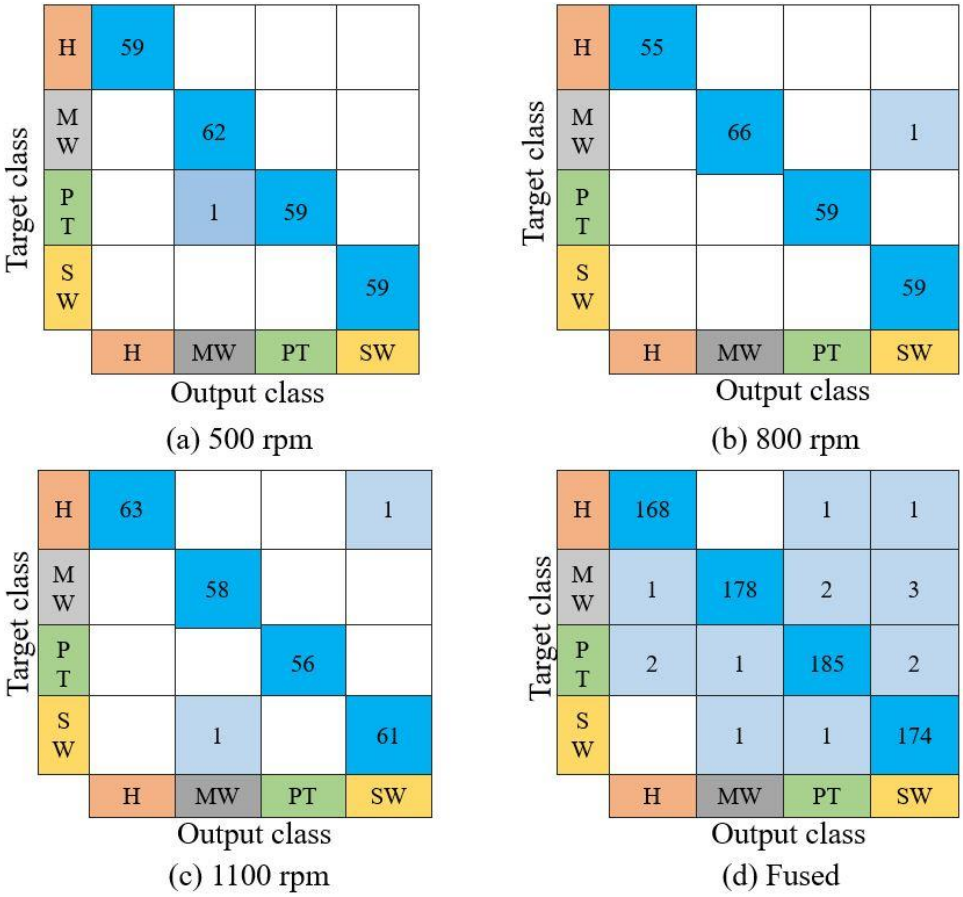

Figure 6.14 Confusion matrixes for proposed model LSTM-GRU at different speeds and a constant torque of 2 Nm.

6.6.2 Validation with other algorithms

The primary aim of this research is to develop a speed-independent model. To achieve this, the proposed hybrid LSTM-GRU model is trained using fused data, and its classification accuracy is compared against other traditional machine learning techniques. To validate the effectiveness of the proposed hybrid LSTM-GRU model, six different traditional classifiers (KNN, ensemble bagged tree (EBT), DT, SVM, linear discriminant analysis (LDA), and naive Bayes (NB)) are employed using the same fused data. Table 6.7 presents the classification accuracy of the suggested hybrid LSTM-GRU model and the six traditional classifiers. The results

demonstrate that the hybrid LSTM-GRU model outperforms the other classifiers in terms of classification accuracy for the multiclass fault detection of polymer gears. These findings highlight the ability of the proposed model to accurately identify multiclass faults in polymer gears.

Table 6.7 Overall classification accuracy of different classifiers.

Classifiers	LSTM-GRU	KNN	EBT	DT	SVM	LDA	NB
Accuracy (%)	97.9	95.4	95.3	93.5	87.9	84.6	80.1

6.6.3 Comparison of proposed work with previous studies

The comparison study between the proposed approach and previously published work is presented in Table 6.8. Analysis of the table reveals that the features extracted using the CEEDMAN-based method outperform other existing methods in terms of performance. Specifically, the proposed method achieves an accuracy of 99.6% in individual conditions and more than 97% in fused conditions. These results highlight the effectiveness of the proposed method in achieving high accuracy in fault classification.

Table 6.8 Comparison of the proposed study classification accuracy with existing works.

Proposed/Existing work	Features	Speed (rpm)	Classifier	Accuracy (%)
Ramteke et al.[149]	Statistical features extracted from FAWT	Fused	LS-SVM	58
Dalian et al. [150]	Features are extracted from EEMD	360	ABC-SVM	94.33
Li et al. [77]	Features are extracted from raw vibration signals	1500	BiLSTM	94
Wang et al. [151]	Features extracted from CCEMDAN	863	CCMEDAN-LSTM	99.5
Proposed work	Features extracted from enhanced signal	500 and 800	LSTM-GRU	99.6
Proposed work	Features extracted from enhanced gear signal	Fused	LSTM-GRU	97.9

*Artificial bee colony algorithm (ABC).

6.7 Conclusions

A hybrid deep learning model that is independent of rotational speed has been developed and tested for multiclass fault detection in polymer gears. The model utilizes LSTM-GRU neural networks within its framework. The complete design and implementation of the model have been presented in this study.

To extract features from the vibration signal, a method called CEEMDAN is employed, which decomposes the signal and applies a sensitive IMF selection method to obtain filtered signals. This facilitates effective feature extraction.

Among the designed models, the proposed LSTM-GRU (model VI) demonstrates superior performance. It achieves the highest classification accuracy, F1-score, and Kappa values of 99.6%, 99.6%, and 98.89% respectively.

Additionally, it exhibits the least computational time compared to the other designed models. On the other hand, model I displays the lowest performance parameters among the design models, while model II has the maximum computational time among the alternatives.

In addition to the proposed design model VI, six traditional machine learning techniques were also investigated and compared. Among these techniques, KNN achieved the highest accuracy. However, the accuracy of the proposed model surpassed that of KNN by 2.5%.

When comparing the results of this study with previous studies that utilized various methodologies, it becomes evident that the proposed model VI is particularly well-suited for fault detection.

The experimental findings strongly demonstrate the effectiveness of the proposed fault diagnosis model in accurately identifying faults of PGs.

Chapter 7

Conclusions and future scope

7.1 Conclusions

Polymer gears have gained significant attention as a viable substitute for conventional metal gears across diverse applications. Extensive research has been conducted in recent decades to explore different design aspects and tooth modification techniques, aiming to enhance the performance and durability of polymer gears. However, the impact of tooth modification on critical properties such as noise and vibration in polymer gears has not been thoroughly investigated. Furthermore, there is a notable absence of studies focused on fault detection techniques for polymer gears, which is crucial for preventing catastrophic failures.

This thesis encompasses two main research aspects related to polymer gears. The first aspect focuses on investigating the influence of teeth modification on vibration and noise emission in polymer gears. Two distinct types of polymer pinion teeth modifications were developed and tested under various speed and load conditions. A comparative analysis was conducted between these modified gears, unmodified gears, and gears paired with steel and polymer counterparts.

The second aspect of this thesis addresses the development of fault detection methods specifically tailored for polymer gears. Several techniques were proposed, including signal processing-based fault detection, machine learning approaches, and deep neural network-based condition monitoring. Vibration signals were acquired from polymer gears under different speeds and load conditions for fault detection purposes. One of the proposed methods involves kurtosis-based VMD and its performance was compared against kurtosis-based EMD and raw signal-based techniques.

Another significant contribution of this thesis lies in the development of machine learning-based condition monitoring techniques. Classifiers such as KNN, SVM, and LDA were trained using different sets of features derived from decomposed signals (EMD and EWT), namely SF, HP, and a combination of SF and HP. The fault classifications of these algorithms were compared. Additionally, a double decomposition-based method was devised to extract feature sets EF, HP, and a combination of EF and HP. These feature sets were employed to train models such as SVM, ensemble learning, and decision tree, and their effectiveness in predicting polymer gear fault classification was evaluated. Furthermore, a novel hybrid deep neural network (LSTM-GRU) was developed utilizing CEEMDAN for polymer gear fault classification.

Based on the findings of this study, the following key conclusions can be drawn:

- The vibration and noise levels increase with an increase in rotational speed and a slight increase in torque for all tested gear pairs. Comparatively, the modified gear pairs exhibit slightly higher levels of noise and vibration in comparison to the unmodified gear pairs.
- Among the modified gear designs, the gear with a hole consistently demonstrates the highest levels of noise and vibration across all operating conditions when compared to the modified gear with a steel pin.
- Under all experimental conditions, the proposed method of kurtosis based VMD outperforms fault detection in polymer gears.
- Furthermore, the CIs extracted from kurtosis-based VMD exhibit good performance in detecting gear faults as compared to CIs extracted from raw signal and kurtosis-based EMD.
- The utilization of KNN-based classification techniques proves effective in detecting faults in polymer gears by utilizing feature sets derived from EWT-based decomposition signals. The introduction

of SF and HP feature sets enhances the classification performance of the model. However, the LDA algorithm consistently exhibits lower classification accuracy across all combinations of feature sets explored in the study.

- The ensemble classifier utilizing EMD-DWT exhibited higher accuracy in classification, whereas SVM showed comparatively lower accuracy.
- The feature sets derived from EMD demonstrated lower accuracy for classifying faults in polymer gears compared to those derived from DWT.
- Six different deep learning models were developed and evaluated for the multiclass fault detection of polymer gears using LSTM-GRU neural networks. CEEMDAN was employed to decompose the vibration signal and extract features using a sensitive IMF selection method. The results demonstrated that the hybrid LSTM-GRU model outperformed the other designed models in terms of both performance and computational time.
- Furthermore, the hybrid model was compared to various traditional machine learning models, and it was found that the hybrid model exhibited superior performance compared to traditional machine learning models.

7.2 Future scopes

- This research can be extended to encompass other polymer gear types, including helical and worm gears, to broaden the scope of fault detection. Additionally, a comparative analysis could be conducted to assess the classification accuracy of polymer spur gears compared to these other polymer gear variants.
- Consider expanding the thesis by investigating the classification of polymer gear faults using noise signals instead of vibration signals,

utilizing the classification models developed in this work. Furthermore, perform a comparative analysis to evaluate the classification accuracy between vibration and noise signal-based approaches.

- Expand the research's horizons by exploring a wider range of fault classes in polymer spur gears. This extension would involve developing methods to accurately classify a broader spectrum of faults, thereby enhancing the comprehensive health monitoring of these systems.
- To enhance the model's performance and address the common issue of imbalanced data in fault classification problems. Investigate various techniques, such as oversampling and under-sampling, to mitigate the impact of imbalanced datasets on classification accuracy.
- Explore the influence of different polymer gear materials on vibration and noise signals. Analyze how different material properties affect the signals and, in turn, their impact on the accuracy of fault classification.
- Evaluate the proposed methodology's performance by applying it to real operational polymer gear datasets. This step will provide practical insights into the effectiveness of the developed classification models in real-world industrial settings.
- This methodology can be extended to developing a system-level fault identification technique.

REFERENCES

[1] Maitra GM. Handbook of gear design. Tata McGraw-Hill Publ Co Ltd 1994;16:536.

[2] Karimpour M, Dearn KD, Walton D. A kinematic analysis of meshing polymer gear teeth. Proc Inst Mech Eng Part L J Mater Des Appl 2010;224:101–15. https://doi.org/10.1243/14644207JMDA315.

[3] Pogačnik A, Tavčar J. An accelerated multilevel test and design procedure for polymer gears. Mater Des 2015;65:961–73. https://doi.org/10.1016/j.matdes.2014.10.016.

[4] Baxter JW, Bumby JR. A comparison of ratings for plastic gears. Proc Inst Mech Eng Part C J Mech Eng Sci 1989;203:31–8. https://doi.org/10.1243/PIME.

[5] Smith Z, Ulrich A. Exploiting the Potential of Plastic Gears. Gear Solut 2012;10:40–7.

[6] Dearn KD, Hoskins TJ, Andrei L, Walton D. Lubrication regimes in high-performance polymer spur gears. Adv Tribol 2013;2013. https://doi.org/10.1155/2013/987251.

[7] Hoskins TJ, Dearn KD, Chen YK, Kukureka SN. The wear of PEEK in rolling-sliding contact - Simulation of polymer gear applications. Wear 2014;309:35–42. https://doi.org/10.1016/j.wear.2013.09.014.

[8] Hasl C, Illenberger C, Oster P, Tobie T, Stahl K. Potential of oil-lubricated cylindrical plastic gears. J Adv Mech Des Syst Manuf 2018;12:1–9. https://doi.org/10.1299/jamdsm.2018jamdsm0016.

[9] Snyder L. At the “PEEK” of the Polymer Food Chain. Gear Technol June 2010:26–8.

[10] Mao K, Li W, Hooke CJ, Walton D. Friction and wear behaviour of

acetal and nylon gears. Wear 2009;267:639–45. https://doi.org/10.1016/j.wear.2008.10.005.

[11] Singh AK, Siddhartha, Singh PK. Polymer spur gears behaviors under different loading conditions: A review. Proc Inst Mech Eng Part J J Eng Tribol 2018;232:210–28. https://doi.org/10.1177/1350650117711595.

[12] Lu Z, Liu H, Zhu C, Song H, Yu G. Identification of failure modes of a PEEK-steel gear pair under lubrication. Int J Fatigue 2019;125:342–8. https://doi.org/10.1016/j.ijfatigue.2019.04.004.

[13] Illenberger CM, Tobie T, Stahl K. Flank load carrying capacity of oil-lubricated high performance plastic gears: Analysis of the pitting development in back-to-back tests. Forsch Im Ingenieurwesen/Engineering Res 2019;83:545–52. https://doi.org/10.1007/s10010-019-00332-x.

[14] Kim CH. Durability improvement method for plastic spur gears. Tribol Int 2006;39:1454–61. https://doi.org/10.1016/j.triboint.2006.01.020.

[15] Senthilvelan S, Gnanamoorthy R. Effect of gear tooth fillet radius on the performance of injection molded Nylon 6/6 gears. Mater Des 2006;27:632–9. https://doi.org/10.1016/j.matdes.2004.12.015.

[16] Jayaswal P, Wadhwani AK, Mulchandani KB. Machine fault signature analysis. Int J Rotating Mach 2008;2008. https://doi.org/10.1155/2008/583982.

[17] A. Davies. Handbook of Condition Monitoring: Techniques and Methodology. 1998.

[18] R. Keith Mobley. An introduction to predictive maintenance. vol. 42. 2002.

[19] Rao S. S. Mechanical vibrations. vol. 9781461404. 2012.

https://doi.org/10.1007/978-1-4614-0460-6.

[20] Ebersbach S, Peng Z, Kessissoglou NJ. The investigation of the condition and faults of a spur gearbox using vibration and wear debris analysis techniques. Wear 2006;260:16–24. https://doi.org/10.1016/j.wear.2004.12.028.

[21] Lebold M, Mcclintic K, Campbell R, Byington C, Maynard K. Review of vibration analysis methods for gearbox diagnostics and prognostics. 54th Meet Soc Mach Fail Prev Technol 2000:623–34.

[22] Eftekharnejad B, Mba D. Seeded fault detection on helical gears with acoustic emission. Appl Acoust 2009;70:547–55. https://doi.org/10.1016/j.apacoust.2008.07.006.

[23] Elforjani M, Mba D. Detecting natural crack initiation and growth in slow speed shafts with the Acoustic Emission technology. Eng Fail Anal 2009;16:2121–9. https://doi.org/10.1016/j.engfailanal.2009.02.005.

[24] Henriquez P, Alonso JB, Ferrer MA, Travieso CM. Review of automatic fault diagnosis systems using audio and vibration signals. IEEE Trans Syst Man, Cybern Syst 2014;44:642–52. https://doi.org/10.1109/TSMCC.2013.2257752.

[25] Bellini A, Immovilli F, Rubini R, Tassoni C. Diagnosis of bearing faults in induction machines by vibration or current signals: A critical comparison. Conf Rec - IAS Annu Meet (IEEE Ind Appl Soc 2008;46:1350–9. https://doi.org/10.1109/08IAS.2008.26.

[26] McFadden PD. Detecting fatigue cracks in gears by amplitude and phase demodulation of the meshing vibration. J Vib Acoust Trans ASME 1986;108:165–70. https://doi.org/10.1115/1.3269317.

[27] Wang W. Early detection of gear tooth cracking using the resonance demodulation technique. Mech Syst Signal Process 2001;15:887–

903. https://doi.org/10.1006/mssp.2001.1416.

[28] Baydar N, Ball A. Detection of gear deterioration under varying load conditions by using the instantaneous power spectrum. Mech Syst Signal Process 2000;14:907–21. https://doi.org/10.1006/mssp.1999.1281.

[29] Sawalhi N, Randall RB. Gear parameter identification in a wind turbine gearbox using vibration signals. Mech Syst Signal Process 2014;42:368–76. https://doi.org/10.1016/j.ymssp.2013.08.017.

[30] Pandya Y, Parey A. Failure path based modified gear mesh stiffness for spur gear pair with tooth root crack. Eng Fail Anal 2013;27:286–96. https://doi.org/10.1016/j.engfailanal.2012.08.015.

[31] Shen C-H, Wen J, Arunyanart P, Choy FK. Vibration Signature Analysis and Parameter Extractions on Damages in Gears and Rolling Element Bearings. ISRN Mech Eng 2011;2011:1–10. https://doi.org/10.5402/2011/402928.

[32] Mark WD, Reagor CP. Static-transmission-error vibratory-excitation contributions from plastically deformed gear teeth caused by tooth bending-fatigue damage. Mech Syst Signal Process 2007;21:885–905. https://doi.org/10.1016/j.ymssp.2006.05.002.

[33] Hu C, Smith WA, Randall RB, Peng Z. Development of a gear vibration indicator and its application in gear wear monitoring. Mech Syst Signal Process 2016;76–77:319–36. https://doi.org/10.1016/j.ymssp.2016.01.018.

[34] E. E. Shipley. Gear failures. Mach Des 1967:1–8. https://doi.org/10.1016/b978-075065154-7/50107-8.

[35] Bajrić R, Sprečić D, Zuber N. Review of vibration signal processing techniques towards gear pairs damage identification. Int J Eng Technol IJET-IJENS 2011;11:124–8.

[36] Nie M, Wang L. Review of condition monitoring and fault diagnosis technologies for wind turbine gearbox. Procedia CIRP 2013;11:287–90. https://doi.org/10.1016/j.procir.2013.07.018.

[37] Giurgiutiu V, Cuc A, Goodman P. Review of Vibration-Based Helicopters Health and Usage. Prevention 2001:1–10.

[38] Samuel PD, Pines DJ. A review of vibration-based techniques for helicopter transmission diagnostics. vol. 282. 2005. https://doi.org/10.1016/j.jsv.2004.02.058.

[39] Lei Y, Lin J, Zuo MJ, He Z. Condition monitoring and fault diagnosis of planetary gearboxes: A review. Meas J Int Meas Confed 2014;48:292–305. https://doi.org/10.1016/j.measurement.2013.11.012.

[40] Randall RB. A new method of modeling gear faults. J Mech Des Trans ASME 1982;104:259–67. https://doi.org/10.1115/1.3256334.

[41] Mcfadden p. d., Smith j. d. A signal processing technique for detecting local defects in a gear from the signal average of the vibration. Proc Inst Mech Eng Part C J Mech Eng Sci 1985;199:287–92. https://doi.org/10.1243/PIME_PROC_1985_199_125_02.

[42] Bonnardot F, El Badaoui M, Randall RB, Danière J, Guillet F. Use of the acceleration signal of a gearbox in order to perform angular resampling (with limited speed fluctuation). Mech Syst Signal Process 2005;19:766–85. https://doi.org/10.1016/j.ymssp.2004.05.001.

[43] Elasha F, Greaves M, Mba D, Fang D. A comparative study of the effectiveness of vibration and acoustic emission in diagnosing a defective bearing in a planetry gearbox. Appl Acoust 2017;115:181–95. https://doi.org/10.1016/j.apacoust.2016.07.026.

[44] Lu B, Li Y, Wu X, Yang Z. A review of recent advances in wind

turbine condition monitoring and fault diagnosis. 2009 IEEE Power Electron Mach Wind Appl PEMWA 2009 2009. https://doi.org/10.1109/PEMWA.2009.5208325.

[45] Parey A, Tandon N. Impact velocity modelling and signal processing of spur gear vibration for the estimation of defect size. Mech Syst Signal Process 2007;21:234–43. https://doi.org/10.1016/j.ymssp.2005.12.011.

[46] Decker HJ, Lewicki DG. Spiral Bevel Pinion Crack Detection in a Helicopter Gearbox. Nasa Tm-2003-212327 Arl-Tr-2958 2003:16.

[47] Mcfadden PD. A revised model for the extraction of periodic waveforms by time domain averaging. Mech Syst Signal Process 1987:83–95.

[48] Delgado-Arredondo PA, Garcia-Perez A, Morinigo-Sotelo D, Osornio-Rios RA, Avina-Cervantes JG, Rostro-Gonzalez H, et al. Comparative Study of Time-Frequency Decomposition Techniques for Fault Detection in Induction Motors Using Vibration Analysis during Startup Transient. Shock Vib 2015;2015. https://doi.org/10.1155/2015/708034.

[49] Zheng J, Cheng J, Yang Y. Generalized empirical mode decomposition and its applications to rolling element bearing fault diagnosis. Mech Syst Signal Process 2013;40:136–53. https://doi.org/10.1016/j.ymssp.2013.04.005.

[50] Vernekar K, Kumar H, Gangadharan KV. Gear Fault Detection Using Vibration Analysis and Continuous Wavelet Transform. Procedia Mater Sci 2014;5:1846–52. https://doi.org/10.1016/j.mspro.2014.07.492.

[51] Zhao X. A method of gear fault detection based on wavelet transform. 2009 Int Conf Bus Intell Financ Eng BIFE 2009

2009:648–51. https://doi.org/10.1109/BIFE.2009.151.

[52] Parey A, Pachori RB. Variable cosine windowing of intrinsic mode functions: Application to gear fault diagnosis. Meas J Int Meas Confed 2012;45:415–26. https://doi.org/10.1016/j.measurement.2011.11.001.

[53] Wang T, Wu X, Liu T, Xiao ZM. Gearbox Fault Detection and Diagnosis Based on EEMD De-noising and Power Spectrum. 2015 IEEE Int Conf Inf Autom ICIA 2015 - Conjunction with 2015 IEEE Int Conf Autom Logist 2015:1528–31. https://doi.org/10.1109/ICInfA.2015.7279528.

[54] German-Sallo Z, Grif HS. Hilbert-Huang Transform in Fault Detection. Procedia Manuf 2019;32:591–5. https://doi.org/10.1016/j.promfg.2019.02.257.

[55] Qiao Z, Lei Y, Li N. Applications of stochastic resonance to machinery fault detection: A review and tutorial. Mech Syst Signal Process 2019;122:502–36. https://doi.org/10.1016/j.ymssp.2018.12.032.

[56] Chen H, Sun Y, Shi Z, Lin J. Intelligent Analysis Method of Gear Faults Based on FRWT and SVM. Shock Vib 2016;2016. https://doi.org/10.1155/2016/1582738.

[57] Jedliński Ł, Jonak J. A disassembly-free method for evaluation of spiral bevel gear assembly. Mech Syst Signal Process 2017;88:399–412. https://doi.org/10.1016/j.ymssp.2016.11.005.

[58] Kotsiantis S. B. Supervised machine learning: A review of classification techniques. Informatica 2007;31:249–68. https://doi.org/10.1007/s10751-016-1232-6.

[59] Jain A.K, Murty M.N FP. Data clustering: A review 2020;21:1–9.

[60] Praveenkumar T, Saimurugan M, Krishnakumar P, Ramachandran

KI. Fault diagnosis of automobile gearbox based on machine learning techniques. Procedia Eng 2014;97:2092–8. https://doi.org/10.1016/j.proeng.2014.12.452.

[61] Li WH, Ding K, Shi TL, Liao GL. Gear Fault Classification Using Kernel Discriminant Analysis. Key Eng Mater 2006;321–323:1556–9. https://doi.org/10.4028/www.scientific.net/kem.321-323.1556.

[62] Samanta B. Gear fault detection using artificial neural networks and support vector machines with genetic algorithms. Mech Syst Signal Process 2004;18:625–44. https://doi.org/10.1016/S0888-3270(03)00020-7.

[63] Ümütlü RC, Hızarcı B, Ozturk H, Kıral Z. Classification of Helical Gear Fault Levels Using Frequency Component Based Statistical Analysis With. Usak Univ J Eng Sci 2018;1:76–86.

[64] Sharma A, Amarnath M, Kankar PK. Novel ensemble techniques for classification of rolling element bearing faults. J Brazilian Soc Mech Sci Eng 2017;39:709–24. https://doi.org/10.1007/s40430-016-0540-8.

[65] Verma JG, Patel S, Kankar PK. Fault diagnosis of gearbox based on ITD-tunable Q-factor wavelet transform. Indian J Pure Appl Phys 2021;59:223–8. https://doi.org/10.56042/ijpap.v59i3.67756.

[66] Zhao L, Ding J, Huang D, Mi B, Ke L, Liu Y. The incipient fault feature enhancement method of the gear box based on the wavelet packet and the minimum entropy deconvolution. Syst Sci Control Eng 2018;6:235–41. https://doi.org/10.1080/21642583.2018.1547885.

[67] Saravanan N, Siddabattuni VNSK, Ramachandran KI. Fault diagnosis of spur bevel gear box using artificial neural network (ANN), and proximal support vector machine (PSVM). Appl Soft

Comput J 2010;10:344–60. https://doi.org/10.1016/j.asoc.2009.08.006.

[68] Chen F, Tang B, Chen R. A novel fault diagnosis model for gearbox based on wavelet support vector machine with immune genetic algorithm. Meas J Int Meas Confed 2013;46:220–32. https://doi.org/10.1016/j.measurement.2012.06.009.

[69] Yin K, Zhai J, Xie A, Zhu J. Feature selection using max dynamic relevancy and min redundancy. Pattern Anal Appl 2023. https://doi.org/10.1007/s10044-023-01138-y.

[70] Vernekar K KH and GK. Engine gearbox fault diagnosis using machine learning approach Article information : J Qual Maint Eng 2018.

[71] Kingma DP, Ba JL. Adam: A method for stochastic optimization. 3rd Int Conf Learn Represent ICLR 2015 - Conf Track Proc 2015:1–15.

[72] Sainath TN, Vinyals O, Senior A, Sak H. Convolutional, Long Short-Term Memory, fully connected Deep Neural Networks. ICASSP, IEEE Int Conf Acoust Speech Signal Process - Proc 2015;2015-Augus:4580–4. https://doi.org/10.1109/ICASSP.2015.7178838.

[73] Yu S, Wickstrom K, Jenssen R, Principe J. Understanding Convolutional Neural Networks with Information Theory: An Initial Exploration. IEEE Trans Neural Networks Learn Syst 2021;32:435–42. https://doi.org/10.1109/TNNLS.2020.2968509.

[74] Jing L, Zhao M, Li P, Xu X. A convolutional neural network based feature learning and fault diagnosis method for the condition monitoring of gearbox. Meas J Int Meas Confed 2017;111:1–10. https://doi.org/10.1016/j.measurement.2017.07.017.

[75] Jiao J, Zhao M, Lin J, Zhao J. A multivariate encoder information based convolutional neural network for intelligent fault diagnosis of

planetary gearboxes. Knowledge-Based Syst 2018;160:237–50. https://doi.org/10.1016/j.knosys.2018.07.017.

[76] Jing L, Wang T, Zhao M, Wang P. An adaptive multi-sensor data fusion method based on deep convolutional neural networks for fault diagnosis of planetary gearbox. Sensors (Switzerland) 2017;17. https://doi.org/10.3390/s17020414.

[77] Li X, Li J, Zhao C, Qu Y, He D. Early Gear Pitting Fault Diagnosis Based on Bi-directional LSTM. 2019 Progn Syst Heal Manag Conf PHM-Qingdao 2019 2019. https://doi.org/10.1109/PHM-Qingdao46334.2019.8942949.

[78] Jiang G, He H, Yan J, Xie P. Multiscale Convolutional Neural Networks for Fault Diagnosis of Wind Turbine Gearbox. IEEE Trans Ind Electron 2019;66:3196–207. https://doi.org/10.1109/TIE.2018.2844805.

[79] Li X, Li J, Zhao C, Qu Y, He D. Early Gear Pitting Fault Diagnosis Based on Bi-directional LSTM. Progn Syst Heal Manag Conf PHM-Qingdao 2019 2019. https://doi.org/10.1109/PHM-Qingdao46334.2019.8942949.

[80] Li X, Li J, Qu Y, He D. Gear pitting fault diagnosis using integrated CNN and GRU network with both vibration and acoustic emission signals. Appl Sci 2019;9. https://doi.org/10.3390/app9040768.

[81] Qu Y, He M, Deutsch J, He D. Detection of pitting in gears using a deep sparse autoencoder. Appl Sci 2017;7. https://doi.org/10.3390/app7050515.

[82] Targett J, Nightingale JE. Thermoplastic gears. Proc Inst Mech Eng Conf Proc 1970;184:184–226.

[83] Düzcükoğlu H, Yakut R, Uysal E. The use of cooling holes to decrease the amount of thermal damage on a plastic gear tooth. J Fail

Anal Prev 2010;10:545–55. https://doi.org/10.1007/s11668-010-9398-8.

[84] Düzcükoğlu H. PA 66 spur gear durability improvement with tooth width modification. Mater Des 2009;30:1060–7. https://doi.org/10.1016/j.matdes.2008.06.037.

[85] İmrek H. Width modification for gears with low contact ratio. Meccanica 2009;44:613–21. https://doi.org/10.1007/s11012-009-9220-4.

[86] Evans SM, Keogh PS. Efficiency and running temperature of a polymer-steel spur gear pair from slip/roll ratio fundamentals. Tribol Int 2016;97:379–89. https://doi.org/10.1016/j.triboint.2016.01.052.

[87] Mertens AJ, Senthilvelan S. Durability of polymer gear-paired with steel gear manufactured by wire cut electric discharge machining and hobbing. Int J Precis Eng Manuf 2016;17:181–8. https://doi.org/10.1007/s12541-016-0023-y.

[88] Li W, Wood A, Weidig R, Mao K. An investigation on the wear behaviour of dissimilar polymer gear engagements. Wear 2011;271:2176–83. https://doi.org/10.1016/j.wear.2010.11.019.

[89] Gábor K, László Z, Róbert K, Gödöllő S. Abrasive wear of polymer-steel gear pairs in diferent soil types. Int Conf Carpathian Euro-Region Spec Ind Syst 2008.

[90] Senthilvelan S, Gnanamoorthy R. Effect of rotational speed on the performance of unreinforced and glass fiber reinforced Nylon 6 spur gears. Mater Des 2007;28:765–72. https://doi.org/10.1016/j.matdes.2005.12.002.

[91] Dighe AD, Mishra AK, Wakchaure VD. Investigation of Wear Resistance and Torque Transmission Capacity of Glass Filled Polyamide and PEEK Composite Spur Gears. Int J Eng Adv Technol

2014:299–303.

[92] Yousef SS, Burns DJ, McKinlay W. Techniques for assessing the running temperature and fatigue strength of thermoplastic gears. Mech Mach Theory 1973;8:175–85. https://doi.org/10.1016/0094-114X(73)90051-7.

[93] Mao K, Hooke CJ, Walton D. Acetal gear wear and performance prediction under unlubricated running condition. J Synth Lubr 2006;23:137–52. https://doi.org/10.1002/jsl.17.

[94] Mertens AJ, Senthilvelan S. Surface durability of injection-moulded carbon nanotube–polypropylene spur gears. Proc Inst Mech Eng Part L J Mater Des Appl 2018;232:909–21. https://doi.org/10.1177/1464420716654308.

[95] Yousef S, Khattab A, Zaki M, Osman TA. Wear characterization of carbon nanotubes reinforced polymer gears. IEEE Trans Nanotechnol 2013;12:616–20. https://doi.org/10.1109/TNANO.2013.2264902.

[96] Yousef S, Visco AM, Galtieri G, Njuguna J. Wear Characterizations of Polyoxymethylene (POM) Reinforced with Carbon Nanotubes (POM/CNTs) Using the Paraffin Oil Dispersion Technique. Jom 2016;68:288–99. https://doi.org/10.1007/s11837-015-1674-3.

[97] Kurokawa M, Uchiyama Y, Nagai S. Performance of plastic gear made of carbon fiber reinforced poly-ether-ether-ketone: Part 2. Tribol Int 2000;33:715–21. https://doi.org/10.1016/S0301-679X(00)00111-0.

[98] Gurunathan C, Kirupasankar S, Gnanamoorthy R. Wear characteristics of polyamide nanocomposite spur gears. Proc Inst Mech Eng Part J J Eng Tribol 2011;225:299–306. https://doi.org/10.1177/1350650111401282.

[99] Hriberšek M, Kulovec S. Preliminary study of void influence on polyamide 66 spur gears durability. J Polym Res 2022;29. https://doi.org/10.1007/s10965-022-03085-4.

[100] Marshek KM, Chan PKC. Wear damage to plastic worms and gears. Wear 1977;44:405–9. https://doi.org/10.1016/0043-1648(77)90154-5.

[101] Hooke CJ, Kukureka SN, Liao P, Rao M, Chen YK. The friction and wear of polymers in non-conformal contacts. Wear 1996;200:83–94. https://doi.org/10.1016/S0043-1648(96)07270-5.

[102] Koffi D, Bravo A, Toubal L, Erchiqui F. Optimized use of cooling holes to decrease the amount of thermal damage on a plastic gear tooth. Adv Mech Eng 2016;8:1–13. https://doi.org/10.1177/1687814016638824.

[103] Mertens AJ, Senthilvelan S. Durability enhancement of polymer gear using compressed air cooling. Proc Inst Mech Eng Part L J Mater Des Appl 2016;230:515–25. https://doi.org/10.1177/1464420715581195.

[104] Düzcükoğlu H. Study on development of polyamide gears for improvement of load-carrying capacity. Tribol Int 2009;42:1146–53. https://doi.org/10.1016/j.triboint.2009.03.009.

[105] Dearn KD. Acoustic Emissions from Polymeric Gears 2009;II.

[106] Nozawa JI, Komoto T, Kawai T, Kumehara H. Tribological properties of polymer-sheet-adhered metal hybrid gear. Wear 2009;266:893–7. https://doi.org/10.1016/j.wear.2008.12.008.

[107] Hoskins TJ, Dearn KD, Kukureka SN, Walton D. Acoustic noise from polymer gears - A tribological investigation. Mater Des 2011;32:3509–15. https://doi.org/10.1016/j.matdes.2011.02.041.

[108] Singh AK, Siddhartha. Noise Emission form Functionally Graded

Materials based Polypropylene Spur Gears - A Tribological Investigation. Mater Today Proc 2018;5:8199–205. https://doi.org/10.1016/j.matpr.2017.11.509.

[109] Sharma V, Parey A. A Review of Gear Fault Diagnosis Using Various Condition Indicators. Procedia Eng 2016;144:253–63. https://doi.org/10.1016/j.proeng.2016.05.131.

[110] Singh P, Harsha SP. Statistical and frequency analysis of vibrations signals of roller bearings using empirical mode decomposition. Proc Inst Mech Eng Part K J Multi-Body Dyn 2019;233:856–70. https://doi.org/10.1177/1464419319847921.

[111] Parey A, El Badaoui M, Guillet F, Tandon N. Dynamic modelling of spur gear pair and application of empirical mode decomposition-based statistical analysis for early detection of localized tooth defect. J Sound Vib 2006;294:547–61. https://doi.org/10.1016/j.jsv.2005.11.021.

[112] Manikumar R, Singampalli RS, J AR. Application of EMD based statistical parameters for the prediction of fault severity in a spur gear through vibration signals. Adv Mater Process Technol 2022;8:2152–70. https://doi.org/10.1080/2374068X.2021.1888499.

[113] Dragomiretskiy K, Zosso D. Variational mode decomposition. IEEE Trans Signal Process 2014;62:531–44. https://doi.org/10.1109/TSP.2013.2288675.

[114] Amarnath M, Praveen Krishna IR. Local fault detection in helical gears via vibration and acoustic signals using EMD based statistical parameter analysis. Meas J Int Meas Confed 2014;58:154–64. https://doi.org/10.1016/j.measurement.2014.08.015.

[115] Huang NE, Shen Z, Long SR, Wu MC, Snin HH, Zheng Q, et al. The empirical mode decomposition and the Hubert spectrum for

nonlinear and non-stationary time series analysis. Proc R Soc A Math Phys Eng Sci 1998;454:903–95. https://doi.org/10.1098/rspa.1998.0193.

[116] Zhong J, Yang Z, Wong SF. Machine condition monitoring and fault diagnosis based on support vector machine. IEEM2010 - IEEE Int Conf Ind Eng Eng Manag 2010:2228–33. https://doi.org/10.1109/IEEM.2010.5674594.

[117] Heydarzadeh M, Kia SH, Nourani M, Henao H, Capolino GA. Gear fault diagnosis using discrete wavelet transform and deep neural networks. IECON Proc (Industrial Electron Conf 2016:1494–500. https://doi.org/10.1109/IECON.2016.7793549.

[118] Lei Y, Zuo MJ. Gear crack level identification based on weighted K nearest neighbor classification algorithm. Mech Syst Signal Process 2009;29:1535–47. https://doi.org/10.1016/j.ymssp.2009.01.009.

[119] Mehmood RM, Lee HJ. Towards emotion recognition of EEG brain signals using Hjorth parameters and SVM 2015:24–7. https://doi.org/10.14257/astl.2015.91.05.

[120] Leite JPRR, Moreno RL. Heartbeat classification with low computational cost using Hjorth parameters. IET Signal Process 2018;12:431–8. https://doi.org/10.1049/iet-spr.2017.0296.

[121] Gilles J. Empirical wavelet transform. IEEE Trans Signal Process 2013;61:3999–4010. https://doi.org/10.1109/TSP.2013.2265222.

[122] Hjorth B. An on-line transformation of EEG scalp potentials into orthogonal source derivations. Electroencephalogr Clin Neurophysiol 1975;39:526–30. https://doi.org/10.1016/0013-4694(75)90056-5.

[123] Prakash J, Kankar PK. Health prediction of hydraulic cooling circuit using deep neural network with ensemble feature ranking technique.

Measurement 2019;151:107225. https://doi.org/10.1016/j.measurement.2019.107225.

[124] Balakrishnama S, Ganapathiraju A. Linear Discriminant Analysis - a Brief Tutorial. Compute 2015.

[125] Ramteke DS, Parey A, Pachori RB. Automated gear fault detection of micron level wear in bevel gears using variational mode decomposition. J Mech Sci Technol 2019;33:5769–77. https://doi.org/10.1007/s12206-019-1123-2.

[126] Pacheco-Chérrez J, Fortoul-Díaz JA, Cortés-Santacruz F, María Aloso-Valerdi L, Ibarra-Zarate DI. Bearing fault detection with vibration and acoustic signals: Comparison among different machine leaning classification methods. Eng Fail Anal 2022;139. https://doi.org/10.1016/j.engfailanal.2022.106515.

[127] Suresh S, Srinivas M, Naidu VPS. Vibration analysis of gearbox fault diagnosis using DWT and statistical features. J Eng Res 2022;10:156–65. https://doi.org/10.36909/jer.10465.

[128] Du NT, Dien NP, Nga NTT. Gear fault detection in gearboxes operated in non-stationary conditions based on variable sideband analysis without a tachometer. Front Mech Eng 2022;8:1–10. https://doi.org/10.3389/fmech.2022.1021222.

[129] Inturi V, Pratyush AS, Sabareesh GR. Detection of Local Gear Tooth Defects on a Multistage Gearbox Operating Under Fluctuating Speeds Using DWT and EMD Analysis. Arab J Sci Eng 2021. https://doi.org/10.1007/s13369-021-05807-0.

[130] W. J. Wang and P. D. Mcfadden. Application of Wavelets to Gearbox Vibration Signals for Fault Detection. J Sound Vib 1996;5:927–39. https://doi.org/10.1109/ICACC.2010.5486917.

[131] Sharma A, Amarnath M, Kankar PK. Feature extraction and fault

severity classification in ball bearings. JVC/Journal Vib Control 2016;22:176–92. https://doi.org/10.1177/1077546314528021.

[132] Saravanan N, Ramachandran KI. Incipient gear box fault diagnosis using discrete wavelet transform (DWT) for feature extraction and classification using artificial neural network (ANN). Expert Syst Appl 2010;37:4168–81. https://doi.org/10.1016/j.eswa.2009.11.006.

[133] Daubechies I, Grossmann A, Meyer Y. Painless nonorthogonal expansions. J Math Phys 1986;27:1271–83. https://doi.org/10.1063/1.527388.

[134] Sharma S, Tiwari SK, Singh S. Diagnosis of gear tooth fault in a bevel gearbox using discrete wavelet transform and autoregressive modeling. Life Cycle Reliab Saf Eng 2019;8:21–32. https://doi.org/10.1007/s41872-018-0061-9.

[135] Zhou ZH. Ensemble methods: Foundation and algorithims. 2012. https://doi.org/10.1201/b11822-34.

[136] Zhaohua Wu NEH. Ensemble empirical mode decomposition: A Noise-Assited. Biomed Tech 2010;55:193–201.

[137] Yeh JR, Shieh JS, Huang NE. Complementary ensemble empirical mode decomposition: A novel noise enhanced data analysis method. Adv Adapt Data Anal 2010;2:135–56. https://doi.org/10.1142/S1793536910000422.

[138] Torres ME, Colominas MA, Schlotthauer G, Flandrin P. A complete ensemble empirical mode decomposition with adaptive noise. ICASSP, IEEE Int Conf Acoust Speech Signal Process - Proc 2011:4144–7. https://doi.org/10.1109/ICASSP.2011.5947265.

[139] Zhang W, Peng G, Li C, Chen Y, Zhang Z. A new deep learning model for fault diagnosis with good anti-noise and domain adaptation ability on raw vibration signals. Sensors (Switzerland) 2017;17.

https://doi.org/10.3390/s17020425.

[140] Li H, Zhao J, Liu J, Ni X. 2256. Application of empirical mode decomposition and euclidean distance technique for feature selection and fault diagnosis of planetary gearbox. J Vibroengineering 2016;18:5096–113. https://doi.org/10.21595/jve.2016.16762.

[141] Zhang Y, Zhou T, Huang X, Cao L, Zhou Q. Fault diagnosis of rotating machinery based on recurrent neural networks. Meas J Int Meas Confed 2021;171:108774. https://doi.org/10.1016/j.measurement.2020.108774.

[142] Haj Mohamad T, Abbasi A, Kim E, Nataraj C. Application of Deep CNN-LSTM Network to Gear Fault Diagnostics. 2021 IEEE Int Conf Progn Heal Manag ICPHM 2021 2021. https://doi.org/10.1109/ICPHM51084.2021.9486591.

[143] Mariıa E. Torres , Marcelo A. Colominas, Gaston Schlotthauer PF. A complete ensemble empirical mode decomposition with adaptive noise. Ieee 2011:4144–7.

[144] Thongpanja S, Phinyomark A, Phukpattaranont P, Limsakul C. Mean and median frequency of EMG signal to determine muscle force based on time dependent power spectrum. Elektron Ir Elektrotechnika 2013;19:51–6. https://doi.org/10.5755/j01.eee.19.3.3697.

[145] Prakash J, Miglani A, Kankar PK. Internal Leakage Detection in Hydraulic Pump Using Model-Agnostic Feature Ranking and Ensemble Classifiers. J Comput Inf Sci Eng 2023;23:1–14. https://doi.org/10.1115/1.4056365.

[146] Hochreiter S, Schmidhuber J. Long Short-Term Memory. Neural Comput 1997;9:1735–80. https://doi.org/10.1162/neco.1997.9.8.1735.

[147] Al Hamoud A, Hoenig A, Roy K. Sentence subjectivity analysis of a political and ideological debate dataset using LSTM and BiLSTM with attention and GRU models. J King Saud Univ - Comput Inf Sci 2022. https://doi.org/10.1016/j.jksuci.2022.07.014.

[148] Yang X lian, Yi S li. Multi-classification of fundus diseases based on DSRA-CNN. Biomed Signal Process Control 2022;77:103763. https://doi.org/10.1016/j.bspc.2022.103763.

[149] Ramteke DS, Pachori RB, Parey A. Automated Gearbox Fault Diagnosis Using Entropy-Based Features in Flexible Analytic Wavelet Transform (FAWT) Domain. J Vib Eng Technol 2021. https://doi.org/10.1007/s42417-021-00322-w.

[150] Yang D, Liu Y, Li S, Li X, Ma L. Gear fault diagnosis based on support vector machine optimized by artificial bee colony algorithm. Mech Mach Theory 2015;90:219–29. https://doi.org/10.1016/j.mechmachtheory.2015.03.013.

[151] Wang P, Zhou Y, Zhang L. Fault Diagnosis Method of Rotating Machinery Based on CEEMDAN-LSTM Model. J Phys Conf Ser 2022;2173. https://doi.org/10.1088/1742-6596/2173/1/012057.

LIST OF PUBLICATIONS

List of Journal Publications:

1. **Kumar, A**., Parey, A. & Kankar, P.K. Supervised Machine Learning Based Approach for Early Fault Detection in Polymer Gears Using Vibration Signals. MAPAN 38, 383–394 (2023). https://doi.org/10.1007/s12647-022-00608-8
2. **Kumar A**., Parey A. & Kankar P. K., Polymer Gear Fault Classification Using EMD-DWT Analysis Based on Combination of Entropy and Hjorth Features. IJPAP 60, 339-346 (2022). DOI: 10.56042/ijpap.v60i4.58431
3. **Kumar, A**., Parey, A. & Kankar, P.K. A New Hybrid LSTM-GRU Model for Fault Diagnosis of Polymer Gears Using Vibration Signals. J. Vib. Eng. Technol. (2023). https://doi.org/10.1007/s42417-023-01010-7
4. **Kumar A**., Parey A. & Kankar P. K., Effect of teeth modifications on vibration and acoustic characteristics of polymer gears. Journal of the Brazilian Society of Mechanical Sciences and Engineering,2023 (**Accepted**)
5. **Kumar A**., Parey A. & Kankar P. K., Early pitting fault detection for polymer gears using kurtosis-VMD based condition indicators. Proceedings of the Institution of Mechanical Engineers, Part O: Journal of Risk and Reliability,2023. (**Revision Submitted**)

List of Conference Publications:

1. **Kumar A**., Parey A. & Kankar P. K., Vibration based fault detection of polymer gear. Materials Today: Proceedings, Volume 44, Part 1, 2021,2116-2120, ISSN2214-7853. https://doi.org/10.1016/j.matpr.2020.12.271.